Oxidative Potential of Ambient Aerosols over Different Regions in India

A Thesis

Submitted for the Award of Ph. D. Degree of

MOHANLAL SUKHADIA UNIVERSITY

in the

Faculty of Sciences

By

Anilbhai Arvindbhai Patel

Under the supervision of

Dr. Neeraj Rastogi

Associate Professor
Geosciences Division
Physical Research Laboratory
Ahmedabad – 380 009, India

DEPARTMENT OF CHEMISTRY
FACULTY OF SCIENCE
MOHANLAL SUKHADIA UNIVERSITY,
UDAIPUR (RAJASTHAN)

2019

Table of Contents

List of Figures

List of Abbreviations

AGL	Above Ground Level
AMS	Aerosol Mass Spectrometer
AM-SL	Above Mean Sea Level
AOA	Ammonia Oxidizing Archaea
APX	Ascorbate Peroxidase
Ar	Argon
b_{abs}	Absorption coefficient of BrC
BB	Biomass Burning
BC	Black Carbon
BDL	Below Detection Limit
BoB	Bay of Bengal
BrC	Brown Carbon
CAT	Catalase
CDOM	Colored Dissolved Organic Matter
CO	Carbon Monoxide
DCFH	Dichlorodihydrofluorescein
DNA	Deoxyribo Nucleic Acid
DOM	Dissolved Organic Matter
DTNB	5′-dithiobis-2-nitrobenzoic acid
DTT	Dithiothreitol
e^-	Electron
EC	Elemental Carbon
EFs	Enrichment Factors
Fe	Iron
FFB	Fossil Fuel Burning
FID	Flame Ionization Detector
GDAS	Global Data Assimilation System
GIDC	Gujarat Industrial Development Corporation
GPX	Guaiacol Peroxidase
H_2O_2	Hydrogen Peroxide
HO-1	Heme Oxygenase
HOA	Hydrocarbon like Organic Aerosol
HULIS	Humic Like Substances
HYSPLIT	Hybrid Single-Particle Langrangian Integrated Trajectory
IC	Inorganic Carbon
IE	Ionization Efficiency

IGP	Indo-Gangetic Plain
ISTRAC	Indian Space Research Organizations Telemetry
KOH	Potassium Hydrogen Phthalate
LNLC	Low Nutrients Low Chlorophyll
LOD	Limit of Detection
LPG	Liquefied Petroleum Gas
LV–OOA	Low Volatile Oxidized Organic Aerosol
LWCC	Liquid Waveguide Capillary Cell
MeOH	Methanol
MLR	Multiple Linear Regression
MQ	Milli-Q
MSA	Methyl Sulphonic Acid
NADH	Nicotinamide Adenine Dinucleotide
NADPH	Nicotinamide Adenine Dinucleotide Phosphate
NDIR	Non-Dispersive Infrared
NE	North Easterly
NE-H	North-Eastern Himalayas
NE-SAC	North-East Space Application Center
NIOSH	National Institute for Occupational Safety and Health
nm	Nanometer
NPOC	Non-Purgeable Organic Carbon
NSS	Non-Sea-Salt
O_3	Ozone
OA	Organic Aerosol
OA	Organic Aerosol
OA	Organic Aerosol
$OH^{\cdot}$	Hydroxide Radical
O_2^{-}	Super Oxide
O_2^1	Singlet Oxygen
OM	Organic Matter
OOA	Oxidized Organic Aerosol
OP	Oxidative Potential
OP_M	Mass Normalized OP
OP_V	Volume Normalized OP
PAHs	Polycyclic Aromatic Hydrocarbons
PBR	Port Blair
PC	Pyrolyzed Carbon
PCU	Passenger Car Unit
PIKA	Peak Integration by Key Analysis
PM	Particulate Matter
PNG	Piped Natural Gas

POPHAA	P-Hydroxyphenyl Acetic Acid
PQN	Phenanthrenequinone
Q-ICP-MS	Quadrupole Inductively Coupled Plasma Mass Spectrometer
R	Correlation Coefficient
R^2	Coefficient of Determination
RH	Relative Humidity
ROS	Reactive Oxygen Species
RSD	Relative Standard Deviation
RTO	Regional Transport Office
-SH	Thiol Group
SIA	Secondary Inorganic Aerosol
SOA	Secondary Organic Aerosol
SOD	Superoxide Dismutase
SPM	Suspended Particulate Matter
SQUIRREL	SeQUential Igor data RetRiEvaL
SV–OOA	Semi Volatile Oxidized Organic Aerosol
SW	Southwesterly
T	Temperature
TN	Total Nitrogen
TNB	2-Nitro-5-Thiobenzoic Acid
TNM-L	Total Nitrogen Measuring Unit
TOC	Total Organic Carbon
TOC-L	Total Organic Carbon Analyzer
HR-ToF-MS	High Resolution Time of Flight Mass Spectrometry
TOT	Thermal Optical Transmittance
TSP	Total Suspended Particulate
UCC	Upper Continental Crust
VOCs	Volatile Organic Compounds
WHO	World Health Organization
WIOC	Water Insoluble Organic Carbon
WSIN	Water Soluble Inorganic Nitrogen
WSIS	Water Soluble Inorganic Species
WSOC	Water Soluble Organic Carbon
WSON	Water soluble Organic Nitrogen
X	Element
μm	micrometer

Chapter 1

INTRODUCTION

1.1. What are atmospheric aerosol ?

Aerosol are defined as solid and/or liquid particles suspended in the atmospheric air. They are also termed as particulate matter (PM), suspended particulate matter (SPM), total suspended particulate (TSP). They are injected into the atmosphere through variety of sources which can be natural as well as anthropogenic. Natural sources include biogenic emissions, sea-salts spray, forest fires, wind-blown mineral dust and volcanic emissions whereas anthropogenic sources include emissions from industries, thermal power plants and vehicles, biomass burning (BB) and waste burning, etc (Fig. 1.1, Seinfeld and Pandis, 2006). The aerosol species include organic and elemental carbon, inorganic species and trace metals including heavy metals. Aerosol are also classified as primary and secondary aerosol. Here, the aerosol emitted directly as particle from the source are called primary aerosol and those formed through the chemical processing of gaseous precursors are called secondary aerosol. They are removed from the atmosphere via two major processes; i.e. dry and wet deposition. The settling of particles can occur by impaction, adhesion, diffusion and gravitation (dry deposition). On the other hand during the wet deposition, particles incorporate to the liquid droplets and form clouds (in-cloud scavenging) and washouts with the precipitation (below-cloud scavenging). Since aerosol are suspended tiny particles in the air, they follow the path of air transport. It is also possible that wind can carry particles great distance (thousands of kilometer) before they get down to the surface. Depending upon their physicochemical properties, typical residence time of aerosol in the lower troposphere varies from few minutes to several days.

Aerosol exhibit wide range of the size varying from a few nanometer (nm) to several micrometer (μm). Based on their sizes, aerosol are classified into four modes; i.e. nucleation, Aitken, accumulation and coarse. The smallest aerosol size can be ~ 1 – 2 nm (i.e. freshly nucleated in the atmosphere and contained few tens of molecules), and the mechanically produced (by quarrying or suspension of mineral dust) particle may be of the highest (~ 100 μm) size in the atmosphere (Prospero et al., 1983). The smallest group of particles, with diameters of ≤ 10 nm, is usually referred to as the nucleation mode, whereas the Aitken mode is comprised of particles

between 10 – 50 nm sizes. Secondary formation of atmospheric aerosol occurs through many processes including nucleation. In this process molecules of low volatility condense onto pre-existing particles causing the growth of those particles (heterogeneous nucleation, ~ 1 – 50 nm) and/or molecules of extremely low vapor pressure will condense with one another to form wholly new particles (homogeneous nucleation, ~ 1 – 2 nm) (Hinds, 1999). Secondary particle formation in the atmosphere occurs mostly by the heterogeneous nucleation process. Particles within the nucleation mode will soon undergo condensational growth and become part of the Aitken mode. In addition to the condensational growth of vapor, particles as a result of coagulation processes (two or more particle cling/accumulate together), soon become a part of the accumulation mode and fall in between the size 50 nm – 1 μm. If we think about a single hair from human's head, the average human hair is about 70 μm in diameter. The size of human hair is ~ 70 times or more than the size of inhalable aerosol (i.e. fine aerosol that falls into nucleation, Aitken and accumulation mode). Particle of accumulation mode significantly influence the incoming visible solar radiation. Coarse mode size particle (> 1 μm) are produced through mechanical processes such as quarrying or suspension of mineral dust, sea-salt spray via bubble bursting during white cap formation etc.

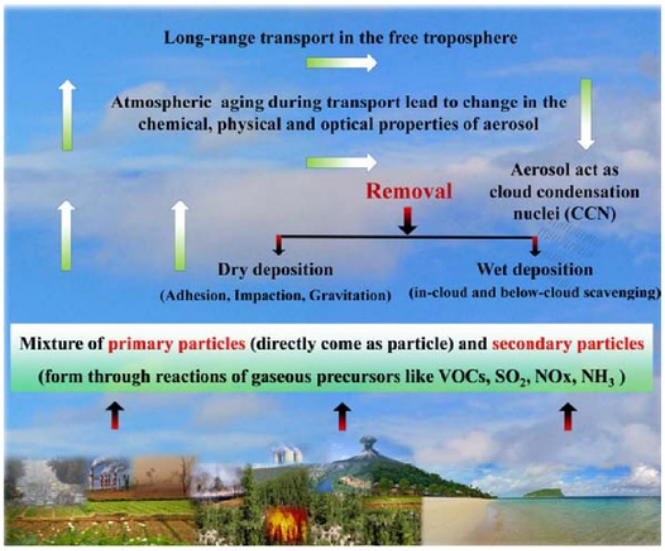

Figure 1. 1. *A pictorial view of aerosol cycling in the atmosphere.*

In general, anthropogenic sources emit fine (< 1 μm) and natural sources produce the coarser (> 1 μm) particle. Atmospheric aerosol size can be specified by various diameter terms, such as geometric, aerodynamic, electrical mobility and optical diameter. Scientists generally define the aerosol size in terms of aerodynamic diameter (i.e. the diameter of unit density sphere that has the same settling velocity as that of particle into consideration in the air).

Aerosol are known to affects Earth's climate (radiation budget and hydrological cycle), aquatic system (biogeochemistry of ocean and lakes), and air quality (human health and visibility reduction) (Ramanathan et al., 2001; Seinfeld and Pandis, 2006). Aerosol also react with several atmospheric trace gases that lead to change in their chemical and physical properties, which can affect their optical and hygroscopic properties as well as bioavailability of nutrients. Although all the effects of aerosol are important, the effect on air quality is gaining specific interest and attention, as it directly relates to public health. Various epidemiological studies have suggested that the human exposure to ambient aerosol is associated with variety of health related issues including cardiovascular and pulmonary diseases (Delfino et al., 2005; Oberdörster et al., 2005; Slaughter et al., 2005; Pope and Dockery, 2006; Pope et al., 2009). One of the widely proposed mechanisms related to how aerosol affect human health is that several types of aerosol, on inhalation, can produce *reactive oxygen species* (ROS) in-situ in human respiratory system (Kumagai et al., 2002; Cheung et al., 2012).

1.2. Aerosol and reactive oxygen species (ROS)

ROS generation by ambient aerosol not only affects human health but also oxidizing capacity of the atmosphere (Cadenas and Davies, 2000; Xu et al., 2015; Hopke, 2015 and references therein); however, the mechanism of ROS generation could be different at different places. Molecular oxygen has two unpaired (in parallel position) electron (e^-) which makes it paramagnetic in nature and hence, is very unlikely to react with other molecules. When molecular oxygen undergoes reaction with other paramagnetic species, which includes but not limited to transition metals and other redox active species present in aerosol, ROS are generated. ROS can be

radicals such as super oxide anion radical ($O_2^{\cdot-}$) and hydroxide radical ($OH^{\cdot}$) as well as non radicals such as hydrogen peroxide (H_2O_2), singlet oxygen (O_2^1), ozone (O_3) etc. ROS can be exogenous (constituents attached to the surface of aerosol) and/or endogenous (formed through in-situ reactions, where aerosol acts as catalyst). Exogenous ROS are also known as particle-bound ROS whereas endogenous are also known as particle-induced ROS. Once they produce they can affect the oxidizing capability of atmosphere, air quality, and all living organisms. Reactivity of ROS is much higher than that of molecular oxygen. As a result, residence time of ROS is very short (a few seconds for $O_2^{\cdot-}$ and $OH^{\cdot}$; whereas, minutes to a day for H_2O_2) (Lesser, 2006). It is noteworthy that $O_2^{\cdot-}$ is more reactive compared to H_2O_2 and $OH^{\cdot}$ is the most reactive form of ROS family.

1.3.1. ROS production and their impact on the atmosphere

During daytime, photochemical reactions generate ROS in the air containing precursors like volatile organic compounds (VOCs), O_3 etc. For example, $OH^{\cdot}$ formation from the reaction of O_3 with alkenes (including biogenic VOCs, Eq 1), alkyl radical reacts with oxygen to form a peroxy radical (Eq 2) and Fenton type reaction could be a significant source of ROS in the atmosphere (Eq 3 and 4) (Paulson and Orlando, 1996). Furthermore, in absence of sunlight, ROS are formed by chemistry of NO_3 radical, where nitrogen oxides undergo reaction with O_3 molecules to form NO_3 radical (Finlayson-Pitts and Pitts, 2000).

$$R_1CH=CHR_2 + O_3 \rightarrow OH^{\cdot} + \text{products} \quad (1)$$

(Terpenes, unsaturated compounds)

$$R^{\bullet} + O_2 \rightarrow RO_2^{\bullet} \quad (2)$$

$$Fe^{2+} + H_2O_2 \rightarrow Fe^{3+} + HO^{\bullet} + OH^- \quad (3)$$

$$Fe^{3+} + H_2O_2 \rightarrow Fe^{2+} + HOO^{\bullet} + H^+ \quad (4)$$

$$Fe^{3+} + O_2^{\cdot-} \rightarrow Fe^{2+} + O_2 \quad (5)$$

Further, hygroscopic organic aerosol (that include secondary organic aerosol (SOA)) can produce ·OH in aqueous phase under daylight conditions; and Fenton type reactions, on the other hand, are capable of producing ROS under dark conditions (Badali et al., 2015). Further, Tong et al., (2016) have documented that ·OH is also formed by the decomposition of SOA in presence of water and iron ions under dark conditions. After production, these ·OH can lead to rapid chemical aging of SOA in the atmosphere. ROS affects the oxidizing capacity of the atmosphere and can also lead to secondary aerosol formation; e.g., oxidation of SO_2 and NO_x in presence of OH· results into the formation of acidic aerosol.

1.3.2. ROS production and their impact on living organism

Figure 1.2 shows the prediction on the fractional deposition of inhaled particles in the nasopharyngeal, tracheobronchial, and alveolar regions of the human respiratory tract during nose breathing based on a mathematical model (*International Commission on Radiological Protection 1994*) (Oberdörster et al., 2005). A redox active fine (< 2.5 μm) aerosol species can go deep into the respiratory tract during inhalation where they can be reduced in-situ by the biological reducing enzymes such as reductive form of nicotinamide adenine dinucleotide phosphate (NADPH) and reductive form of nicotinamide adenine dinucleotide (NADH) (Hiura et al. 1999, 2000; Kumagai et al. 1997; Nel et al. 1998; Kumagai et al., 2002). These NADH and NADPH enzymes are present in mitochondria and they are capable of handling e^- transportation processes occurring in the cell during the respiration. The reduced redox active aerosol species transfer e^- to the molecular oxygen, which then converts to its reduced form $O_2^{\cdot-}$. It further undergoes reduction to form H_2O_2 and OH through well known Fenton and Haber–Weiss processes (Fig. 1.3). They are collectively termed as ROS. Here, it is important to note that aerosol act as catalyst and hence it keeps producing ROS until they are removed from the place of generation. These in-situ formed ROS are known as endogenous ROS or, particle induces ROS. Capacity of aerosol to produce ROS is also termed as their *oxidative potential (OP)*.

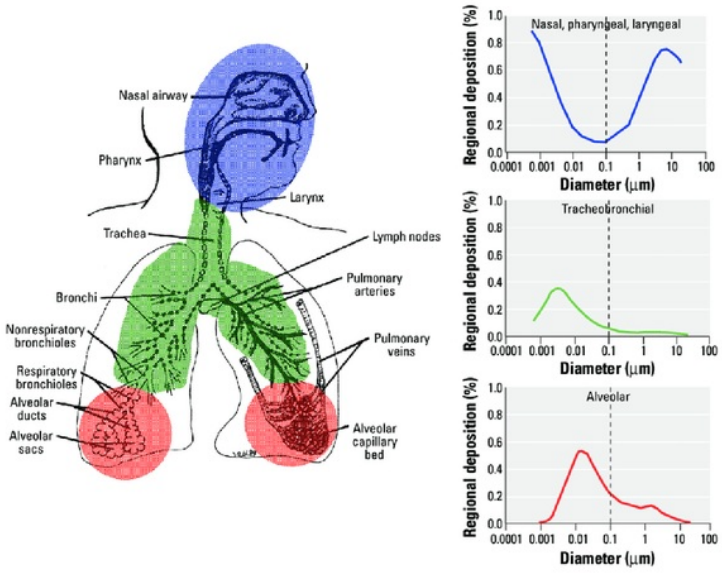

Figure 1. 2. *Predicted fractional deposition of inhaled particles in the nasopharyngeal, tracheobronchial, and alveolar region of the human respiratory tract during nose breathing (Oberdörster et al., 2005).*

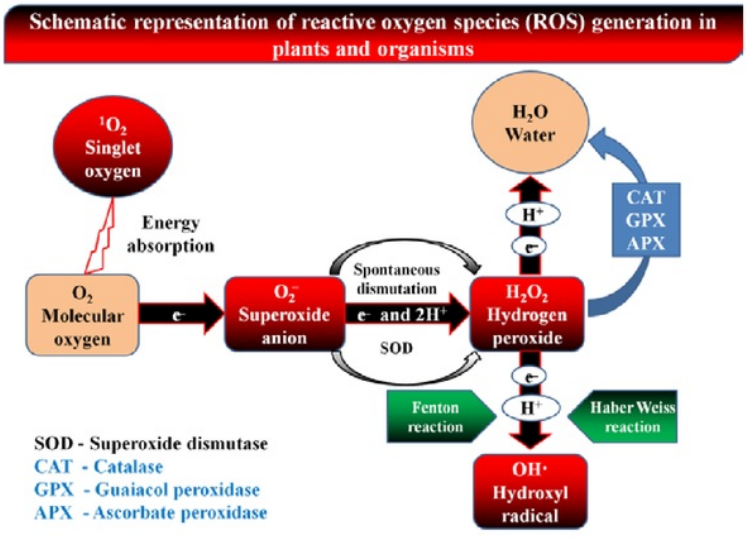

Figure 1. 3. *Schematic representation of how the reactive oxygen species form in living organisms.*

Oxidants (such as ROS) are required in human body as they act against pathogens and maintain the immune system (Morgan and Liu, 2011; Nauseef, 2014; Dunn et al., 2015). However, balance between oxidants and antioxidant is also necessary for all the living organisms. Antioxidants are nothing but vitamins that we take as food. If by any chance we exposed to regions where aerosol have more capability to generate in-situ ROS, the imbalance is developed which favors oxidants and disfavors antioxidants. This situation is said to be under oxidative stress (Barrera, 2012 and references therein). It further may result into inflammation, cell damage and sometimes even cell death. It is because these highly reactive ROS are able to damage all the macromolecules including lipids, proteins, deoxyribonucleic acid (DNA) etc. For example, ROS can cause damage to cellular membrane by process called lipid peroxidation. Cellular membranes are made up of fatty acids which contains unsaturated portion (carbon–carbon double bond) in their structure. ROS can easily attack on this unsaturated portion of fatty acid and generate carbon centered radical fatty acid. This radical fatty acid can further reacts with molecular oxygen to give lipid peroxyl radical which can further reacts with other free fatty acid and produce a fatty acid radical and a lipid peroxide, and so on (Fig. 1.4, Ayala et al., 2014). This lipid peroxidation process can have numerous health effects such as increase in membrane rigidity, alteration in permeability etc (Dix and Aikens, 1993).

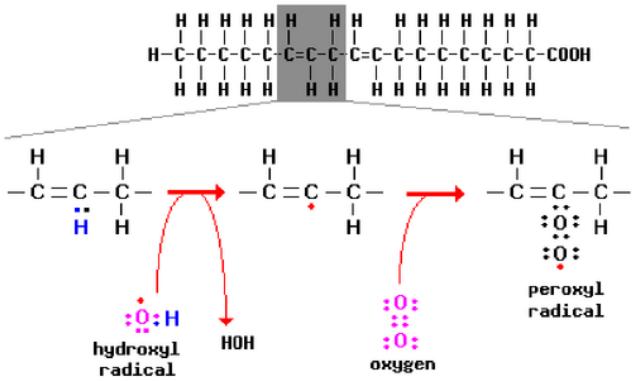

Figure 1. 4. *Lipid peroxidation by ROS in cellular membrane in living organisms (VIVO Pathophysiology;*

(http://www.vivo.colostate.edu/hbooks/pathphys/topics/radicals.html)

ROS can also be produced into the plant cell through photosensitized reaction. Further, salt stress and/or drought can generate ionic and osmotic stress in the plant cell, which reduces CO_2 supply to leaf and that causes reduction of photosynthetic e^- transport chain and hence produce ROS (Kiddle et al., 2003). These ROS can react immediately with other metabolites present in plant cells which may cause cell damage and plant death. ROS thus sometimes infested and induce oxidative stress in human body and hence affect living organisms including plants (Fig. 1.5).

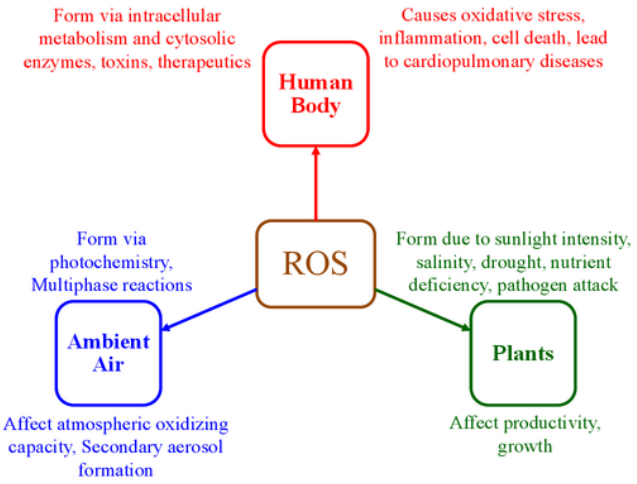

Figure 1. 5. *Schematic diagram depicting how reactive oxygen species (ROS) affect atmospheric chemistry as well as health of human and plants (Rastogi and Patel, 2017).*

1.3. Review of work already done on the subject

Current regulations to protect health are based on ambient aerosol mass without considering their chemical composition. While aerosol mass often exhibits good correlations with toxicity, the toxicity of aerosol is likely more complicated than mass alone, and may be defined by a combination of properties including number concentration, size, surface area, and chemical composition (Perrone et al., 2013; Charrier et al., 2015; Patel and Rastogi, 2018a). These properties determine where aerosol will deposit in the lungs, how it will interact with the body, and how much

oxidative stress it will produce (Oberdörster et al., 2005). The picture is further complicated by the fact that aerosol is a complex mixture of particles from various primary and secondary sources with different degrees of atmospheric processing. Aging changes both size distribution and chemical composition of aerosol, making sources harder to differentiate and potentially changing the toxicity of the aerosol over time. Transition metals (such as Fe, Cu, Zn, Cr, Co, Ni) and quinones are among a few known chemical species which can generate ROS (Charrier and Anastasio, 2012 and references therein).

1.3.1. Research gap identified in the proposed field of investigation

Emissions from variety of combustion sources such as crop residue, woods, cow dung cakes, vehicles, thermal power plants, and industries are reported to be major contributors to ambient aerosol over India. These emissions lead to very high concentration of fine particles over different regions of India (Sarkar et al., 2013). Inhalation of particles containing transition metals (such as Fe, Cu, Zn, Cr, Co, Ni), and/or organic compounds (such as quinones, polycyclic aromatic hydrocarbons (PAHs)), and/or other unknown species can initiate the formation of ROS. However, it is yet to be established that which particles, in addition to metals and quinones, causes the generation of ROS and what is the role of their physicochemical characteristics. ROS generation may cause oxidative stress, inflammation or cell death that lead to various diseases, as discussed above. Many researchers have documented optical, physical and chemical properties of aerosol over different regions of India; however, studies on OP of ambient aerosol i.e., capacity of aerosol to produce ROS, are non-existing in India and limited in the world (Rastogi and Patel, 2017 and references therein).

1.4. Implications

Outcome of this study has important implications in various fields of research such as Atmospheric Chemistry, Medicine, Epidemiology, Toxicology, and Agriculture. Several types of chemical species in aerosol have high potential to generate ROS in the atmosphere as well as in human and plants body. The abundance of chemical species with high ROS generation capacity provides a measure of

toxicity level over a given region during specific seasons. Identification of these chemical species is inevitable to understand their major sources in the atmosphere, which in turn is important in designing appropriate mitigation strategies to reduce these sources.

1.5. Major Objectives

- To determine the OP of ambient aerosol collected from regions dominated by different sources and meteorological conditions,
- To investigate the dependence of the OP on aerosol mass concentration vis-à-vis chemical composition,
- To identify specific sources/processes producing species with high OP over the study regions.

1.6. Structure of thesis

Chapter 1 presents introduction of ambient aerosol and their role in the generation of reactive oxygen species in the atmosphere as well as living organisms. It also presents a review of work done including research gap, and major objectives of the study.

Chapter 2 presents the atmospheric aerosol sampling strategy over different regions of India dominated by different sources and meteorological conditions. It further covers analytical scheme developed and adopted for the measurement of oxidative potential and chemical constituents present in the aerosol sample.

Chapter 3 presents the oxidative potential of ambient aerosol over upper, middle and lower regions of the Indo-Gangetic Plain. It also discusses how the oxidative potential is being affected by aerosol chemical composition derived from intense biomass burning as well as derived through long-range transport over the Indo-Gangetic Plain.

Chapter 4 presents the oxidative potential of ambient aerosol over remote locations such as high altitude site (Mount Abu) and marine environments (the Arabian Sea and Port Blair). It discusses how the seasonal changes in chemical

composition of aerosol affects oxidative potential over high altitude site Mount Abu. It further discusses how the anthropogenic (continental outflow) and natural (open ocean or desert) aerosol affects the oxidative potential over ocean.

Chapter 5 presents the oxidative potential of ambient aerosol over different micro-environments over a big urban city in the western India, Ahmedabad. It represents the role of aerosol derived from industries, traffic related sources, residential zone on the oxidative potential.

Chapter 6 summarizes the key findings of the present study along with the scope of future research wok on the subject.

Chapter 2

AEROSOL SAMPLING AND CHEMICAL ANALYSIS

2.1. Introduction

Aerosol are comprised of several components such as mineral dust, sea-salts, carbonaceous fraction, inorganic fraction etc. in the atmosphere. Details about the chemical analysis of aerosol species such as EC, OC, WSOC, WSON, WSIS and trace metals have been reported from our Lab (Rastogi and Sarin, 2005, 2014, 2016, Ram and Sarin, 2009, 2011; Rajput et al., 2013, 2014). Along with the chemical analysis, this chapter introduces the measurements of aerosol oxidative potential, a new initiative in India.

It is an established fact that redox active PM such as quinones and transition metals catalyze the ROS production in human body through transferring electron from biologically reducing enzyme such as reduced form of nicotinamide adenine dinucleotide phosphate (NADPH) to molecular oxygen (O_2). Several cell based and cell free methods are available to study ROS in vivo and in vitro (Cho et al., 2005; Godri et al., 2011; Venkatachari et al., 2005). Among the available methods for the measurement of ROS generated through particles, those widely used are p-hydroxyphenylacetic acid (POPHAA) and dichlorodihydrofluorescein (DCFH) methods. However, none of these methods cover the entire range of ROS which can be produced by particles. In addition to measure the concentration of ROS generated by aerosol, it is important to measure the capability of aerosol to generate ROS (also termed as oxidative potential, OP). Dithiothreitol (DTT) assay is documented to be mainly used for determining OP of quinones and some trace metals, whereas POPHAA and DCFH assay measures only H_2O_2 concentration.

This chapter presents sampling strategy and analytical protocols of aerosol collected from different sites. Results are presented in subsequent chapters (number 3, 4 and 5). DTT assay was chosen to determine OP of aerosol because its response correlate well with biological markers like Heme oxygenase (HO-1) expression in cells (Li et al., 2003), and exhaled nitric oxide fraction in human subjects (Delfino et al., 2006).

2.2. Strategy and field campaigns

To measure the aerosol composition and OP over sites dominated by different sources and meteorological conditions, different strategic locations were chosen in India and surrounding oceans. Among these locations, three sites cover the Indo-Gangetic Plain (IGP) where one was in upper IGP (Patiala), one in central IGP (Kanpur), and one in lower IGP (Shillong). A high altitude site (Mount Abu) and two marine sites (Bay of Bengal and Arabian Sea) were also chosen for aerosol sampling. In addition, samples were also collected from various micro-environments over the big city (Ahmedabad) of western India. All the sampling locations are depicted in Fig. 2.1.

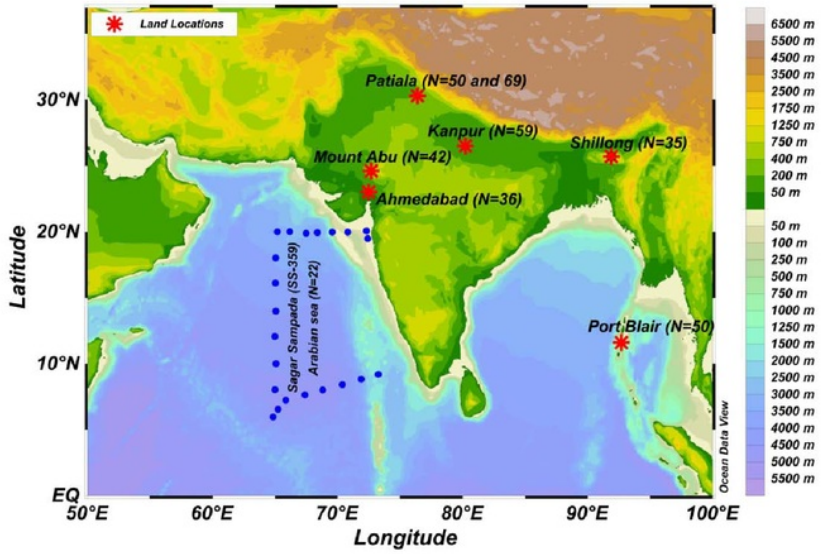

Figure 2. 1. *Map showing geographical locations of sampling sites over different regions over India. Color bar represents topography (i.e. height of locations above/below mean sea level).*

2.3.1. The Indo-Gangetic Plain (IGP)

The Indo-Gangetic Plain is also known as the Indus-Ganga Plain and the North Indian River Plain. It is a 630 million acre fertile plain covering most of northern and eastern India, the eastern parts of Pakistan, virtually all of Bangladesh and southern plains of Nepal. The region is named after the Indus and the Ganges

rivers and encompasses a number of large urban areas. The IGP is adjacent to the unique topography with the Himalayan range of mountains to the north and hills to the south. On regional scale, IGP spread over northern India receives large amount of air pollutants due to various anthropogenic activities such as emissions from vehicles, industries, large-scale post-harvest biomass burning (BB), and bio-fuel burning, which result into deterioration of air quality.

2.2.2.1. Patiala: A semi-urban site situated in the upper IGP

The sampling was carried out at ~ 250 m above mean sea level (amsl) at terrace of the Physics department, Punjabi University, Patiala, Punjab (30.2 ºN and 76.3 ºE). Punjab province is a part of northern IGP, which is known for agriculture and farming. The site is surrounded by agriculture fields (nearest distance ~ 1 km). Roughly, 84% of the land of the state is being used for farming (Singh et al., 2014). The site is also surrounded by thermal power plants and big industries (in and around Ludhiana, Amritsar, and Lahore (Pakistan) in the northwest direction) within 200 km. Post-monsoon period, i.e. October and November months, is influenced by enhanced level of carbonaceous aerosol and pollutants concentration due to large scale post-harvest paddy-residue burning over this site. Patiala is associated with shallower boundary level and thus highly influenced by frequent fog events during January and December months (i.e. winter). Emissions from bio-fuel (Cowdung cake, Shisham, Babool etc.) and fossil fuel burning (FFB) largely influence the study region during winter. More details of the sampling site can be found in Patel and Rastogi, (2018a).

To assess the $PM_{2.5}$ (particulate matter with aerodynamic diameter less than or equal to 10 μm) chemical composition along with their OP, day and night pair samples were collected on tissuquartz filters using high volume sampler (flow rate: 1.13 m^3 min^{-1}). Sampling was carried out on tissuquartz filters (PALLFLEX, 2500QAT-UP, 20 cm × 25 cm) on daily basis during winter (10th January to 3rd February, 2014, n = 50) and post-monsoon (11th October to 15th November, 2014, n = 69). Average daytime and nighttime temperature (T) and relative humidity (RH) during post-monsoon months were 28.9°C and 22°C, and 48% and 63%, respectively, whereas those during winter months were 18°C and 10°C, and 63% and 91%, respectively.

2.2.2.2. Kanpur: an urban site in the middle of IGP

Nestling on the banks of the eternal Ganga, Kanpur stands as one of North India's major industrial centers with its own historical, religious and commercial importance with a population of ~ 3.0 million. Kanpur lies in the central IGP, which witness extremes of temperature. It can drop to a minimum of 0°C in the winters whereas it can rise up to 48°C in summers. Kanpur experiences severe fog in December and January months whereas; excessive dry heat is accompanied by dust storms during in summer months. Kanpur has been a major hub of leather, pharmaceutical, textiles, chemicals and steel industries. Emissions from vehicles, biofuel, wood and coal burning, industrial activities, brick kilns, and thermal power plant plumes over Kanpur contributes to fine aerosol loading which make its air quality worst. During winter, regional BB is among the major contributors to aerosol loadings at this location.

$PM_{2.5}$ sampling had been carried out on daily basis (24 hours integrated) at a site located on the campus of Indian Institute of Technology, Kanpur (26.5 °N, 80.3 °E; 142 m amsl) during the 20th of December, 2015 to the 6th of February, 2016. A total of 59 samples were collected on tissuquartz filters (PALLFLEX, 2500QAT-UP, 20 cm × 25 cm) using high volume sampler (flow rate: 1.13 m^3 min^{-1}). The study period witnessed several severe fog conditions with high RH (up to 100%) and low temperature conditions (lowest temperature: approximately 4 °C).

2.2.2.3. Shillong: a high altitude site in the lower IGP

Shillong is situated in the foot-hills of the north-east Himalayas (NE-H). Being a hill station in the lower IGP, Shillong appears ideal to monitor the transformation of aerosol during long-range transport of pollutants from the upwind regions of IGP and south-east Asia. Local bio-fuel burning is often observed in Shillong.

The sampling was carried out at Barapani (25.7 °N, 91.9 °E; 1064 m amsl), situated ~20 km upwind of the Shillong main town. A total of 35 $PM_{2.5}$ samples were collected every 3rd day (24 hours integrated) on tissuquartz filters (PALLFLEX, 2500QAT-UP, 20 cm × 25 cm) using high volume sampler (flow rate: 1.13 m^3 min^{-1})

during 11th of January, 2017 to 21st of April, 2017. The sampler was kept at ~10 m height inside the campus of North-East Space Application Center (NE-SAC).

2.3.2. Remote locations

2.2.2.1. Mount Abu: a high altitude site in western India

The geographic location of sampling site "Guru Shikhar" in Mount Abu (hereafter Mt. Abu, 24.6 ºN, 72.7 ºE, 1680 amsl) is the highest peak of the Aravalli range of mountains. The Thar Desert and the Arabian Sea are located ~300 km northwest and ~400 km southwest of Mt. Abu, respectively. The wind pattern shows a typical contrast between May-August (strong southwesterlies) and November-February (weak northeasterly winds). Air-masses during southwest monsoon bring substantial moisture and clean air from Arabian Sea in contrast to continental air-masses from the northeast which bring pollutants to sampling site through long-range transport. More details of the sampling site can be found in Patel and Rastogi, (2018b). Apart from these, site also experiences free tropospheric conditions during December-January) winter months due to lower boundary layer height. Mt. Abu is therefore an ideal choice for monitoring regional air quality over western India. Precipitation occurs during July to September which roughly averages around 600 mm rainfall every year (SW-monsoon).

A total of 42 PM_{10} samples were selected from the 100 samples which collected weekly over the period of two years (10th March 2014 to 25th May 2016, 48 hours integrated sampling for each sample) on tissuquartz filters (PALLFLEX, 47 mm) using low volume sampler (Envirotech APM 550, flow rate 1.0 m^3 hr^{-1}). Sampling during monsoon period (mid July to September) was not carried out due to logistic issues.

2.2.2.2. Marine atmospheric boundary layer

The Arabian Sea

Long-range transport of aerosol and aging processes such as heterogeneous reaction, condensation, coagulation, evaporation, aggregation, oxidation and reduction in the air can alter their physicochemical properties. Continental transport

of nutrients may affect ocean productivity through wet/dry deposition. Land-locked by three sides, the Arabian Sea is an ideal place to study of continental aerosol transported to marine environment.

A total of 22 atmospheric PM_{10} samples (integration time: 10 to 18 hours) were collected onboard ORV Sagar Sampada (SS#359) on tissuquartz filters (PALLFLEX, 2500QAT-UP, 20 cm × 25 cm) while sailing over the Arabian Sea (Fig. 1). Air temperature (T) and relative humidity (RH) during the cruise varied from 26.4 to 31.9°C, and 66 to 85%, respectively. Prevailing winds were westerly, and weak (varied from 5 – 19 km h^{-1}) during initial period but became relatively intense (varied from 16 – 26 km h^{-1}) during the latter period of cruise.

Port Blair (Bay of Bengal)

Port Blair (PBR) is the administrative capital of the Andaman and Nicobar Islands, a union territory of India situated in the Bay of Bengal (BoB), which is confined by land from three sides. It is home to more than one lakh people. PBR is situated at a distance of 1300 km from the Indian mainland West Bengal, the lower part of the IGP. Southern part of PBR encompasses forests and mangroves. PBR has several thousand automobiles, an airport, and a port, and hence a fair amount of local anthropogenic activity.

A high volume sampler (flow rate: 1.13 m^3 min^{-1}) was deployed on the terrace of ISTRAC (Indian Space Research Organizations Telemetry, Tracking and Command Network, 11.62 ºN, 92.72 ºE) building, 60 m amsl. A total of 50 PM_{10} samples were collected on daily basis (24 hours integrated) on tissuquartz filters (PALLFLEX, 2500QAT-UP, 20 cm × 25 cm) using high volume sampler (flow rate: 1.13 m^3 min^{-1}) during February to April months of 2013. During these months, study site receives anthropogenic aerosol transported mainly from the IGP-India and Southeast Asia.

2.3.3. Micro-environments

2.2.3.1. Ahmedabad: a big urban site in the western India

Ahmedabad (23.0 ºN, 72.6 ºE, 49 amsl) is the 7th largest mega city of India with a population of about 6.3 million. It is located in western India. The Thar Desert and the Arabian Sea are situated ~500 km northwest ~100 km southwest direction respectively Thus, it receives both natural and anthropogenic aerosol under tropical conditions, which makes it a great natural laboratory for aerosol studies. Days of May and June months (summer) over Ahmedabad often experiences ~ 47°C.

A total of 36 PM_{10} samples were collected (24 hours integrated sampling) on tissuquartz filters using a high volume air sampler (flow rate: 1.13 m^3 min^{-1}) in parallel over five different micro-environments over Ahmedabad (i.e. Bapunagar, Narol, Paldi, Income Tax and Science City) with a weekly frequency during May to June, 2017. Here, the Bapunagar, Paldi and Science city are residential zones in different parts of Ahmedabad. Income Tax is a big commercial zone with heavy traffic. Narol is an industrial site (i.e., Textiles, Dye, Printing, etc.) with unpaved Gujarat Industrial Development Corporation (GIDC) inter-connecting road (i.e., Industrial Zone) and nearby (~7 kms) Pirana dumping site.

2.3. Aerosol Sampling

2.3.1. Description of air samplers

High volume air sampler (Fig. 2.2a) with mass flow control is capable of 24-hour continuous sampling of $PM_{2.5}$, PM_{10} or total suspended particulate (TSP). They feature a high speed motor, durable all-weather shelter and ruggedized electronic components for accurate sampling. During the sampling, it is essential to clean the pistons inside the high volume samplers regularly otherwise, they may get chocked and affect efficient sampling. Similarly, the teflon ring used during $PM_{2.5}$ sampling needs cleaning on regular basis followed by application of fresh silicon oil/Grease.

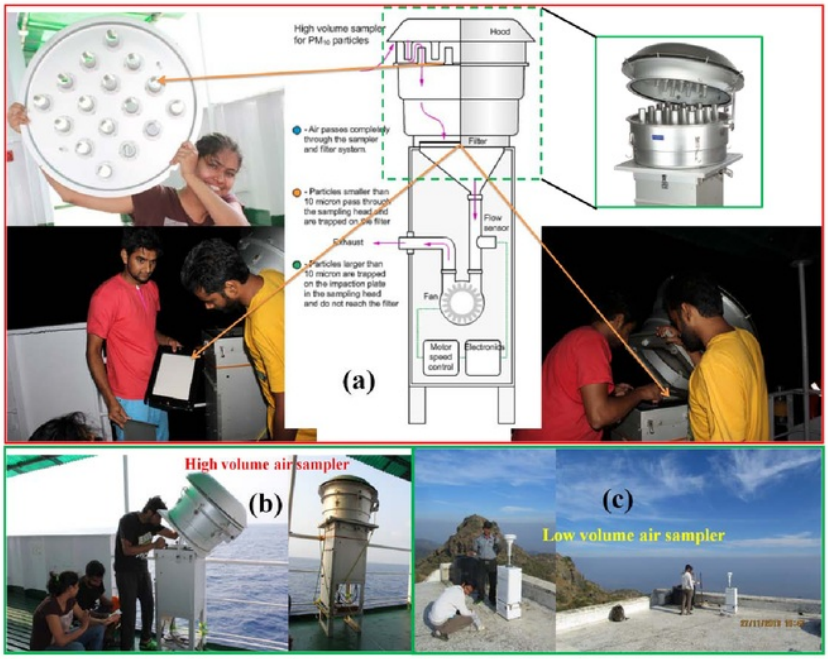

Figure 2. 2. *A pictorial view of different parts of air sampler during some of the campaigns; (a) shows the schematic of sampler, whereas, (b) and (c) shows the preparation of sampling using high volume air sampler (over the Arabian Sea) and low volume air samplers (over the Mount Abu), respectively.*

Aerosol sampling at each of the above mentioned strategically locate sites was carried out using high (Thermo) and low (Environtech) volume air samplers. Sampling was performed on pre-combusted (~ 400°C) tissuquartz filters (PALLFLEX, 2500QAT-UP, 20 cm × 25 cm) over all the sites except that for Mt. Abu. For Mt. Abu, sampling was performed on 47 mm diameter circular pre-baked tissuquartz filters (PALLFLEX, 2500QAT-UP). Pre-combustion at such high temperature was performed to reduce the blank content, e.g. volatile organic compounds (VOCs). The flow rates of high and low volume samplers were calibrated before and after sampling period and found to be within the uncertainty of 5%. Sample filters were stored in deep freezer (~ -20°C) immediately after collection.

2.4. Chemical analysis

2.4.1. Analytical strategy

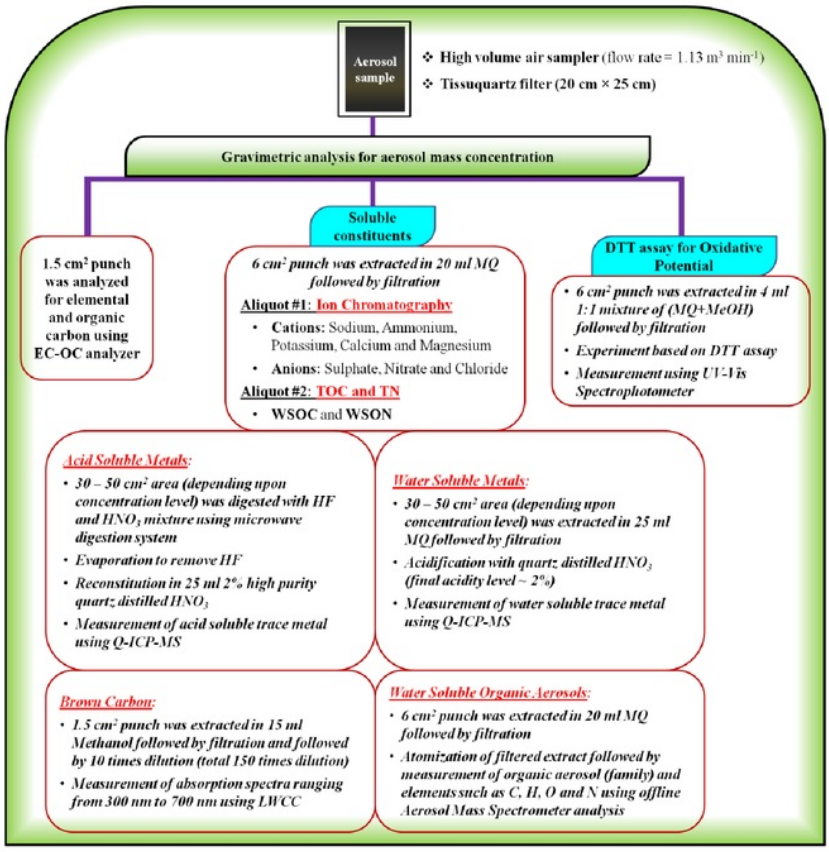

Figure 2. 3. *Analytical scheme for chemical analysis of aerosol samples.*

2.4.2. Gravimetric analysis for aerosol mass concentration

Filters were kept for 24 h equilibration at a RH of ~ 40–45% and T of ~ 23–25 °C before and after aerosol loading followed by weighing using high precision balance (Sartorius, model LA130S-F, accuracy: ±0.1 mg). The subtraction product (pre-weight minus post-weight, usually aerosol mass in µg) of each sample was then

normalized with respective air volume (m^3) filtered during sampling hours to get ambient aerosol mass concentration (i.e. $\mu g\ m^{-3}$).

2.4.3. Elemental Carbon and Organic Carbon

Elemental carbon (EC) and organic carbon (OC) were quantified using EC-OC analyzer (Model, 2000; Sunset Laboratory, USA) with temperature cycle as per National Institute for Occupational Safety and Health 5040 (NIOSH)-5040 thermal optical transmittance (TOT) protocol (Rastogi and Sarin, 2009, Rajput et al., 2011, Rastogi et al., 2014).

EC-OC analyzer consist of four components: sample oven, oxidizer (manganese dioxide, MnO_2), methanator, and detector (Birch and Cary, 1996).

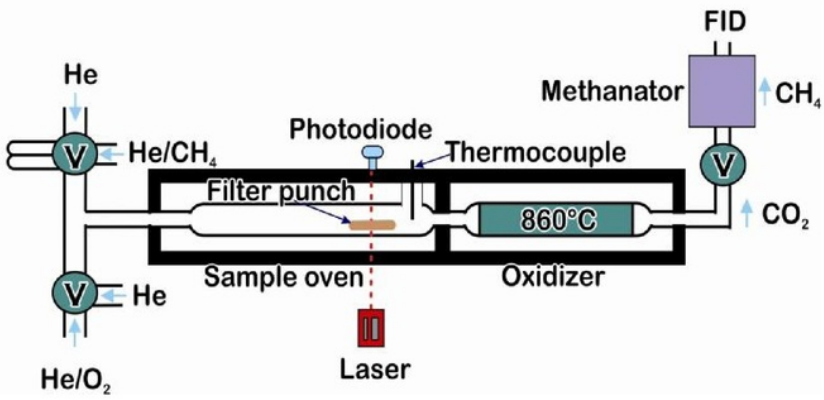

Figure 2. 4. *Schematic for thermo-optical EC-OC analyzer, adopted from Sunset Laboratory Manual.*

A known rectangular area punch (1.5 cm^2) of aerosol sample is kept on a quartz boat and placed inside the front oven (i.e. sample oven). EC and OC fraction deposited on filter area are quantified in two stage manners.

During the first stage, volatilization of OC is occurred in inert atmosphere (100% He) when front oven undergo step-wise heating from room temperature to 310 °C for 80 s, 310 °C to 475 °C for 60 s, 475 °C to 615 °C for 60 s, 615 °C to 870 °C for 60 s. All volatilized products are then sent to MnO_2 oxidizer unit (860 °C) where OC fractions are quantitatively converted to CO_2 gas.

In second stage, the oven is cooled to below 550 °C for 60 s. Hereafter, the atmosphere is changed from inert to oxidized (i.e. a mixture of oxygen (10% O_2) and helium gas (90% He, vol/vol)). Front oven temperature is then increased step-wise from 550 °C to 625 °C for 45 s, 625 °C to 700 °C for 45 s, 700 °C to 775 °C for 45 s, 775 °C to 850 °C for 45 s, and 850 °C to 900 °C for 120 s. Evolved EC fractions are then sent to oxidizer in the same manner as OC fractions.

Oxidized products of evolved fraction of OC and EC in step-wise manners (i.e. CO_2) go to methanator. Here, CO_2 is swept out of the MnO_2 oxidizing oven in the helium stream, mixed with hydrogen gas and passed through a heated nickel catalyst where they reduced to CH_4 and subsequently quantified in flame ionization detector (FID). A fixed volume of methane (5% methane in Helium as an internal standard) is being injected at the last of each run to monitor the efficiency of FID. A known concentration (20 µg) of sucrose, an external standard, is used frequently during the analysis to maintain the data quality.

EC-OC analyzer for thermal optical transmittance (TOT) protocol uses He-Ne laser of 678 nm wavelength to correct the pyrolyzed carbon. Initial transmittance is attributed to actual EC fraction and is recorded during each run. During analysis of OC, a fraction of OC gets pyrolysis due to higher temperature and inert atmosphere. At this point, transmittance decreases as pyrolyzed carbon (PC) also absorbs (acts as EC). Hereafter, by converting the atmosphere from inert to oxidizing, EC and PC get oxidized and, the point when transmittance reaches to its initial value is described as split point between OC and EC. Hence, PC which does not evolve in the first stage is not a part of EC but actually of OC. Therefore, OC = OC1 + OC2 + OC3 + OC4 + PC and EC = PC + EC1 + EC2 + EC3 + EC4 + EC5 + EC6 - PC.

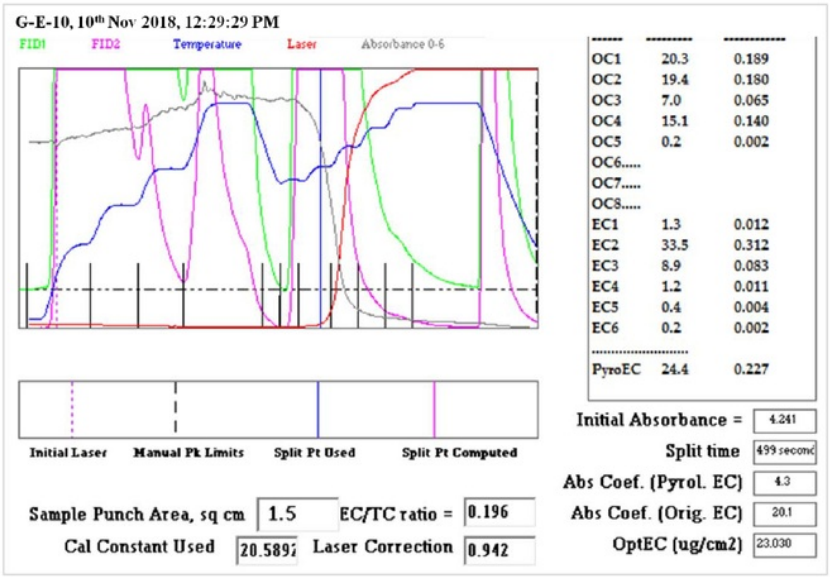

Figure 2. 5. *A typical thermogram of a sample analyzed on thermo optical EC-OC analyzer.*

Various blank filters were also analyzed in the same manner as samples (Table 1) and reported OC and EC data are blank corrected. About 20% of samples were repeated to ascertain analytical precision and is found to be within ±5% for both OC and EC.

2.4.4. Water Soluble Organic Carbon

A known filter punch (usually 6 cm^2) of aerosol sample was extracted in Milli-Q (MQ) water (specific resistivity≥ 18.2 MΩ) using repeated ultrasonication for 30 min (3 × 10 min cycle) in pre-cleaned polypropylene vial and subsequently, filtered with tissuquartz filters (25 mm, pore size 0.45 µm) followed by quantification of water soluble organic carbon (WSOC) fraction using a total organic carbon analyzer (TOC, Shimadzu, model TOC-L CPH). As per the optimized analytical procedure in our lab, 50 µl of each filtered extract is introduced to TOC analyzer using auto-sampler (Shimadzu, model ASI-L), then acidified using 5% HCl and sparged (sparge gas and flow: 80 ml zero air, sparge time: 1.0 minute) to remove inorganic carbon (IC, generally carbonates/bi-carbonates are escaped in the form of

CO_2). Sample extract minus IC is then injected inside the combustion tube (kept at 680 °C) where it get oxidized to CO_2 by Platinum catalyst (Pt-Al_2O_3). The evolved CO_2 is then carried using carrier gas (i.e. zero air) to non-dispersive infrared (NDIR) detector for the quantification of carbon content (i.e. non-purgeable organic carbon (NPOC)). Specifically, the technique uses high purity gas (zero air, purity 99.9%) for sparging the acidified sample to eliminate IC fraction. Thus the obtained quantity of NPOC is also generally called as WSOC. The analyzer measures absorption at 4.3 μm (CO_2 absorb strongly) according to Lambert-Beer's law using non-dispersive method, i.e. IR is not spectrally dispersed.

Various standards are diluted from the 1000 mgC/L stock solution (made using potassium hydrogen phthalate, KHP in MQ) for the instrument calibration. Several blanks were run in the same way as sample and were subtracted from each sample. ~ 20% of samples were repeated to ascertain analytical precision and is found to be within ±5%.

2.4.5. Water Soluble Organic Nitrogen

Total nitrogen monitor (Shimadzu, model TNM-L ROHS) is assembled with TOC-L. Both the measurements (i.e. WSOC and total nitrogen, TN) are performed simultaneously. Here, total nitrogen compounds are decomposed at a high temperature (~ 680 °C) and oxidized using platinum as a catalyst (Pt-Al_2O_3) to nitric oxide (NO), and subsequently detected by chemiluminescence detector. The measured quantity is nothing but the total soluble nitrogen. Water soluble organic nitrogen (WSON) is obtained by subtracting the water soluble inorganic nitrogen (WSIN, i.e. $N-NH_4^+ + N-NO_3^-$) from TN.

Standards for TN are suitably diluted from 1000 mg/L high purity analytical grade KNO_3 (stock solution made in MQ water) for instrument calibration.

2.3.2.1.1. Water Soluble Inorganic Species using Ion Chromatography:

Filtered extract (details are given above) was further analyzed in Ion Chromatograph (IC, Model DIONEX ICS-5000 DC-5) for the quantification of water

soluble inorganic species (WSIS, also called as major ions). IC has four components; auto sampler, ion exchange column, suppressor and detector. Here, a mixture of major ions (such as anions: {sulphate [SO_4^{2-}], nitrate [NO_3^-] chloride [Cl^-]}, and cations: {sodium [Na^+], ammonium [NH_4^+], potassium [K^+], calcium [Ca^{2+}] and magnesium [Mg^{2+}]}) present in water extract of sample interact with stationary and mobile phase that further result in the separation of each ions. Stationary phase is bound inside the cation column (Dionex IonPac^{TM} CS16, 5 × 250 mm) and anion column (Dionex IonPac^{TM} AS23, 4 × 250 mm). Whereas, mobile phase, 30 mM methyl sulphonic acid (MSA) for cation and a mixture of 4.5 mM carbonate + 0.8 mM bi-carbonate solutions for anions are passed through cations and anion column respectively. Mobile phase carries ~ 25 – 100 µl sample (injection volume is selected depending upon concentration) and each ion is further eluted from the columns based on retention time. The mobile phase carries these eluted ions to suppressor followed by the quantification in conductivity detector (Thermo Scientific, P/N 061830). The function of suppressor is to reduce the background of eluent and to increase the sensitivity for the sample ions. Measurement of cations and anions are done simultaneously.

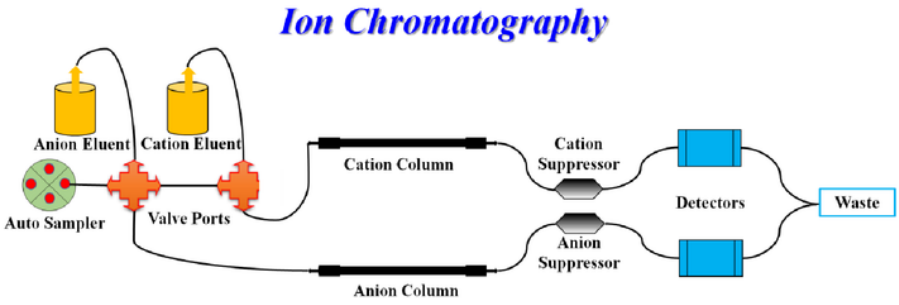

Figure 2. 6. *Schematic for Ion Chromatography.*

In optimized protocol of our lab, 1000 mg/L stock solution of each cation (using high purity analytical grade $NaNO_2$, $(NH_4)_2SO_4$, KNO_3 $CaCl_2.2H_2O$ and Mg metal, Merck) were made. Mixed standards were made by suitably dilution of stock solutions for the instrument calibration for cations. For anions, anion multi element

standard II (1000 mg/L in H_2O, HC409399, Merck) was used by suitable dilution for the instrument calibration.

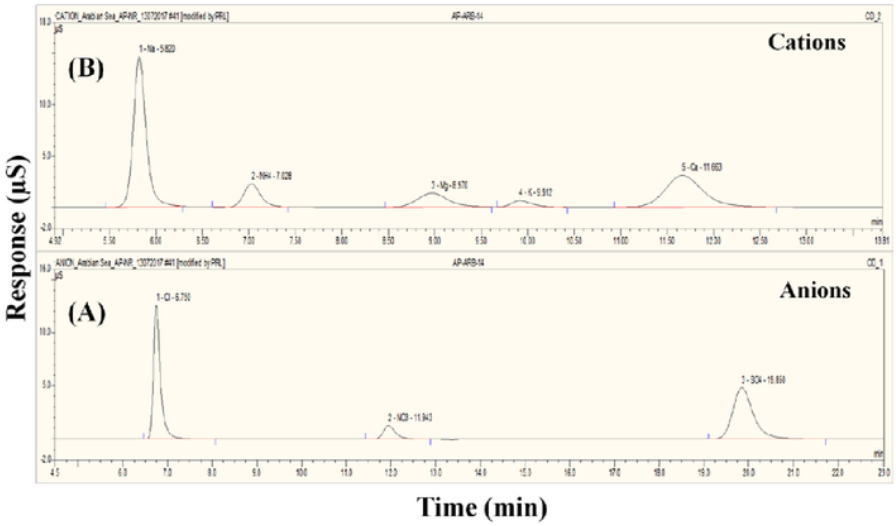

Figure 2. 7. *Typical chromatogram for (A) Anions and (B) Cations.*

2.4.6. Metals using Q-ICP-MS

Quadrupole inductively coupled plasma mass spectrometer (Q-ICP-MS, Thermo-X series) is used to quantify trace level (as low as ng/L) metal content (such as Li, Be, B, Al, Ti, V, Cr, Mn, Fe, Co, Ni, Cu, Zn, Ga, As, Se, Kr, Sr, Mo, Ag, Cd, Se, Sb, Ba, Pb, etc) present in sample. Among all the study sites described above, aerosol samples from Patiala (January 2014) and Ahmedabad sites were quantified for total content of each metals using acid digestion method. Whereas, samples collected from Patiala (October-November 2015), Kanpur, Shillong and Arabian sea sites were quantified for water-soluble fraction of each metals by leaching aerosol samples in MQ water.

For the complete digestion, punch of 30 – 50 cm^2 area (depending upon concentration level) of each sample was digested with HF and HNO_3 mixture using microwave digestion system (Start D, Milestone). Digested samples were further evaporated to remove HF, and then reconstituted in 2% high purity quartz distilled HNO_3 (Merck). Removal of HF is indeed necessary as it can react with the quartz

material (part of ICP-MS instruments). Generally, nitrate salts of metals are soluble and hence HNO_3 was used to digest samples.

For water-soluble content of metals, 30 – 50 cm^2 punch (depending upon concentration level) of each samples were extracted in MQ using repeated ultrasonication for 30 min (3 × 10 min cycle) in polypropylene sample vials. These extracts were then filtered with tissuquartz filters (25 mm, pore size 0.45 μm) to remove insoluble fraction. Filtered extracts were then acidified using high purity quartz distilled HNO_3 (final acidity level ~ 2%).

Generally, mass spectrometers are comprised of three parts: ion source, mass separation device and the detector. Our laboratory has multi-element trace element analysis technique, i.e. Q-ICP-MS, with Argon (Ar) plasma as a source for ionization, quadrupole for mass separation device and dual-stage discrete dynode electron multipliers as detector. The sample (in liquid form) is introduced through nebulizer, where it is converted into a fine aerosol mist using a stream of Ar gas. Sample aerosol is then rapidly dried, dissociated, atomized and ionized into the central region of the plasma (6500 K). The quadrupole mass analyzer then filters out non-analyte, matrix, and interfering ions, allowing only desired analyte ions of a single mass-to-charge ratio (m/z) to be transmitted to the detector. The detector receives and amplifies an ion signal that is proportional to concentration, as determined through calibration.

For instrument calibration, standards of different known concentrations have been diluted from 23 multi elements stock solution (i.e. 1000 mg/L, Merck). Sample runs were bracketed by external laboratory calibration standards and certified United States Geological Survey (USGS) standard reference material (W1-basalt) that had yielded an external precision of ~10%. For drift correction, internal standard (^{115}In) was used. Several blank filters were also measured in the same way as samples and reported values in this study are corrected for blank. Analyses of several samples were repeated and found to be within 5%.

2.4.7. Brown Carbon using LWCC

Mostly methanol (MeOH) is used for extraction of various polar organic compounds but certain group of non-polar organic compounds are also fairly soluble in MeOH (Verma et al., 2012), if not completely soluble (described below with full details). Further a recent study showed that 85% of organic aerosol can be extracted using MeOH. For this reason, we chose MeOH as a solvent to get the information of organic chromophores, Brown Carbon (BrC), based on absorption spectra. In general, BrC is expressed as their absorption coefficient in UV region (b_{abs}, i.e. 365 nm), nevertheless, other chromophore may peak at different wavelengths (Satish et al., 2017). With this information in mind, 1.5 cm^2 punches (depending upon concentration level) from each aerosol samples were extracted in MeOH using ultrasonication for 30 min (3 × 10 min cycle). Extracts were further introduced into liquid waveguide capillary cell (LWCC, World Precision Instrument, Sarasota, FL, 2m path length (l)) through Acrodisc syringe filters (with GHP membrane, 0.45 µm, 25 mm) to remove insoluble particles including BC and dust. This LWCC was coupled to a portable UV-Vis spectrophotometer (Model, USB-4000) along with Deuterium and Tungsten Halogen lamps (DT-Mini-2, Ocean Optics). The high resolution absorption spectra were saved from 300 nm to 700 nm wavelengths for each filtered extract. Reference spectrum was employed with MeOH to remove any artifacts from solvent. For detailed analytical protocol for the measurement of BrC, reference is made to Satish and Rastogi, 2019.

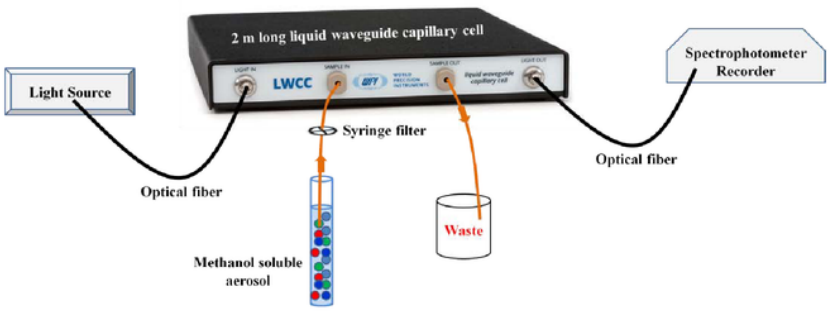

Figure 2. 8. *A schematic representation of BrC measurement.*

Absorption coefficient at given wavelength (b_{abs_λ}) was quantified as follows:

$$b_{abs\_\lambda} = (A_{\lambda} - A_{700}) \times V_{extract} \times \left(\frac{\text{Total filter area}}{\text{Area of filter aliquot used}}\right) \times \left(\frac{\ln(10)}{Va \times l}\right) Mm^{-1} \ldots \ldots \ldots \text{Eq (1)}$$

Here, A_λ is the absorption at wavelength λ, and A_{700} is reference absorption (for base line drift correction) at wavelength 700 nm. $V_{extract}$ = volume (ml) of MeOH used for extraction. Va is a volume of air (in m^3) filtered during sampling hours and l is cell path length (2 m). In general, λ = 365 nm is used to characterize the BrC. It is because 365 nm is far enough from the UV region to avoid the interference from non-organic compounds such as Nitrate. Also humic (high molecular weight compounds) like substances (HULIS) absorb strongly at this wavelength (Hecobian et al., 2010). However, our purpose to record absorption spectra was to get the information about chromophores that are present in aerosol sample and its capability to generate ROS (if any). In present study, absorption coefficient at different wavelength (representative of chromophores) were measured and correlated with ROS generation capability.

2.4.8. Water Soluble Organic Aerosol using AMS

A water-soluble fraction of organic aerosol (OA) over five different locations in Ahmedabad have been measured using High Resolution Time of Flight Aerosol Mass Spectrometer (HR-ToF-AMS). In principle, it measures chemical composition (such as organic families, elements {C, H, O, N} and inorganic species) with desired time resolution in high sensitivity V mode (Rastogi et al., 2018; Singh et al., 2019).

For offline AMS analysis, a 6 cm^2 punch of aerosol sample was extracted in MQ followed by filtration through Acrodisc syringe filters (with GHP membrane, 0.45 µm, 25 mm) to remove insoluble particles. This extract was atomized via aerosol generator (Topas, ATM 226) continuously and directed to the AMS via silica gel drier (outlet RH = 20%) for 20 minute to get the aerosol characteristics of a given sample. Atomized aerosol is subjected to vaporization using heated tungsten surface (at 600 °C) in high vacuum (~ 10^{-8} Torr). Here, the volatile and semi-volatile contents of the aerosol flash vaporized followed by ionization via electron bombardment from AMS filament. This process is called hard electron impact (ionization energy = 70 eV) and almost all the organic molecules get fragmented by this process. Ionized fragments are then analyzed for their mass in Time of Flight mass spectrometry (ToF-MS). Ionization efficiency (IE), particle velocity and inlet flow calibrations were performed using established standard protocols (Canagaratna

et al., 2007). Obtained data were than processed using the standard AMS data analysis software – SeQUential Igor data RetRiEvaL (SQUIRREL) and Peak Integration by Key Analysis (PIKA) written in IGOR (Wavemetrics, Inc., Lake Oswego; Canagaratna et al., 2007), to obtain the mass concentrations of different organic aerosol families.

2.4.9. Black Carbon using Aethalometer

Semi-continuous measurements of Black carbon (BC) were also performed simultaneously using Aethalometer (model: AE-31, Magee Scientific, USA) with 5 min integration time at few of the above listed sites.

It monitors optical attenuation (absorbance) of light at seven wavelengths (370, 470, 520, 590, 660, 880 and 950 nm) with a typical half-width of 20 nm (Hansen, 2005). However, the measured mass concentration of BC at 880 nm is considered as the standard as it has maximum absorption at this wavelength. The principle of Aethalometer is to measure the change in attenuation of light passing through spot (where aerosol are continuously collected) on the filter for a given interval of time. Assuming BC is only absorbing component in the atmospheric aerosol, a linear relationship between BC mass concentration and the attenuation of light is used to determine the BC mass concentration (Snyder and Schauer, 2007). Aethalometer uses a constant attenuation cross section, i.e., 16.6 m^2 g^{-1}, to determine the BC mass concentration. The analytical uncertainty in BC measurements is about ± 2% (as reported in the manual).

2.4.10. Dithiothreitol (DTT) assay for oxidative potential

It is an established fact that redox active PM such as quinones, polycyclic aromatic hydrocarbons (PAHs), transition metals etc. can catalyze the ROS production process in human body through transferring an electron from biologically reducing enzyme such as reduced form of nicotinamide adenine dinucleotide phosphate (NADPH) to molecular oxygen (O_2). Several cell based and cell free methods are available to study ROS in vivo and in vitro (Cho et al., 2005; Godri et al., 2011; Venkatachari et al., 2005). In studies carried out during this Ph.D. work, a DTT assay, an acellular method, is used to measure the OP of soluble ambient PM,

where DTT mimics the biologically reducing enzymes (Cho et al., 2005; Li et al., 2009). DTT activity has been found to be well correlated with soluble organic compounds but, not with metals (Cho et al., 2005). In contrast, other study had shown some metals to be significant drivers for the observed DTT activity (Charrier and Anastasio, 2012). However, an important limitation of DTT assay is that it does not respond to all the compounds which have capability to generate ROS (or contribute to OP) (Cho et al., 2005; Venkatachari and Hopke, 2008; Hu et al., 2008; Charrier and Anastasio, 2012). At the same time, DTT assay is most widely used acellular assay because its response correlates well with biological markers like Heme oxygenase (HO-1) expression in cells (Li et al., 2003), and exhaled nitric oxide fraction in human subjects (Delfino et al., 2006).

In vitro OP of ambient PM was assessed using the DTT method described in Cho et al. (2005) and Charrier and Anastasio (2012) with slightly modified steps, where the use of trichloro acetic acid was avoided (Li et al., 2009; Eiguren-Fernandez et al., 2010; McWhinney et al., 2013, Patel and Rastogi, 2018a and b). A 6 cm^2 punch of PM sample filter was extracted using 4 ml 1:1 mixture of MeOH and MQ, followed by ultrasonication for 30 min (3 cycle, 10 min each). The use of (MeOH+MQ) mixture for extraction was decided based on the polarity index of MeOH (i.e. 5.1) and water (i.e. 10.2). Mostly MeOH is used for extraction of various polar organic compounds but certain group of non-polar organic compounds are also fairly soluble in MeOH (Verma et al., 2012), if not completely soluble. Water, on the other hand cannot dissolve non-polar compounds but can dissolve large fraction of polar compounds compared to MeOH (as per the polarity index). To attain the maximum soluble fraction of organics (for both polar as well as non-polar) present in PM, we have used mixture of MeOH and water. However, this mixture may not dissolve all the species, and therefore, the word 'soluble fraction' should be appropriate for the work carried out in this thesis. Subsequently, insoluble suspended particles were removed from the extract through filtration using 25 mm diameter tisssuquartz filter (0.45 µm pore size, PALLFLEX, 2500QAT-UP), and 0.25 ml of the filtered extract were incubated at 37 °C with 100 µM DTT made in 0.1 M (7.4 pH) phosphate buffer solution in an amber color glass vials (to avoid photochemical reactions). These vials were continuously shaken in water bath with shaker (LSB-

0155, Daihan Lab Tech). At various time intervals (such as 0, 10, 20 and 30 min), a known aliquot of reaction mixture was taken out from the vial and immediately reacted with 10 mM 5, 5′-dithiobis-2-nitrobenzoic acid (DTNB). The remaining DTT in this aliquot immediately converts DTNB to its yellow colored product i.e., 2-nitro-5-thiobenzoic acid (TNB), which is directly proportional to remaining DTT concentration in each vials. Subsequently, it was measured with UV-VIS spectrophotometer (UV-1800, Shimadzu) at 412 nm wavelength (Fig. 2.11x). TNB is stable for ~ 2 h at room temperature (Charrier and Anastasio, 2012; Li et al., 2009). The remaining DTT concentration was plotted as a function of time, and the linear DTT consumption rate (moles of DTT consumed per minute, also referred as oxidative potential (OP) or DTT activity) was calculated, which is proportional to the concentration of redox active PM species.

As per the optimized protocol in our lab for calibration of DTT assay, various standards of known concentrations were suitably diluted from 1M stock DTT solution (Merck) and were added to 10 mM DTNB. Subsequently, the developed yellow colored TNB was measured using UV-VIS spectrophotometer.

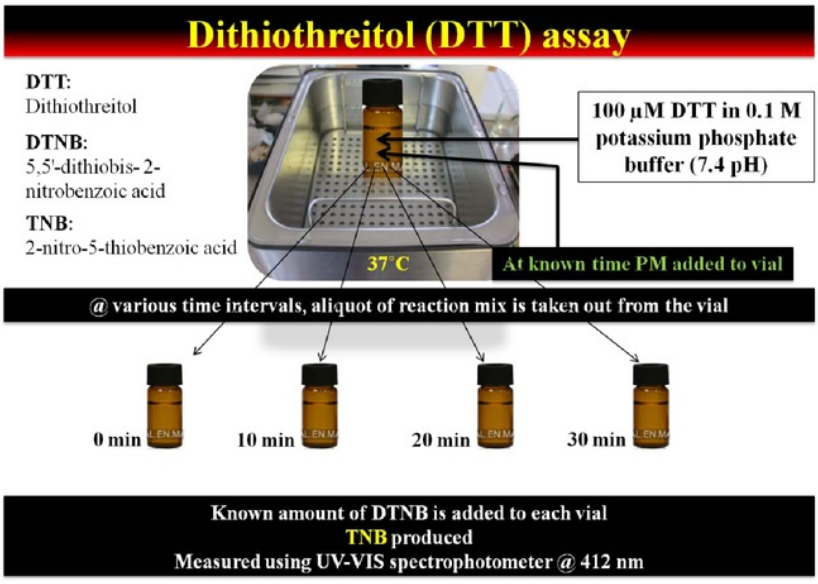

Figure 2. 9. *Schematic for Dithiothreitol assay.*

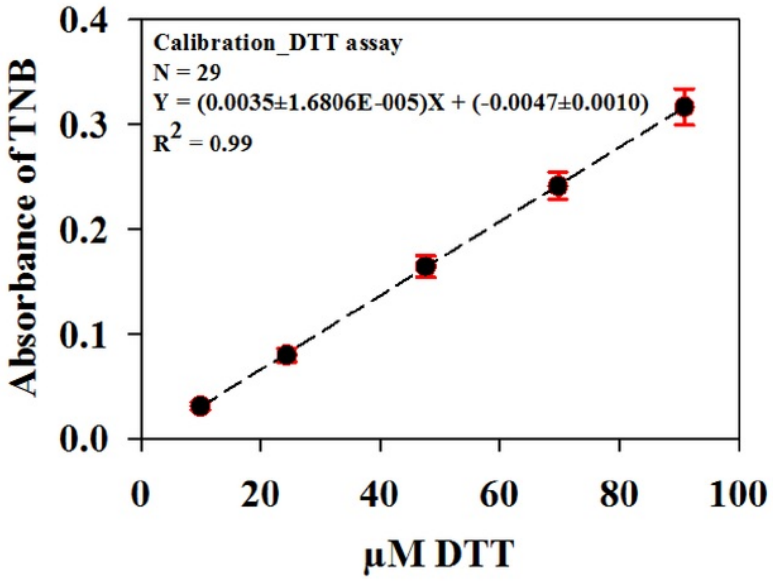

Figure 2. 10. *DTT assay calibration using UV-Vis spectrophotometer during the entire study period (i.e. 2015 to 2019).*

Reaction mechanism for DTT assay:

Step #1:

Step #1a: *It is demonstrated that the redox-active quinone can effectively catalyze the transfer of electrons from DTT to oxygen.*

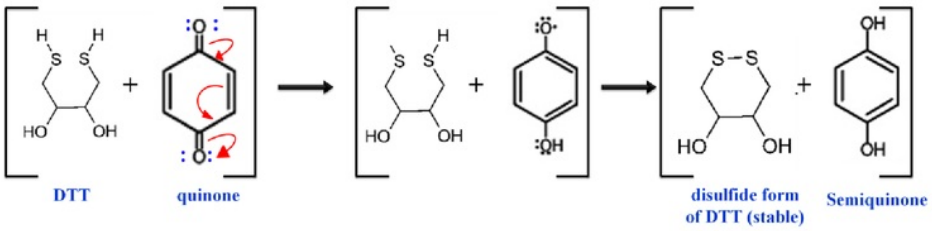

Step #1b: *In the simultaneous reaction with step #1a, generation of superoxide and hydrogen peroxide takes place.*

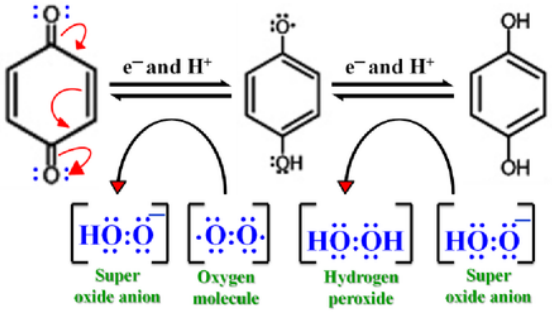

Step #2: *The thiol group (-SH, here DTT) are more reactive and immediately reacts with disulfide bond (~S-S~, here DTNB) and generate DTT-disulfide and TNB. DTT is reducing agent. Once oxidized, it forms stable six member ring.*

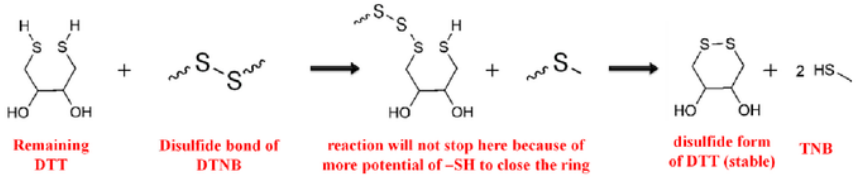

Despite of being present at very low concentration (i.e. ng m^{-3}), semi quinones are generally more damaging to cells as they can catalyze the generation of H_2O_2. It further converts to the most damaging ·OH radical through Fenton and Haber reactions. Quinone and semi quinone along with iron (Fe) present in PM may exceed the level of ROS. Hence, the activity of these redox active species needs to be measured.

To get the optimum pH for the DTT assay, Li et al., (2009) had performed an experiment with three reaction systems; i.e. DTT + Anthrone + DTNB, DTT + 1,4-Naphthoquinone (NQ) + DTNB and DTT + 9,10- Phenanthrenequinone (PQ) + DTNB, in the pH range of 3.8 – 11.0 (Fig. 2.11Y). They have found that almost 100% of DTT was transformed to DTT-Disulfide (or 100% TNB produced) by the catalyst 9,10-PQ, 40% by the catalyst 1,4-NQ, and 0% by Anthrone at pH ranging from 7.0 - 8.0. However, above pH 8.0, alkaline decomposition of DTNB was

occurred for all systems. Based on these results, we can use pH 7.3 for the DTT assay to obtain a highly sensitive, moderate catalytic redox reaction rate, which also agrees with human blood's pH (i.e. around 7.3).

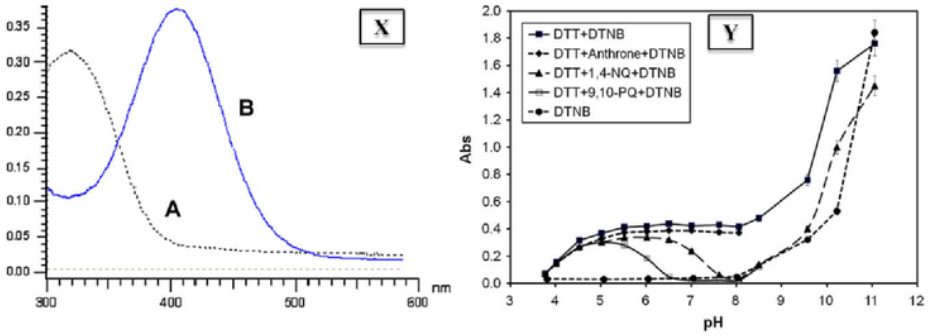

Figure 2. 11. *[X] shows UV–VIS absorption spectrum for A = DTNB and B = TNB. [y] shows the effect of pH on reaction between DTT and DTNB in presence of various catalysts. It is adopted from Li et al., (2009).*

Each batch of 5 samples was included with a blank (4 samples plus 1 blank) and the respective blank values were subtracted from measured DTT activity of each sample. To maintain the quality of data, all the samples and blanks were run in duplicates or triplicates and samples were not accepted until relative standard deviation (RSD) values of duplicates/triplicates were within 5%. Further to check the reproducibility of measurements, about 20% samples were repeated on different days and found to be consistent within 5–10%. Limit of detection (LoD, as per n = 84 blanks) for DTT assay is 0.27 µM DTT min^{-1}.

The validation of DTT assay was assessed by measuring the DTT consumption rate for a given standard and compared with the documented value (Charrier and Anastasio, 2012). Towards this, the consumption rate of DTT (100 µM initial concentration) in presence of 0.05 µM 9,10-Phenanthrenequinone (PQN) was measured and found to be 0.74 ± 0.10 µM DTT min^{-1} (n = 7). The measured slope is similar to that documented by Charrier and Anastasio (2012) (0.71 ± 0.09 µM DTT min^{-1}) for the same amount of PQN.

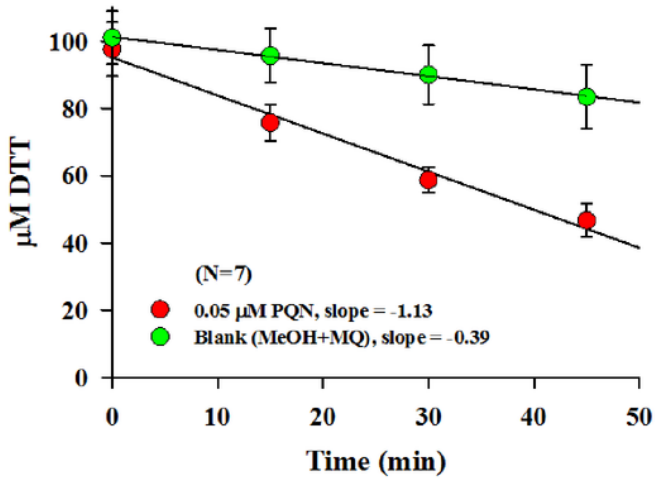

Figure 2. 12. *Validation of DTT assay in our lab. DTT consumption rate in presence of 0.05 µM 9,10-Phenanthrenequinone (PQN).*

2.5. Data quality

Table 2. 1. *Summary of average concentration and standard deviation of chemical constituents (µg/filter) present in blank tissuquartz filter (i.e. 400 square cm, including procedure blank) throughout the study period (2015 to 2019).*

Constituents	OC	EC	WSOC	TN	Na^+	NH_4^+	Mg^{2+}	K^+	Ca^{2+}	Cl^-	NO_3^-	SO_4^{2-}
Average	1535	659	253	34	4		4	3	4		1	8
SD	479	951	186	12	3		2	2	2		1	5

Water-soluble metals[#]																			
Metals	Li	B	Al	Cr	Mn	Fe	Co	Ni	Cu	Zn	Ga	Sr	Mo	Ag	Cd	Ba	Tl	Pb	Bi
Average	310	226	2057	281	305	903	300	62	189	275	329	221	85	394	41	411	243	296	199
SD	6	167	3073	16	66		3	49	213	538	6	28		56	2	136	5	20	10
Acid-soluble metals[‡]																			
Average		47	1493	18	10	246		13	3	20	2.1	5			0.9	37	0.5	2.5	0.1
SD		13	1187	14	8	197		6	3	12	0.4	4			0.3	26	0.5	2.1	0.4

[#]ng metal/filter

[‡]µg metal/filter

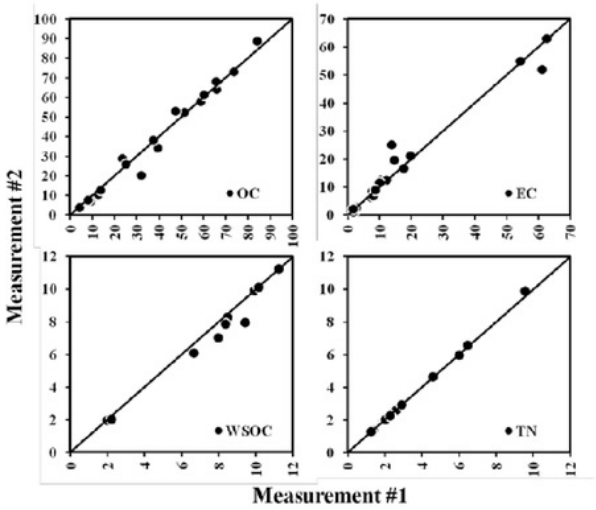

Figure 2. 13. *Repeat measurements of the OC and EC (µg/square cm filter), WSOC and TN (µg/ml) in aerosol samples. Solid line in each scatter plot represents 1:1 agreement between measurement #1 and #2.*

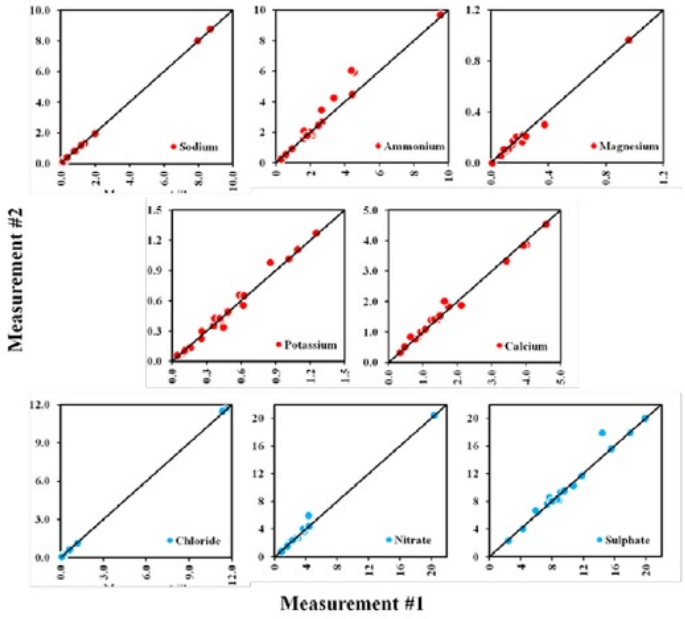

Figure 2. 14. *Repeat measurements of the major ions (µg/ml) in aerosol samples. Solid line in each scatter plot represents 1:1 agreement between measurement #1 and #2.*

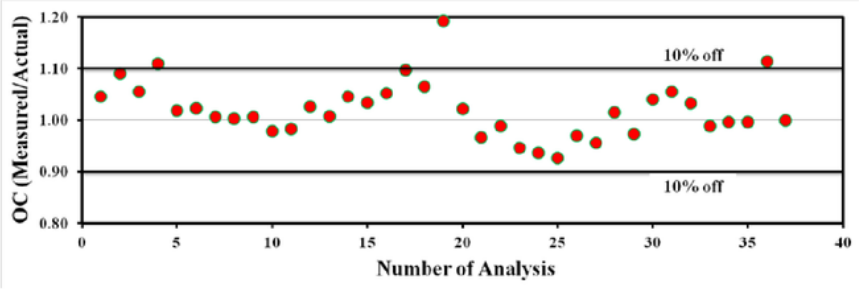

Figure 2. 15. *Analytical accuracy for OC using potassium hydrogen phthalate (KHP) standard on EC-OC analyzer.*

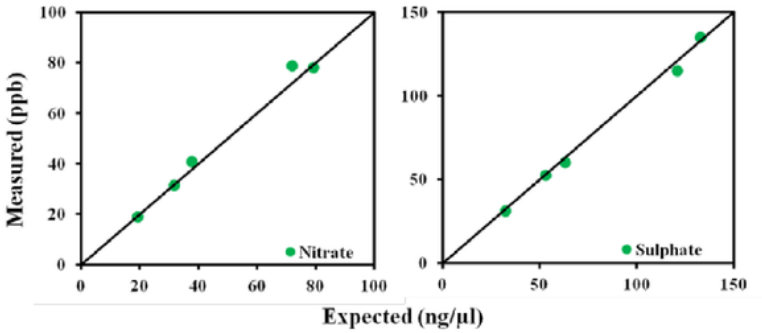

Figure 2. 16. *Validation of standards made in our laboratory (which is used for instrument calibration) as per the optimized protocol.*

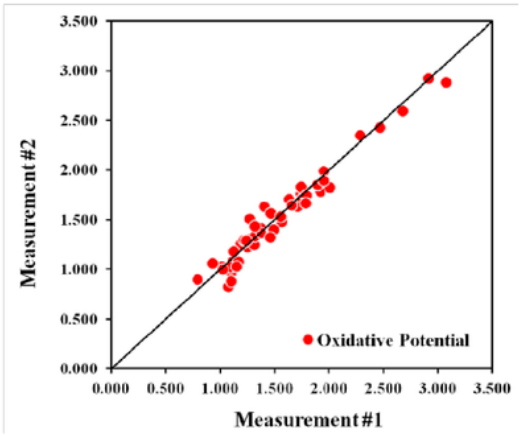

Figure 2. 17. *Repeat measurements of the oxidative potential (DTT consumed per min in presence of aerosol) in samples. Solid line in scatter plot represents 1:1 agreement between measurement #1 and #2.*

Chapter 3

OXIDATIVE POTENTIAL OF AMBIENT AEROSOL OVER THE INDO-GANGETIC PLAIN

This chapter briefs about the wintertime spatial variability of $PM_{2.5}$ chemical composition and their OP over upper (Patiala), middle (Kanpur), and lower regions (Shillong) of the Indo-Gangetic Plain (IGP). In addition, $PM_{2.5}$ sampling was also carried out during the autumn season over Patiala to infer the effect of emissions from intense biomass burning on aerosol OP. As the measured OP is only due to the soluble fraction of $PM_{2.5}$, results of this work can be considered as the lower limit of OP of $PM_{2.5}$ from the study regions.

3.1. Patiala: a semi-urban site located in the upper IGP

3.1.1. A case study during winter (representing aerosol from mixed sources)

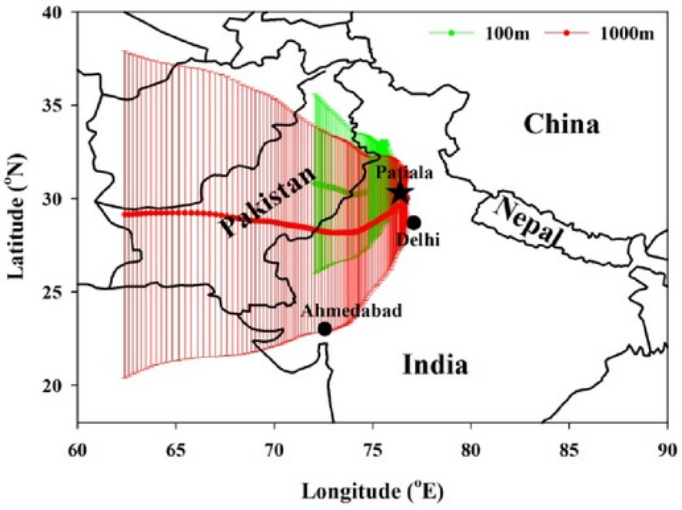

Figure 3. 1. *Map is showing sampling location Patiala with five day air mass back trajectories at two different altitudes (100 m and 1000 m) during the sampling period (January 10th to February 3rd, 2014, Patel and Rastogi, 2018a).*

3.1.1.1. $PM_{2.5}$ mass concentration and composition

Ambient $PM_{2.5}$ mass concentration varied from 59 to 312 μg m^{-3} (average: 150 ± 53, 1σ) with the highest value associated with the famous regional festival

"LOHRI" in Punjab. In this festival, widespread bonfires (source of particulates and gaseous species) are arranged in the night for gathering and celebration at several places throughout the state. Statistical data for ambient aerosol mass concentrations, carbonaceous aerosol (OC, EC and WSOC), water soluble inorganic species (WSIS, i.e., major ions such as SO_4^{2-},NO_3^-, Cl^-, Na^+, NH_4^+, K^+, $Ca^{2+}$and Mg^{2+}) and trace metals (Al, Mn, Fe, Ni, Cu, Zn and Pb) are presented in Table 3.1. Most of the measured constituents during "LOHRI" event exhibited more than double mass concentration than the average of rest of the samples. Further, BC_{370} also exhibited ~1.5 times higher mass concentration than BC_{880} during LOHRI which is attributed to emissions from bonfire. On average, $PM_{2.5}$ were composed of ~ 31% WSIS (estimated by adding the concentrations of all the measured cations and anions), ~ 37% organic matter (OM, from the measured concentration of OC), 5% EC, and ~ 1% trace metals; whereas, the remaining portion was unidentified (Rastogi et al., 2015).

3.1.1.2. Trace metals in $PM_{2.5}$

Trace metals concentrations in $PM_{2.5}$ over the study site were considerable and followed the order Zn > Al > Pb > Fe > Mn > Cu > Ni (Table 3.1). Metal concentrations were similar to those documented over IGP (Kulshrestha et al., 2009; Sudheer and Rengarajan, 2012 and references therein). To investigate the dominant source of trace metals (continental crust vis-à-vis anthropogenic activity) over the study region, enrichment factors (EFs) of Fe, Mn, Pb, Cu, Ni and Zn were estimated using equation (1) where Al is used as a reference element for upper continental crust (UCC) (Arimoto et al., 1989; Rastogi and Sarin, 2009).

$$EFx = (X/Al)_{aerosol} / (X/Al)_{UCC} \qquad (1)$$

A general understanding to infer estimated EF is that if it is close to unity, it indicates that the element (X) is primarily derived from UCC. Higher EFs values for a given trace element suggest its larger contribution from anthropogenic sources. The EFs values for Pb (range: 330 – 15780; average: 4030 ± 3900, 1σ), Cu (40 – 800; 200

± 180), Ni (30 – 300; 130 ± 68) and Zn (290 – 24900; 4730 ± 5720) suggest their predominant contribution from anthropogenic sources (Ntziachristos et al., 2007), whereas that for Fe (0.4 – 4.5; 1.2 ± 0.8) and Mn (3 – 35; 12 ± 9) suggest that the Fe and considerable portion of Mn in collected $PM_{2.5}$ were largely derived from UCC over the study region.

3.1.1.3. Oxidative potential of soluble $PM_{2.5}$

OP_V varied from 1.3 to 7.2 nmol DTT min^{-1} m^{-3} (3.8 ± 1.4), which is several times higher than those documented over different sites in USA (Hu et al., 2008; Ntziachristos et al., 2007; Verma et al., 2014), Europe (Perrone et al., 2016), and China (Liu et al., 2014) (Table 3.4). In Bangalore India, OP_V for the ambient particle is reported to be 0.79 ± 0.13 nmol DTT min^{-1} m^{-3} (Vreeland et al., 2016), which is significantly lower than that observed over Patiala. On the contrary, OP_M varied from 13 to 50 pmol DTT min^{-1} μg^{-1} (27 ± 8) over the study region, which is similar or somewhat lower than those observed over Orinda (Ntziachristos et al., 2007), Atlanta (Verma et al., 2014), and Los Angeles (Hu et al., 2008) (Table 3.4). The higher OP_V over the study site is attributed to higher $PM_{2.5}$ mass concentration over the study region in comparison to documented studies (Table 3.4). High $PM_{2.5}$ mass concentration is expected to have relatively high concentration of species with high OP, although they may or may not be in same proportion in each sample. Further, volume normalized OP during "LOHRI" was found almost double (7.2 nmol DTT min^{-1} m^{-3}) than the average of rest of the study period (3.7 nmol DTT min^{-1} m^{-3}). On the contrary, mass normalized OP was not influenced during this period, likely due to simultaneous increasing in DTT-inactive secondary inorganic aerosol (SIA) (discussed later in detail). Fig. 3.2 depicts the relationship of $PM_{2.5}$ mass concentration with OP_V and OP_M. Here, it is interesting to note that OP_V increased linearly with $PM_{2.5}$ mass concentration ($R = 0.66$, $p < 0.001$, Fig. 3.2a) whereas, OP_M exhibited large scatter with highly variable OP for similar $PM_{2.5}$ mass concentrations (Fig 3.2b). This observation suggests that OP depends more on $PM_{2.5}$ composition rather than its mass concentration. If OP_M is independent of composition, then it is

expected to remain unchanged with changing PM mass concentration, which is not the case. This observation has several implications. It suggests that documentation of OP_M is better representative of aerosol DTT activity. However, in terms of $PM_{2.5}$ dose reaching human respiratory system, use of OP_V is inevitable, as dose will depend on the volume of air inhaled by a person. There may be bias if one directly relates $PM_{2.5}$ mass concentrations with mortality, morbidity, risk factors for various diseases etc. over different regions and ignore particle composition, as often done in epidemiological studies (Pope and Dockery, 2006). However, extensive study is required to identify the best parameter (s) representing particle ROS generation capacity, which is PM mass at present. Furthermore, Table 3.1 shows that OP_V correlates well with several aerosol species on volume basis ($\mu g\ m^{-3}$) at considerable significance level ($p < 0.05$). It could be due to the fact that the sources of major aerosol components also produce DTT-active species in somewhat similar proportion. $PM_{2.5}$ mass concentration is found to be 3 – 10 times higher than the reported values over different sites in the world (Table 3.4), suggesting the people living in the IGP inhale more PM mass that can cause severe health problems. However, their effects are not yet assessed.

Table 3. 1. *Statistical data (range, average and standard deviation (±1σ)) of measured species concentrations (μg m^{-3}) in aerosol, and correlation coefficient (R) of volume and mass normalized species concentrations with OP_V and OP_M, respectively for daytime, nighttime, and all samples. Values marked in red and bold font are significant at $p < 0.05$.*

Constituents (n=48)	Min	Max	Avg	SD	Day (n=24)	Night (n=24)	All (n=48)	Day (n=24)	Night (n=24)	All (n=48)
					R with (OP_V)			R with (OP_M)		
$PM_{2.5}$	59	312	150	53	**0.51**	**0.77**	**0.66**	-	-	-
OP_V (nmol DTT min^{-1} m^{-3})	1.3	7.2	3.8	1.4	-	-	-	-	-	-
OP_M (pmol DTT min^{-1} μg^{-1})	13.1	49.6	26.6	8.4	-	-	-	-	-	-
OC	10.3	75.3	25.9	11.2	**0.54**	**0.76**	**0.68**	0.37	0.27	**0.31**
EC	3.0	16.9	7.4	2.7	**0.68**	**0.67**	**0.67**	**0.66**	**0.42**	**0.54**
WSOC	8.2	28.2	15.0	4.3	**0.54**	**0.69**	**0.60**	**0.54**	0.16	**0.29**
Cl^-	BDL#	10.8	1.7	1.8	**0.45**	**0.75**	**0.61**	-0.09	-0.04	0.01
NO_3^-	1.8	35.3	15.0	7.5	**0.40**	**0.75**	**0.61**	**-0.54**	-0.23	**-0.36**
SO_4^{2-}	4.4	32.1	17.6	7.2	0.24	**0.50**	**0.31**	**-0.62**	-0.34	**-0.45**
NH_4^+	3.2	21.4	11.5	4.7	0.29	**0.67**	**0.50**	**-0.61**	-0.36	**-0.49**
Na^+	BDL#	0.6	0.2	0.1	**0.45**	**0.77**	**0.65**	0.22	0.34	0.28
K^+	0.7	5.7	2.0	0.8	**0.55**	**0.71**	**0.65**	**0.45**	0.24	**0.36**
Mg^{+2}	BDL#	0.2	0.0	0.0	0.09	0.42	0.24	-0.14	0.30	0.07
Ca^{+2}	BDL#	0.3	0.1	0.1	0.42	0.55	0.49	0.07	0.06	0.05
BC_{370}	2.8	21.6	7.9	3.5	**0.71**	**0.73**	**0.68**	**0.69**	0.29	**0.40**
BC_{880}	2.6	16.2	7.8	2.9	**0.60**	**0.66**	**0.63**	0.37	0.21	0.27
Al*	BDL#	501	170	150	0.24	-0.10	0.09	**0.45**	0.32	**0.37**
Mn*	3	78	19	14	**0.60**	**0.49**	**0.52**	0.21	0.32	0.26
Fe*	26	380	129	72	**0.59**	0.36	**0.45**	0.36	0.35	**0.33**

Ni*	BDL[#]	17	6	4	**0.61**	0.33	**0.46**	**0.65**	**0.41**	**0.52**
Cu*	3	144	15	20	0.33	0.32	**0.29**	0.19	0.10	0.12
Zn*	58	6362	929	1119	**0.42**	**0.50**	**0.43**	-0.02	0.12	0.04
Pb*	16	1309	214	226	0.11	**0.61**	0.25	-0.22	0.11	-0.13

**Concentrations are in ng m^{-3}, [#]Below detection limit*

Table 3. 2. *Statistical data (range, average and standard deviation (±1σ)) of measured species concentrations (μg m^{-3}) and OP_V (nmol DTT min^{-1} m^{-3}) for the samples collected during daytime and during nighttime and day/night ratio.*

Volume-normalized	Day				Night				Day/Night Ratio			
	Min	Max	Avg	SD	Min	Max	Avg	SD	Min	Max	Avg	SD
$PM_{2.5}$	59	236	154	47	61.6	312.1	145.2	59.2	0.42	2.37	1.19	0.56
OP_V	1.9	6.7	3.8	1.3	1.3	7.2	3.8	1.5	0.39	1.77	1.03	0.34
OC	11.4	42.0	25.3	8.0	10.3	75.3	26.5	13.8	0.53	1.85	1.07	0.43
EC	3.0	10.5	7.2	2.0	3.0	16.9	7.6	3.2	0.36	1.76	1.06	0.44
WSOC	8.7	22.8	16.3	3.8	8.2	28.2	13.8	4.5	0.66	2.62	1.26	0.46
Cl^-	BDL[#]	4.1	1.0	0.9	0.5	10.8	2.3	2.3	0.13	2.85	0.86	0.80
NO_3^-	1.8	27.2	15.1	6.6	4.5	35.3	15.0	8.4	0.25	4.93	1.42	1.25
SO_4^{2-}	5.2	32.1	20.8	6.9	4.4	25.1	14.3	5.9	0.35	5.79	1.79	1.28
NH_4^+	3.4	20.6	12.4	4.4	3.2	21.4	10.6	5.0	0.33	5.26	1.55	1.27
Na^+	BDL[#]	0.4	0.2	0.1	0.0	0.6	0.2	0.1	0.32	2.81	1.18	0.64
K^+	0.7	3.5	2.0	0.6	0.9	5.7	2.0	0.9	0.35	2.05	1.05	0.42
BC_{370}	2.8	11.3	6.8	2.2	4.3	21.6	9.0	4.2	0.39	1.53	0.83	0.34
BC_{880}	2.6	11.3	7.2	2.5	4.2	16.2	8.3	3.1	0.34	1.82	0.91	0.38
Al[*]	23	501	266	134	115	409	225	86	0.88	3.51	1.50	0.67
Mn[*]	6	78	21	16	3	41	18	11	0.18	6.27	1.73	1.54
Fe[*]	40	380	146	76	26	303	111	66	0.23	4.61	1.73	1.15
Ni[*]	BDL[#]	17	6	5	1	12	5	4	0.00	3.21	1.26	0.70
Cu[*]	3	26	13	6	3	144	18	28	0.07	4.19	1.45	1.09
Zn[*]	154	6362	1034	1340	58	2845	823	862	0.06	19.5	3.03	4.29
Pb[*]	35	1309	269	283	16	547	159	133	0.12	12.3	3.16	3.63

[*]*Concentrations are in ng m^{-3},* [#]*below detection limit*

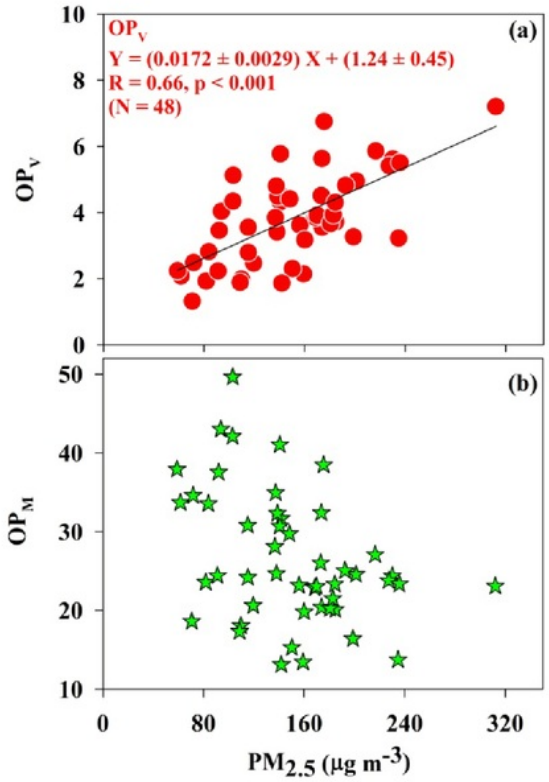

Figure 3. 2. *Scatter plot of $PM_{2.5}$ mass concentration with (a) OP_V and (b) OP_M.*

3.1.1.4. Source (s)/Process (es)/Species responsible for observed OP

The major focus of this study is to investigate the major source (s)/process (es)/species responsible for observed DTT activity, and most of the discussions are based on OP_M. To investigate this, linear regression analysis was performed between OP_M and mass normalized (ng species per µg $PM_{2.5}$) species concentrations. OP_M exhibited a significant positive correlation ($p < 0.05$) with carbonaceous aerosol (OC, EC, BC and WSOC), whereas significant negative correlation ($p < 0.05$) with secondary inorganic aerosol (SIA) such as SO_4^{2-}, NO_3^- and NH_4^+ (Table 3.1). These observations infer that carbonaceous aerosol are DTT-active whereas SIA either reduces the DTT activity of ambient particles or they are independent of observed

DTT activity, because in both cases they are expected to correlate negatively with DTT activity. In order to assess whether SIA reduces DTT activity or not, a laboratory experiment was conducted. Towards this, four aliquots of a standard (0.05 µM PQN) were taken and three of them were spiked with different amount of lab-made SIA (Fig. 3.3). Here, SIA mass fraction was calculated by adding the mass fractions of SO_4^{2-}, NO_3^- and NH_4^+. Consumption rate of DTT in all four aliquots was found to be more or less uniform (~ 0.71 µM DTT min^{-1}), irrespective of amount of SIA added. However, when it was normalized to added SIA mass (i.e., DTT activity/µg SIA), it showed decreasing trend. It is because addition of SIA increases PM mass but not DTT activity. This experiment confirms that SIA do not affect DTT activity.

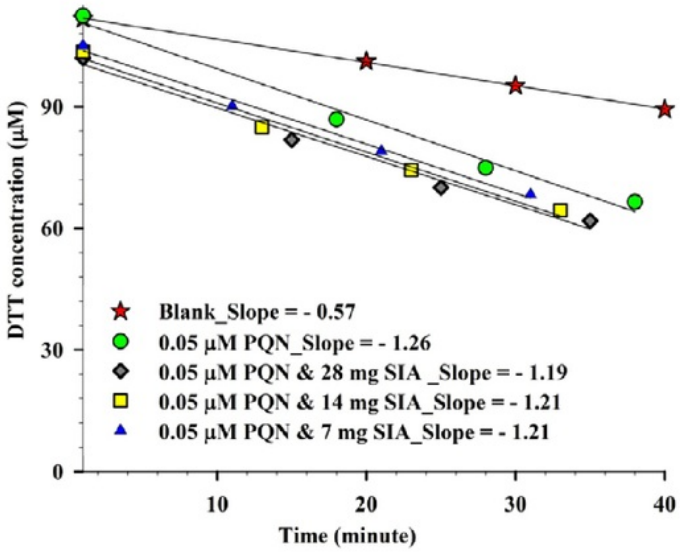

Figure 3. 3. *Consumption rate of DTT in presence 0.05 µM PQN as well as mixture of 0.05 µM PQN and different amount of lab-made SIA.*

The positive R values of the OP_V versus the mass concentrations of SIA species, and the negative R values related to the OP_M versus the normalized mass had been reported in earlier literature also (Hu et al., 2008; V. Verma et al., 2014; Verma et al., 2012). Further, trace metals, except Ni, were not found to be significantly

correlated with DTT activity (Table 3.1). Although redox activity of many of transition metals in biological mechanism is well established, they do not respond in DTT assay. The inactivity of transition metals for DTT assay has been documented in literature (Cho et al., 2005; Xiong et al., 2017). Moreover, measured OP is just due to soluble fraction of $PM_{2.5}$. Thus, acid digested trace metals cannot be compared directly with OP. The observed positive and significant correlation between DTT activity and Ni might be due to its co-variability with EC.

Further, ratios of daytime to nighttime volume normalized OC, EC and K^+concentrations were close to unity (Table 3.2), which suggests more or less uniform contribution of these species from different sources during the day and nighttime of winter season. However, based on the relationship of OP_M with measured aerosol species in daytime and nighttime samples, it was observed that some species (such as WSOC, K^+, BC_{370}) exhibits different relationship with DTT activity during day and night (Table 3.1). It could be due to several reasons such as changes in meteorological conditions (during day and night) affecting DTT activity and/or presence of some species change overall DTT activity of PM (discussed later). Meteorological conditions (such as temperature and relative humidity) play important role in secondary aerosol formation, in changing atmospheric abundances of semi-volatile aerosol, and in fog formation. These processes can change chemical properties of PM components and thus, their DTT activity.

Mass normalized EC exhibits a significant positive correlation with OP_M in the day ($R = 0.66$, $p \leq 0.001$) and night ($R = 0.42$, $p \leq 0.04$) samples, suggesting DTT-active species (or their precursors) came from same source from where EC came in ambient aerosol (Table 3.1, Fig. 3.4). Cho et al. 2005 had also documented that EC correlate positively with DTT activity, and attributed it to the co-emissions of EC and DTT-active species. EC can be emitted from various combustion sources (mainly fossil fuel (FFB) and/or biomass burning (BB)). In order to investigate whether there is any difference in the DTT activity level of species derived from FFB vis-à-vis BB, a ratio of BC_{370}/BC_{880} is used as a color scale in Fig. 3.4. Here, the ratio

of BC_{370}/BC_{880} less than or equal to 1.0 in the sample would indicate that carbonaceous species are predominantly derived from FFB sources, whereas ratio greater than 1.0 would suggest the relative dominance of BB sources (Herich et al., 2011; Wang et al., 2011; Park and Son, 2017). Higher DTT activities were found to be related to higher BC_{370}/BC_{880} ratios (Fig. 3.4), suggesting the emission from BB sources are likely more DTT-active, however, to draw firm conclusion, further studies with specific markers are required. In addition, a significant positive correlation of mass normalized K^+ with OP_M during day (Table 3.1) also suggests that the emissions from biomass burning could be considerable source for the species with higher OP; however, the specific species cannot be identified using the measurements done in this study. Here, it is relevant to state that K^+ has been shown as a good marker of biomass burning emissions over the IGP in earlier studies (Rastogi et al., 2016).

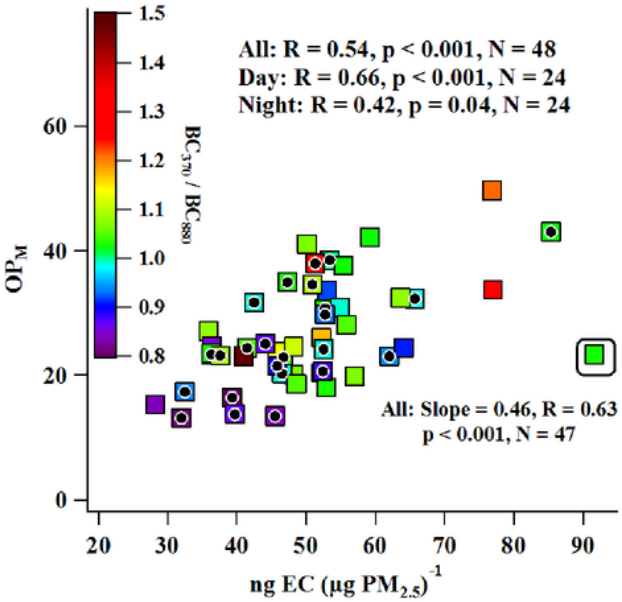

Figure 3. 4. *Scatter plot between OP_M and mass normalized EC. Color scale shows BC_{370} / BC_{880} ratio in corresponding sample. Black dots in the square represent day time samples.*

During investigation, it was also observed that the outlier point in Fig. 3.4 not only corresponds to highest EC mass fraction but also highest EC mass concentration (16.9 μg m^{-3}), however, mass normalized DTT activity of this sample was relatively low. Interestingly, high SIA mass fraction was also associated with the same sample. DTT activity of samples appears to be decreasing with increasing SIA mass fraction as SIA are DTT-inactive (as discussed earlier) (Table 3.1). It was also observed that daytime SIA shows a significant negative correlation with OP_M ($R = -0.62$, $p < 0.005$) whereas, nighttime correlation was not significant at 0.05 level (figure not shown), which is attributable to higher SIA mass fraction during daytime. It was also observed that SIA mass fraction remains low (~ 0.15 – 0.30) in samples collected during fog events (usually occur at night), but high (~ 0.18 – 0.41) during non-foggy hours as well as during the days after foggy nights. This observation further suggests that dominance of SIA in ambient $PM_{2.5}$ can cause an artifact. As per this artifact, SIA appear to reduce mass normalized DTT activity (as discussed earlier). Some studies have also demonstrated that SIA are DTT-inactive (Cho et al., 2005; Ntziachristos et al., 2007; Verma et al., 2012b).

3.1.1.5. Secondary Particles and OP

Present study shows that ~ 60% of $PM_{2.5}$ composition was dominated by SIA and OM. $PM_{2.5}$ composition also suggests that the emissions from BB contributes more to carbonaceous aerosol than those from FFB (Rastogi et al., 2015). In addition, filter based averaged WSOC/OC ratio was ~ 0.60, which implies that majority of OC was secondary organic aerosol (SOA). It also implies that SIA and SOA i.e., secondary particles dominate $PM_{2.5}$ composition over the study site during winter, which was also documented by Rastogi et al. 2016. In this study, WSOC mass fraction showed a significant positive correlation with OP_M during daytime ($R = 0.54$, $p < 0.05$) but large scatter was observed during nighttime (Table 3.1). It was also observed that the WSOC in samples collected during foggy period exhibited larger scatter with OP_M. To investigate it further, a linear relationship of OP_M with WSOC was examined separately in samples collected during foggy and non-foggy periods

(Fig. 3.5). WSOC showed a positive relationship with OP_M during non-foggy period whereas no relationship was observed during foggy period (Fig. 3.5a and c). It can be attributed to the partitioning of DTT-active and inactive water-soluble species to aqueous phase (fog), which was not collected by $PM_{2.5}$ sampler due to size restriction. Since OP_M exhibited positive correlation with the mass fraction of WSOC and negative correlation with the mass fraction of SIA (Table 3.1), it was investigated whether WSOC/SIA ratio can be used as a measure of OP by secondary particles. It was observed that OP_M exhibits a significant positive correlation with WSOC/SIA ratio ($R = 0.77$, $p < 0.001$) in the samples collected during non-foggy period, whereas large scatter was observed in samples collected during foggy period (Fig. 3.5b and d). Another interesting observation was a significant positive correlation of OP_M with WSOC/SIA ratio ($R=0.69$, $p=0.01$) for samples collected on the days following foggy nights with the slope ~1.5 times higher than that observed during non-foggy period (Fig. 3.5b and d). The attribution of ROS activity of fog to dissolved organic substances using DCFH probe was also observed by Decesari et al. 2017, which documented that WSOC alone explains 98% of the variability in the fog water ROS levels. However, the ROS generation capacity of WSOC might not be similar in both cases as the assays were different. Enhancement of the slope of OP_M and WSOC/SIA ratio linear relationship in samples collected during day time following the foggy nights in comparison to that in samples collected during non-foggy period might be due to the production of redox-active species by fog processing. It could be due to many reasons such as aqueous phase chemistry of SOA formation produces more DTT-active species in comparison to SOA formed through non-aqueous phase chemistry or, it could be partitioning of DTT-active species to aqueous phase during fog events which releases when fog dissipates. Firm conclusions cannot be drawn due to sample limitation. However, our observation suggests taking up semi-continuous measurements of ROS in polluted environment under foggy and non-foggy conditions to understand what enhances the DTT activity of ambient PM after fog dissipation. Circled points in Fig. 3.5b were not considered in linear regression

analysis. These points are the samples which were collected immediately after rain events during the sampling period.

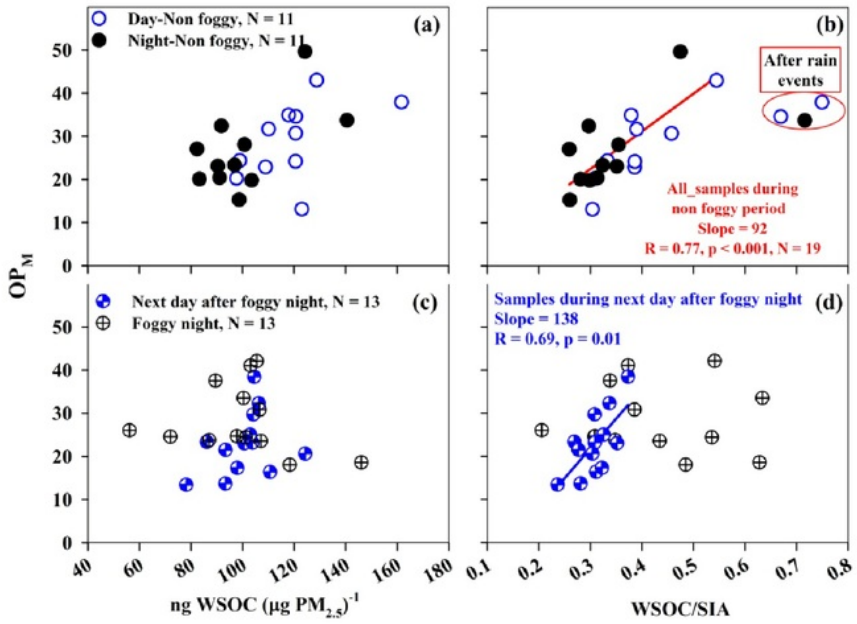

Figure 3. 5. *Scatter plots of OP_M with WSOC mass fraction and WSOC/SIA ratio during non-foggy (a, b) and foggy (c, d) periods. Regression analysis in scatter plot (b) includes all the samples (N=19) except three circled points. Regression in scatter plot (d) includes only samples collected just next day after foggy night (N=13).*

3.2. Kanpur: an urban site located in the middle of the IGP

3.2.1. Variability in $PM_{2.5}$ mass and chemical composition

The $PM_{2.5}$ mass concentration over the Kanpur city ranged from 79 to 336 µg m^{-3} (167 ± 53) during winter 2016, which was similar to that observed over Patiala during winter 2014. The large variability in observed in $PM_{2.5}$ mass over the two different sites can be attributed to dominance of specific sources (FFB, BB) along with meteorological conditions during the winter months. Moreover, species from combustion related sources such as OC, EC and K^+ varied from 14 – 63 µg m^{-3} (33 ±

11), 3 – 12 μg m^{-3} (7 ± 3) and 0.8 – 3. 5 μg m^{-3} (1.8 ± 0.5) over Kanpur, and 10 – 75 μg m^{-3} (26 ± 11), 3 – 17 μg m^{-3} (7 ± 3) and 0.7 – 5.7 μg m^{-3} (2.0 ± 0.8) over Patiala, respectively (Tables 3.1 and 3.3, Fig. 3.7). Further, SIA varied from 15 – 61 μg m^{-3} (38 ± 12) and 12 – 80 μg m^{-3} (44 ± 18) over Kanpur and Patiala respectively. Although the study periods were two distinct years, the comparison suggests that chemical composition over Kanpur and Patiala were similar during winter months.

3.2.2. Aerosol OP

OP_V varied from 2.7 – 10.1 nmol DTT min^{-1} m^{-3} (5.5 ± 1.5) over Kanpur and 1.3 – 7.2 nmol DTT min^{-1} m^{-3} (3.8 ± 1.4) over Patiala, whereas, OP_M varied from 19 – 58 pmol DTT min^{-1} μg^{-1} (34 ± 8) over Kanpur and 13 – 50 pmol DTT min^{-1} μg^{-1} (27 ± 8) over Patiala. Though there was no statistically significant difference in $PM_{2.5}$ mass concentration, the average values of OP_V and OP_M observed over Kanpur were significantly higher ($p < 0.001$) than those observed over Patiala, the upwind region of IGP (Tables 3.1 and 3.3). Fig. 3.6 depicts a comparison of linear relationships of OP_V with chemical components over the over Kanpur and Patiala. The slope (nmol DTT min^{-1} μg^{-1}) hints intrinsic OP of $PM_{2.5}$ and chemical constituent such as WSOC, OC, EC and (Fig. 3.6a, b, c and d). Similar slopes for the $PM_{2.5}$ and chemical constituent such as OC and EC over Kanpur and Patiala suggests their similar intrinsic OP. The intrinsic OP for $PM_{2.5}$ observed over Kanpur was a factor of ~ 2.0 lower compared to that observed over Hangzhou city, China (Wang et al., 2019).

Table 3. 3. *Statistical data (range, average and standard deviation (±1σ)) of measured species concentrations (μg m^{-3}), OP_V and OP_M of $PM_{2.5}$ over Kanpur.*

Components	Min	Max	Average	SD
$PM_{2.5}$	79	336	167	53
OP_V	2.7	10.1	5.5	1.5
OP_M	19	58	34	8
Cl^-	0.04	4.64	0.46	0.83
NO_3^-	5	25	15	5
SO_4^{2-}	5	29	15	6
Na^+	0.13	0.99	0.28	0.14
NH_4^+	3	14	8	3
Mg^{+2}	0.02	0.08	0.03	0.02
K^+	0.8	3. 5	1.8	0.5
Ca^+	0.03	0.35	0.15	0.07
WSOC	9	45	22	8
WSTN	5	36	17	8
OC	14	63	33	11
EC	3	12	7	3
WSON	BDL[#]	19	8	5
Al[*]	2	27	12	7
Ti[*]	BDL	3.19	1.15	0.61
V[*]	0.37	4.93	2.05	1.21
Cr[*]	BDL	3.96	0.77	0.73
Fe[*]	2	53	17	10
Mn[*]	BDL	52	7	8
Fe[*]	5	70	24	13
Co[*]	BDL	0.22	0.04	0.04
Ni[*]	BDL	1.32	0.21	0.49
Zn[*]	23	411	162	85
Cu[*]	0.4	10.9	2.7	2
As[*]	1	26	5	6
Se[*]	0.55	6.73	2.22	1.35
Cd[*]	BDL	40	5	6
Sb[*]	BDL	26	3	4
Tl[*]	BDL	1.9	0.28	0.32
Pb[*]	7	3099	188	504
Bi[*]	108	1376	618	333

[*]values are in ng m^{-3}, [#]below detection limit

Table 3. 4. *Comparison of $PM_{2.5}$ mass concentration, OP_V and OP_M (range, average and standard deviation ($\pm 1\sigma$) measured in this study with those documented in literature.*

	Patiala[a]	Kanpur[b]	Beijing[c]	Los Angeles[d]	Orinda[e]	Atlanta[f]	Mexico City[g]
$PM_{2.5}$ ($\mu g\ m^{-3}$)	59–312 (150±53)	79–336 (167±53)	50–410 (140)	5–10 (7±2)	15–44 (26±10)	5–25	33–71
nmol DTT min^{-1} m^{-3} (OP_V)	1.3–7.2 (3.8±1.4)	2.7–10.1 (5.5±1.5)	0.11–0.49 (0.19)	0.10–0.16 (0.13±0.02)	0.37–2.50 (0.96±0.66)	–	–
pmol DTT $min^{-1}$$\mu g^{-1}$ (OP_M)	13–50 (27±8)	19–58 (34±8)	–	14–24 (19±4)	21–75 (38±21)	10–50	25–40

[a]Patiala (Semi-Urban, N = 48), [b]Kanpur (Urban, N = 59), [c]Liu et al., 2014, Beijing (Urban, N = 54), [d]Hu et al., 2008, Los Angeles(Urban, N = 6), [e]Ntziachristos et al., 2007, Orinda (Urban, N = 8), [f]Verma et al., 2012, Atlanta (Urban, N = 8), [g]De Vizcaya-Ruiz et al., 2005, Mexico (Urban, May, N = 3).

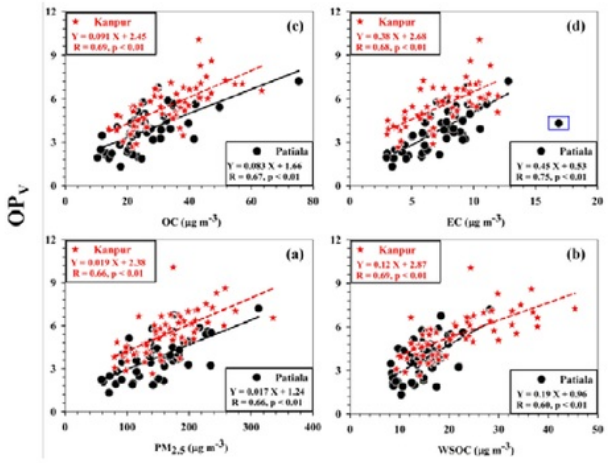

Figure 3. 6. *Scatter plots showing comparative linear relationships between OP_V and (a) $PM_{2.5}$ (b) WSOC (c) OC (d) EC mass concentrations over Kanpur and Patiala.*

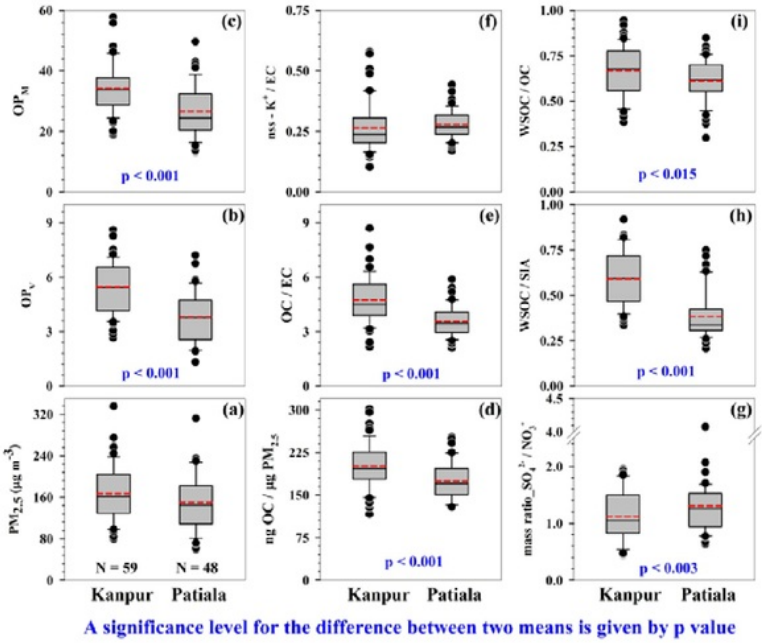

Figure 3. 7. *Box-Whisker plot depicts variability of $PM_{2.5}$ mass concentration along with OP_V and OP_M, and characteristics ratios. The box portion of the box plot is given by two lines at the 25th and 75th percentile, whereas a line is drawn inside the box at the 50th percentile represents median value. Two whisker boundaries are at the 10th and 90th percentile. Outlier boundaries are given at the 1st and 99th percentiles. Short dashed red line within the box represents mean.*

WSOC showed a factor of ~ 1.6 lower slope over Kanpur (0.12) compared to that observed over Patiala (0.19), suggesting its higher intrinsic OP over Patiala (Fig. 3.6b). As described in previous section, $PM_{2.5}$ composition suggests that the emissions from BB contributes more to carbonaceous aerosol than those from FFB (Rastogi et al., 2015). In addition, average primary WSOC and secondary WSOC contribution to total WSOC concentration over Patiala was ~ 20% and 80%, respectively, which implies that majority of WSOC were SOA. On the contrary, average primary WSOC and secondary WSOC contribution to total WSOC concentration over Kanpur was ~ 60% and 40%, respectively. This observation suggests that intrinsic OP of WSOC that formed through secondary processes is more

responsible for generation of ROS compared to that emitted primarily from source (s) over the study regions in IGP.

Using Na^+ as a reference element for sea-salt correction (Keene et al., 1986), the non-sea-salt (nss) components of Ca^{2+}, K^+ and SO_4^{2-} were calculated (average nss-K^+: 99%, nss-Ca^{2+}: 95% and nss-SO_4^{2-}: 99%) for Kanpur winter 2016 samples. The observed nss fractions suggest insignificant sea-salts contribution to these species. Moreover, nss-K^+ (99%) and nss-SO_4^{2-} (100%) showed insignificant sea-salts contribution to these species over Patiala for winter 2014. Further, nss-K^+/EC ratio was similar for Kanpur and Patiala, suggesting that the contribution of aerosol from primary combustions sources were more or less same (Fig. 3.7f). However, significant higher OC fraction (~ 1.15 times, $p < 0.001$) and higher WSOC/SIA (1.6, $p < 0.001$) over Kanpur compared to Patiala could be the reason for observed higher averaged OP_V and OP_M (Fig. 3.7b, c, d and h). As per our lab experiment described in previous section, it is relevant to say that SIA are DTT-inactive.

3.3. Shillong: a high altitude site located in the lower IGP

To study the atmospheric aging of aerosol travelling through the Indo-Gangetic Plain and Southeast Asia, Shillong suits well due to its favorable meteorology (such as wind pattern) during winter months. $PM_{2.5}$ sampling had been carried out over Barapani, Shillong (25.7 °N, 91.9 °E; 1064 m amsl) during 11th January, 2017 to 21st April, 2017 to characterize ambient aerosol and their role in ROS generation.

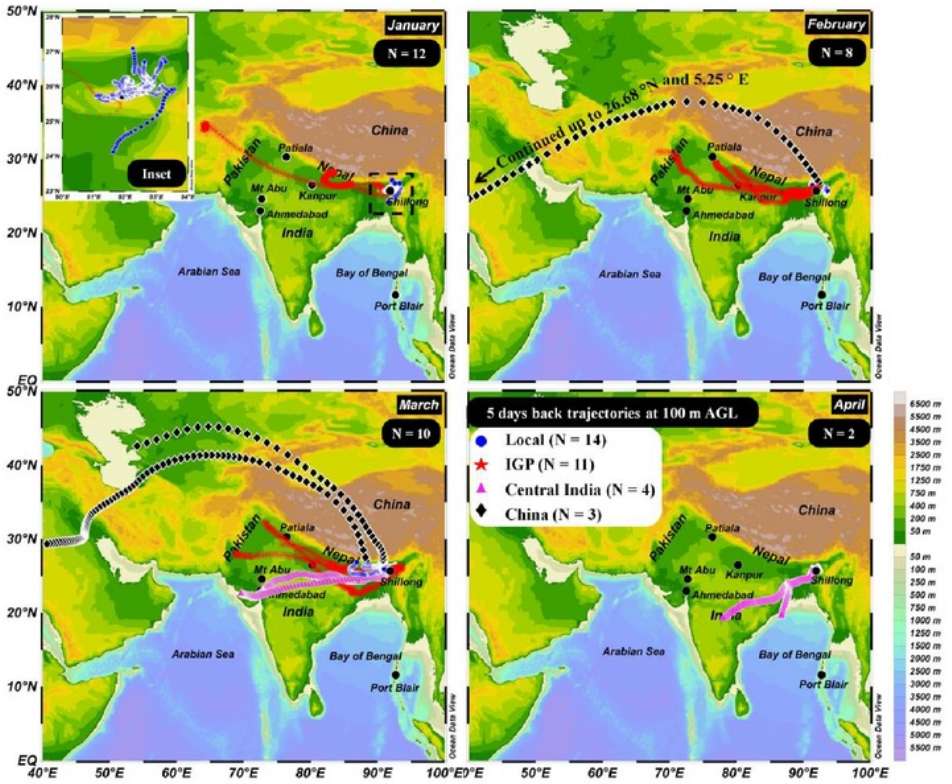

Figure 3. 8. *Five day back trajectories ending at 100 m above ground level from sampling location at Shillong is shown for each sample. Inset in January shows dominated contribution from local emission sources.*

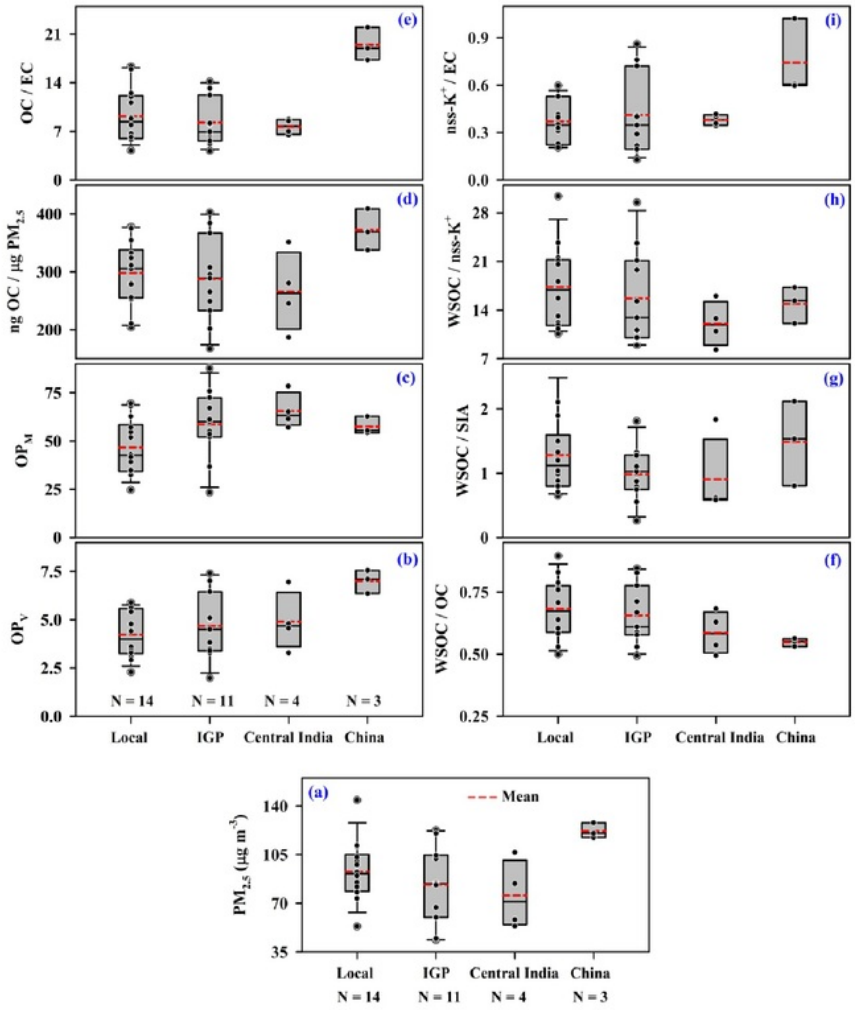

Figure 3. 9. *Box-Whisker plots depicting variability of $PM_{2.5}$ mass concentration along with OP_V and OP_M, and characteristics ratios of species in samples appear to come from different regions. For the details of box plot, lines and symbols, refer to caption of Figure 3.7.*

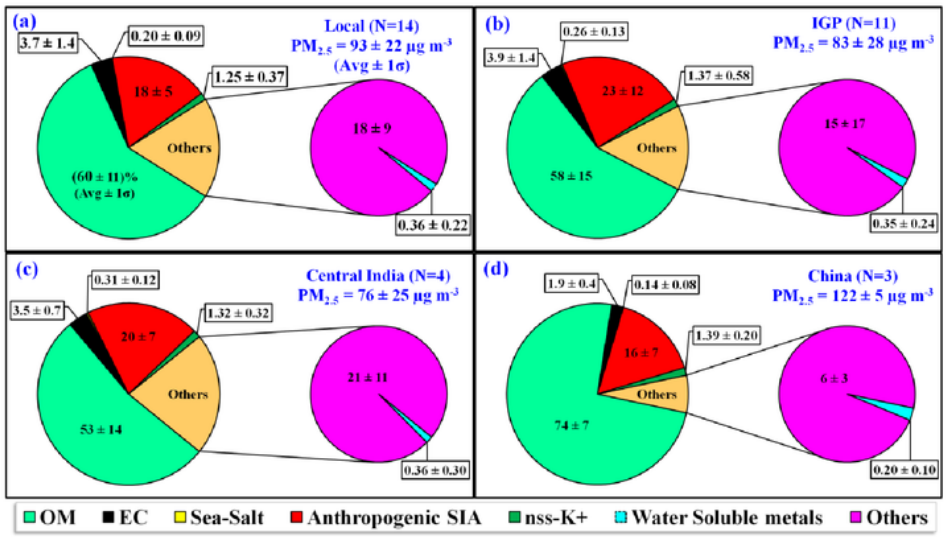

Figure 3. 10. *$PM_{2.5}$ chemical composition for four different categories: (a) Local, (b) IGP, (c) Central India and (d) China.*

$PM_{2.5}$ mass concentrations over Shillong varied from 44 to 144 µg m^{-3} (90 ± 25, 1σ). Further, five day back trajectories ending at 100 m above ground level (AGL) were analyzed using Hybrid Single-Particle Langrangian Integrated Trajectory (HYSPLIT) model using the Global Data Assimilation System (GDAS, 1 degree, global, 2006-present) as input. As per air mass back trajectories, the entire study period was classified into four different categories, i.e. Local (fresh emissions, N = 14), IGP (long-range transport from the upper IGP, N = 11), Central India (long-range transport from central India, N = 4) and China (long-range transport from Arab, Saharan and China regions, N = 3) (Fig. 3.8). Further, Using Na^+ as a reference element for sea-salt correction (Keene et al., 1986), the nss fraction of K^+, Mg^{2+}, Ca^{2+} and SO_4^{2-} were calculated. The observed nss fractions suggest insignificant sea-salts contribution to these species (average nss faction in each ion was greater than 96%). Moreover, major sources of aerosol contributing to PM_{10} were estimated using various proxies as described in Patel and Rastogi, 2018b. We used Na^+ as proxy for sea-salts (1/3.5 of seal-salts) and (NH_4^+, NO_3^- and nss-SO_4^{2-}) as proxy for anthropogenic sources, along with contribution from organic matter (OM, considered

as 1.9 times that of OC which is used for aged aerosols, Kiss et al., 2002; Yttri et al., 2007) and EC.

Averaged $PM_{2.5}$ mass concentration for these four categories over Shillong were 93 ± 22, 83 ± 28, 76 ± 25 and 122 ± 5 μg m^{-3} for Local, IGP, Central India and China, respectively. OP_V varied from 1.98 to 7.55 nmol DTT min^{-1} m^{-3} with an average values of 4.23 ± 1.24, 4.68 ± 1.71, 4.90 ± 1.52 and 7.00 ± 0.60 nmol DTT min^{-1} m^{-3} for Local, IGP, Central India and China, respectively. OP_M varied from 23 to 88 pmol DTT min^{-1} μg^{-1} with an average value of 47 ± 14, 59 ± 18, 66 ± 9 and 57 ± 5 pmol DTT min^{-1} μg^{-1} for Local, IGP, Central India and China, respectively. A dose of exposure level in terms of OP_V over Shillong was about 4 to 100 times higher than those reported for $PM_{2.5}$ over Athens urban-background (Paraskevopoulou et al., 2019), Lecce urban-background (Pietrogrande et al., 2018), Atlanta rural (Fang et al., 2015) and Netherlands urban-background (Janssen et al., 2014) sites and comparable to those observed over the semi-urban site located upwind in the IGP (Patel and Rastogi, 2018a). OP_M values of $PM_{2.5}$ over Shillong were higher than those observed over Athens urban-background (Paraskevopoulou et al., 2019), Atlanta rural (Fang et al., 2015) and Lecce urban-background (Pietrogrande et al., 2018), whereas comparable with the Netherlands urban-background (Janssen et al., 2014). These observations reflect a relatively high exposure risk and intrinsic oxidative toxicity of aerosol over Shillong.

The OC/EC ratio is often used to differentiate the relative dominance of biomass vis-à-vis fossil fuel burning sources (Turpin and Huntzicker, 1995; Rastogi et al., 2016) and/or secondary formation processes. Ambient aerosol from fossil fuel combustion sources shows lower OC/EC≲(2.0), whereas highe r ratio (> 4.0) in aerosol denotes prominent contribution from biomass burning and/or secondary organic aerosol formation during atmospheric aging. Samples with back trajectories across the China (category-China) showed ~2 times higher OM fraction compared to the other categories (Figs 3.8, 3.9d and 3.10d). This also reflected in the form of highest $PM_{2.5}$ mass concentration for China-Category (mean was statistically

different for China compared to other categories, $p < 0.001$). Further, a high OC/EC ratio (17 to 22, Fig. 3.9e) and nss-K^+/EC ratio (0.60 to 1.02, Fig. 3.9i) for China category indicate the strong influence from biomass burning emissions to these samples. Primary particle, nss-K^+, is often used as a tracer for emissions from biomass burning. If the observed higher OC/EC ratio could be due to presence of secondary organic aerosols formed through precursors emitted from sources other than biomass burning then one would not expect high nss-K^+ in these samples for China category. Averaged nss-K^+/EC ratio (0.74) for China category matches well with those observed over Patiala (0.70, Rastogi et al., 2016) during post-harvest paddy residue burning period which also indicates a strong influence of biomass burning. Further, OC component in China category samples can be considered as less aged since it showed relatively lower WSOC/OC ratio (ranging from 0.53 to 0.56, Fig. 3.9f). On the other side, less OC/EC (ranging from 4 to 16) ratios and relatively high WSOC/OC ratio (ranging from 0.49 to 0.90) for IGP and Central India categories compared to China indicates atmospheric processing of $PM_{2.5}$ while travelling across the respective regions (Fig. 3.9e and f). OP does not only depend upon the aging but likely depends on the species which are going under atmospheric aging. Aerosol derived from the primary combustion sources may be redox active. Further, their OP may increase (changed to more redox active chemical structure) or decrease (becomes redox inactive) when it undergoes atmospheric aging. Polycyclic aromatic hydrocarbons (PAHs) are derived largely from combustion sources (such as BB and/or FFB), and their atmospheric aging often results into oxygenated PAHs (i.e. quinones), the most responsible species for OP. For example, Li et al., 2000 found that HO-1 expression (a biological marker for induced oxidative stress) for oxygenated PAHs is more potent than PAHs. Verma et al., 2015 and Xiong et al., 2017 have recently demonstrated the importance of atmospheric aging in enhancing the overall capability of ambient PM to generate ROS.

Referring to the present study, mean OP_V values of Local, IGP and Central India categories were ~ 1.5 times higher and that for China category. Overall, OP_V observed over Shillong during winter 2017 were ~ 5 – 9 times higher compared to

that reported over Mount Abu, a high altitude site in western India, during winter and spring months (i.e. January – April, 2016) (Patel and Rastogi, 2018b). Likewise, mean OP_M values for the above classified categories were found ~ 3 to 5 times higher compared to those observed over Mount Abu during the above said period. It is important to note that PM_{10} composition over Mount Abu was dominated by mineral dust (averaged 30 and 80% during winter and spring months, respectively). On the contrary, $PM_{2.5}$ composition over Shillong was found to be dominated by OM fraction (averaged 60, 58, 53 and 74% for Local, IGP, Central India and China, respectively, Fig. 3.10). DTT assay is reported to be most active for organics (Cho et al., 2005) which likely resulted into high OP_M over Shillong. Furthermore, OC fraction in $PM_{2.5}$ was 17% and 20% over Patiala and Kanpur respectively, located in the upwind of Shillong. On the contrary, Shillong was dominated by ~ 30% of OC fraction in $PM_{2.5}$. As a result, OP_M values were found to be a factor of ~ 1.5 to 2 higher over Shillong as compared to those observed over Patiala and Kanpur. It highlights the intrinsic OP of OC component in $PM_{2.5}$ over Shillong.

3.4. Effect of biomass burning on aerosol OP: A case study

Emission of aerosol and their gaseous precursors from post-harvest paddy-residue burning during October–November every year results into poor air quality downwind in the IGP (Rajput et al., 2014; Rastogi et al., 2014; Singh et al., 2016). Further, Singh et al. 2008 have documented that ~ 60 % of the population in Punjab state live in the rice growing areas and exposed to poor air quality due to burning of rice stubbles during October–November every year. In the same review article, Singh et al. 2008 have reported ~ 10 % increase in the number of asthma patients, as per the medical records of the civil hospital of Jira, within 20 – 25 days of the burning period every season. It was, thus, important to study aerosol OP during these months in the IGP. Day and night (10 h integrated time) pair of $PM_{2.5}$ samples (N = 69) were collected every day before (N = 20, pre-burning), during (N = 36, burning), and after (N = 8, post-burning) a large-scale paddy residue burning from 11th October to 15th November 2014. There were 5 samples between pre-burning and burning period

which were largely influenced by firecracker burning collected during the famous festival "Diwali".

3.4.1. $PM_{2.5}$ mass concentration and biomass burning markers

$PM_{2.5}$ mass concentration ranged from 108 to 325 µg m^{-3} (average: 175 ± 59, 1σ) and 213 to 503 µg m^{-3} (average: 367 ± 89, 1σ) during day and nighttime, respectively, during burning period, which were ~ 1.7 times higher than the rest non-burning periods (except Diwali). The higher concentrations of $PM_{2.5}$ along with carbonaceous aerosol during burning period were, as obvious, observed due to large scale post-harvest paddy residue burning in the open fields. The variability found in $PM_{2.5}$ mass concentration (108 to 503 µg m^{-3}) during present study burning period is somewhat higher than those reported earlier from the same site during the same period in 2008, 2010 (60-390 µg m^{-3}, Rajput et al., 2013) and 2011 (21-400 µg m^{-3}, Rastogi et al., 2016). However, OC and EC mass fractions were somewhat lower than those reported earlier (Rajput et al., 2013). Singh et al. (2015) reported the year-round data and found the highest mass concentrations of $PM_{2.5}$ and PM_1 during paddy-residue burning period from the same study site, which was attributed to the dominance of submicron size aerosol in the atmosphere. Furthermore, biomass burning (BB) markers such as OC/EC and K^+/EC were found to be correlated strongly and positively ($R \geq 0.80$, $p < 0.05$) with OP_V during the burning period (discussed in latter section). Carbon monoxide (CO) can be utilized to highlight the primary emissions from combustion source. If primary combustion sources are dominating, one would expect lower WSOC/CO ratio; however, this ratio during the burning period was not much different from non-burning period. This observation suggests the dominance of primary aerosol from BB. In addition, a strong correlation between CO and OP_V and during burning period ($R = 0.71$, $p < 0.05$) suggests the role of BB derived primary aerosol species on their OP.

On an average, the Diwali period was observed to be loaded with ~ 2.2 and ~ 1.3 times higher $PM_{2.5}$ mass concentration as compared to non-burning and burning periods, respectively. It is relevant to state that the Diwali is a festival of lights, which

is celebrated during autumn in India, and is also marked with huge burning of fireworks across India. However, the highest value of $PM_{2.5}$ mass concentration (503 µg m^{-3}) was associated with burning period. The characteristics K^+/EC ratio was highest during the Diwali period because the firecrackers are made up of ~75 % potassium nitrate, ~15 percent organic material (charcoal) and ~10 percent sulfur (Rastogi et al., 2019 and references therein).

3.4.2. $PM_{2.5}$ chemical composition and OP

As this study period was influenced by paddy-residue burning and $PM_{2.5}$ mass was consist of 26% of OC, OP normalized to OC mass (pico mole DTT consumed per minute per µg of OC mass or OP (µg OC)$^{-1}$ or activity (µg OC) $^{-1}$ or intrinsic OP of OC or OP_{OC}) is used to obtain the intrinsic OP of organics. The OP_V varied from 2 to 25 nmol DTT min^{-1} m^{-3} (average: 12 ± 5, 1σ) with the highest average during burning (14 ± 5 nmol DTT min^{-1} m^{-3}), followed by post-burning (12 ± 2 nmol DTT min^{-1} m^{-3}), and followed by more or less equal contribution during pre-burning (8 ± 3 nmol DTT min^{-1} m^{-3}) and Diwali period (9 ± 1 nmol DTT min^{-1} m^{-3}) (Table 3.5). OP_V for burning and post-burning period were not statistically different, however, these values are statistically higher than those observed during Diwali and pre-burning period. OP_V values (7 – 25 nmol DTT min^{-1} m^{-3}) found during the burning period were 10 – 14 times higher than those reported worldwide (0.02 – 3.5 nmol DTT min^{-1} m^{-3}) (Paraskevopoulou, et al., 2019 and references therein). This is an important observation as the inhaled dose of $PM_{2.5}$ with high OP can severely affect people living in the study region. Furthermore, OP_M varied from 17 to 89 pmol DTT min^{-1} μg^{-1} (54 ± 17) with an average highest during post-burning (78 ± 9 pmol DTT min^{-1} μg^{-1}), followed by more or less equal contribution during burning (55 ± 12 pmol DTT min^{-1} μg^{-1}) and pre-burning period (51 ± 18 pmol DTT min^{-1} μg^{-1}), followed by the Diwali period (29 ± 7 pmol DTT min^{-1} μg^{-1}) (Table 3.5).

OP_V during burning period was ~ 1.7 times higher than pre-burning period but more or less similar to that found during post-burning period. On the contrary, OP_M

during post-burning period was ~ 1.4 times higher than pre-burning and burning period. Fig. 3.11 shows the scatter plot between OP_V and $PM_{2.5}$ mass concentrations for pre-burning, Diwali, burning and post-burning period. The slope gives the information about OP_M, which is the intrinsic property of $PM_{2.5}$ and independent of exposure levels. It was observed that post-burning period contained 2 – 3 times higher slope compared to those found during pre-burning and burning period. It suggests that atmospheric aging of BB derived $PM_{2.5}$ species could have led to higher OP_M during post-burning period. Furthermore, a third axis (WSOC/OC ratio) is used as a color scale in Fig. 3.11a. The higher intrinsic OP (i.e. slope) during post-burning period was associated with the higher WSOC/OC ratio in contrast to that observed during the burning period. The higher fraction of water insoluble organic carbon (WIOC) during paddy residue burning period, some of which probably soluble in methanol, might have emitted to the atmosphere, and could have contributed to the observed highest OP_V values. Further, a ratio of BC_{370}/BC_{880} was used as a color scale in Fig. 3.11b. Here, as discussed in the previous section, the ratio of BC_{370}/BC_{880} less than or equal to 1.0 in the sample would indicate that carbonaceous species are predominantly derived from FFB sources, whereas ratio greater than 1.0 would suggest the relative dominance of BB sources (Herich et al., 2011; Wang et al., 2011; Park and Son, 2017). Higher individual OP_V values were found to be associated with higher (> 1.0) BC_{370}/BC_{880} ratios (Fig. 3.11b), representing the emission from BB sources are more DTT-active.

Table 3. 5. *Variability (along with average ± standard deviation, 1σ) of $PM_{2.5}$ mass concentration (μg m^{-3}), OP_V (nmol DTT min^{-1} m^{-3}) and OP_M (pmol DTT min^{-1} μg^{-1}) for pre-burning, Diwali, burning and post-burning periods.*

Constituents	Overall (N = 69)	Pre-Burning (N = 20)	Diwali (N = 5)	Burning (N = 36)	Post-Burning (N = 8)
$PM_{2.5}$ (μg m^{-3})	91 – 503 (229 ± 115)	91 – 373 (154 ± 59)	259 – 424 (340 ± 74)	108 – 503 (271 ± 122)	139 – 191 (156 ± 19)
OP_V	2 – 25 (12 ± 5)	2 – 13 (8 ± 3)	8 – 11 (9 ± 1)	7 – 25 (14 ± 5)	10 -16 (12 ± 2)
OP_M	17 – 89 (54 ± 17)	17 – 83 (51 ± 18)	23 – 40 (29 ± 7)	33 – 78 (55 ± 12)	65 – 89 (78 ± 9)

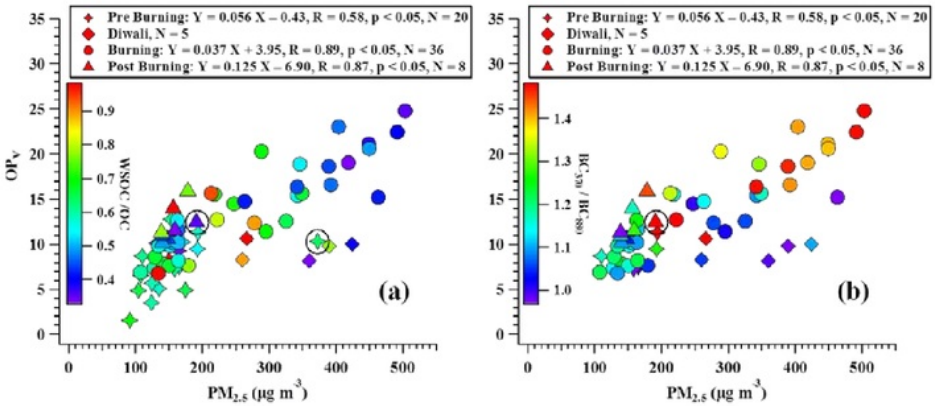

Figure 3. 11. *Scatter plot between OP_V and $PM_{2.5}$ mass concentrations for pre-burning, Diwali, burning and post-burning period along with color scale for (a) WSOC/OC ratio and (b) BC_{370}/BC_{880} ratio in corresponding samples. Samples in open black circles are excluded (as outliers) from the regression analysis.*

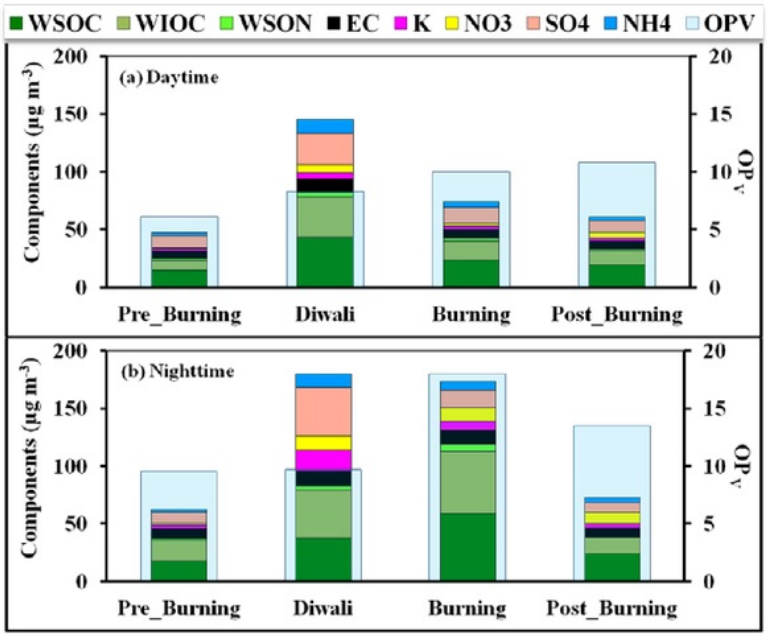

Figure 3. 12. *$PM_{2.5}$ chemical composition along with OP_V is averaged for pre-burning, Diwali, burning and post-burning period for (a) daytime and (b) nighttime.*

In Fig. 3.12, the nights during the burning period were associated with higher concentrations of WSOC and WIOC constituents in $PM_{2.5}$ which likely caused a very high OP. However during Diwali period, in comparison to daytime, the nights were associated with the higher concentration of DTT-inactive water soluble inorganic species such as K^+, NO_3^- and SO_4^{2-}; therefore, OP was not much higher in comparison to daytime values during Diwali.

3.4.3. Oxidative potential and Brown Carbon

Biomass burning is reported to be one of the major sources for the brown carbon (BrC) species emissions over the study site (Srinivas et al., 2016). BrC are high molecular weight organic species such as humic like substances (HULIS). OC mass is found to be ~15 – 36% of total $PM_{2.5}$ mass during burning period. To ascertain OP of water-soluble and water-insoluble BrC, methanol-soluble BrC has also been analyzed in the present study. Cheng et al., 2016 showed that 85% of organic aerosol can be extracted using methanol. In general, BrC is expressed as their absorption coefficient (b_{abs}) at 365 nm. OP_V exhibited similar temporal variation with the methanol-soluble BrC measured at 365 nm at significant higher levels during the burning period (Fig. 3.13a). Among all combustion sources, the biomass burning has been reported to contribute highest to the OP caused by HULIS (Ma et al., 2018). Since BrC is a fraction of OC, the intrinsic OP of OC (i.e. ROS generation capacity of OC, represented as OP_{OC}) is examined in the present study. OP_{OC} was ~ 1.6 times higher during the post-burning period (352 ± 48 pmol DTT min^{-1} $(\mu g\ OC)^{-1}$) as compared to that during burning period (223 ± 77 pmol DTT min^{-1} $(\mu g\ OC)^{-1}$). WSOC/OC was also higher during the post-burning period, suggesting secondary organics may have high OP likely due to the aging of OC during the post-burning period (Fig. 3.13b). The averaged OP_{OC} values observed during burning and post-burning period are ~ 17 and ~ 27 times higher, respectively, than those observed for the samples collected in close proximity to the trash-burning piles in Bangalore, India (Vreeland et al., 2016).

Moreover, BrC absorption at 365 nm (b_{abs_365}) is shown to be mainly associated with HULIS compounds, nevertheless, other chromophore may peak at different wavelengths (Satish et al., 2017). In the present study, absorptions coefficient at 405 nm, 420 nm and 450 nm (representing nitro-aromatic light absorbing compounds) are chosen to get information about the BrC composition. Ratios of b_{abs_405} / b_{abs_365}, b_{abs_420} / b_{abs_365} and b_{abs_450} / b_{abs_365} showed similar trend with NO_3^- fraction as well as with OP_{OC} during the burning period. These all trends were found to be increasing during post-burning period (Fig. 3.13b), suggesting aging of nitro-aromatics emitted from paddy burning can be more DTT-active. BrC composition is reported to be strongly dependent on the meteorological conditions such as RH and T (Satish et al., 2017). Different absorption coefficient ratios and OP_{OC} were examined for day and night time for the samples collected during burning and post-burning periods (Fig. 3.14). The abundances of BrC chromophores absorbing at 405 nm 420 nm and 450 nm were low during the burning compared to post-burning period, and hence the observed OP_{OC}. Interestingly during nighttime of post burning period, a strong and significant positive correlations between OP_{OC} and ratios such as b_{abs_405} / b_{abs_365} (slope = 10862, R = 0.97, p = 0.025, N = 4), b_{abs_420} / b_{abs_365} (slope = 8188, R = 0.99, $p < 0.01$, N = 4) and b_{abs_450} / b_{abs_365} (slope = 8200, R = 0.99, p = 0.01, N = 4) were observed (Fig. 3.14). Here it is relevant to say that nitro-phenol and nitro-catechol are reported to be dominant light absorbing compounds in $PM_{2.5}$ particles that absorbs strongly at higher wavelengths (i.e. 400 nm to 450 nm in visible region) over the regions impacted by biomass burning (Claeys et al., 2012; Lin et al., 2015). DTT response to the mixture of nitrogen containing bases in alkaloids (HULIS family) and quinone from rice straw burning are reported to have more than the sum of individual responses (Dou et al., 2015). This synergistic effect could be responsible for observed higher OP_V during burning and post-burning period over the study site compared to values reported in the literature by Paraskevopoulou et al. (2019).

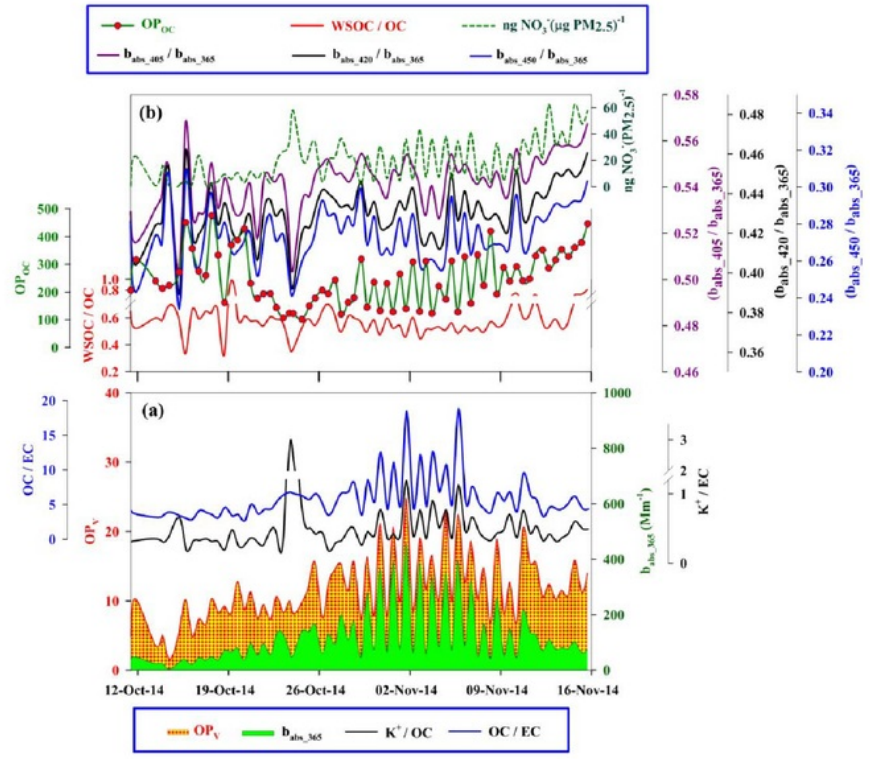

Figure 3. 13. *Temporal variability of (a) OP_V along with biomass burning markers and b_{abs} at 365 nm as representative of BrC and, (b) OC mass normalized OP along with $PM_{2.5}$ mass normalized nitrate, WSOC/OC ratio, BrC chromophores absorption coefficient ratios such as b_{abs_405} / b_{abs_365}, b_{abs_420} / b_{abs_365} and b_{abs_450} / b_{abs_365}.*

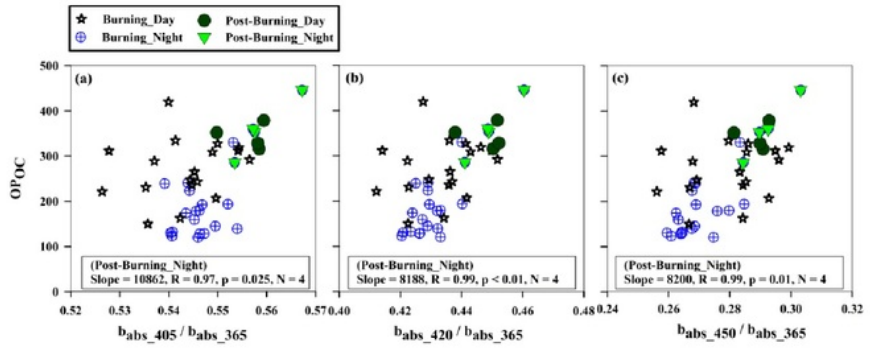

Figure 3. 14. *Scatter plot between OP_{OC} and BrC chromophores absorption coefficient ratios such as (a) b_{abs_405} / b_{abs_365} (b) b_{abs_420} / b_{abs_365} and (c) b_{abs_450} / b_{abs_365}.*

3.4.4. Multivariate regression analysis of OP responsible $PM_{2.5}$ components

In order to examine $PM_{2.5}$ species responsible for the observed OP, a multiple linear regression (MLR) analysis was performed for the samples collected during burning and post-burning period. MLR studies are often performed for this purpose (Bates et al., 2015; Argyropoulos et al., 2016). Species that exhibited significant positive linear relationships with OP_V were selected to establish the MLR model. MLR were employed using OC and NO_3^- mass concentration for burning and non-burning (includes pre- and post-burning only; Diwali data points were excluded from the MLR analysis) (Table 3.6). Statistical regression for MLR showed that a coefficient of determination with $R^2 = 0.64$ for non-burning period was not as strong as that found during the burning period ($R^2 = 0.84$). It suggests that either OC and NO_3^- or those co-emitted and/or formed with these species were majorly responsible $PM_{2.5}$ species for the observed OP_V during the burning period. A large NO_3^- aerosol contribution to $PM_{2.5}$ mass along with significantly higher ROS activity ($P = 0.06$) does not necessarily mean that NO_3^- aerosol are producing ROS because DTT assay is reported to be inactive for secondary inorganic species (such as NH_4^+, SO_4^{2-} and NO_3^-) (Patel and Rastogi, 2018a). Furthermore, it is interesting to note that intercepts in the MLR model equations for non-burning (4.27) and burning period (7.29) are half of the averaged OP_V (i.e. 9 nmol DTT min^{-1} m^{-3} and 14 nmol DTT min^{-1} m^{-3}, respectively) suggesting that 50% of the chemically measured OP_V can be predicted by OC and NO_3^- aerosol species present in the $PM_{2.5}$. Results suggest that OC and NO_3^- aerosol species could be utilized to predict a total of 84% of OP_V during burning period (Fig. 3.15).

Table 3. 6. *Multiple linear regression analysis results of OP_V (nmol DTT min^{-1} m^{-3}) with OC and NO_3^- mass concentration (µg m^{-3}) during non-burning and burning period.*

Factors	*Coefficients*	*Standard Error*	*t Stat*	*P-value*
Non-burning; N = 28, R = 0.80, R^2 = 0.64, Adj R^2 = 0.62, Std Err = 2.02				
Intercept	4.27	1.09		
OC	0.10	0.04	2.69	0.012
NO_3^-	0.56	0.13	4.39	0.000
Burning; N = 36, R = 0.92, R^2 = 0.84, Adj R^2 = 0.83, Std Err = 2.11				
Intercept	7.29	0.73		
OC	0.06	0.02	3.02	0.005
NO_3^-	0.30	0.16	1.91	0.065

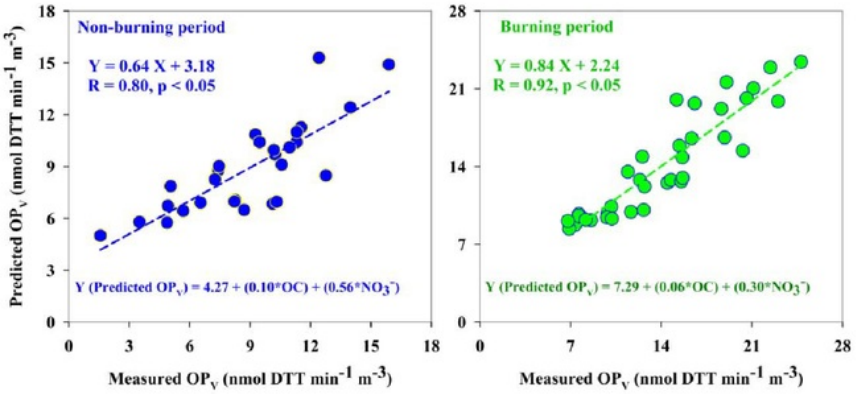

Figure 3. 15. *Linear regression analysis between measured and predicted OP_V for non-burning and burning periods.*

3.4.5. Comparison of paddy-residue burning 2014 and winter 2014 (mixed source derived) OP

Furthermore, correlations between OP_V and atmospheric mass concentrations of $PM_{2.5}$, OC and WSOC were compared for winter (January 2014) and paddy-residue burning (October-November, 2014) period over Patiala (Fig. 3.16). The slope

gives important information about the intrinsic properties of $PM_{2.5}$ components. OP_V exhibited a strong and positive correlation with $PM_{2.5}$ mass concentration during paddy-residue burning period ($m = 0.037$, $R = 0.89$, $p < 0.05$) with ~ 2.0 times higher slope compared to that reported for winter ($m = 0.017$, $R = 0.66$, $p < 0.05$) (Patel and Rastogi, 2018a) (Fig. 3.16a and b). It is attributed to dominant contribution of DTT-active species from BB to $PM_{2.5}$ during study period, which are expected to have higher OP. An average OP_V was ~ 3.5 times higher during burning period compared to that observed during winter. OP_V was correlated significantly with $PM_{2.5}$, OC and WSOC concentration during winter (R varied from 0.59 to 0.68), likely due to the influence from mixture of multiple sources contributing to mass but not significantly to DTT activity. On the contrary, better correlations for the same species were observed during the burning period (R varied from 0.89 to 0.91) suggesting that BB-derived organics would be the major responsible component for the observed OP. Overall, the slopes for OP_V versus OC and WSOC scatter plots during the burning period were similar to that observed during winter (Fig. 3.16 c, d, e, f). On the contrary, the slope for the scatter plot between OP_V and OC during daytime burning period (0.112) was ~ 1.3 times higher compared to that observed during winter period (0.083, Fig. 3.16d). On average, OC fraction during the nighttime burning period (29%) was ~ 1.3 times higher than that observed during the daytime (22%). The higher values of OP_V were associated with the higher OC mass concentration during the nighttime of burning period. However, the intrinsic OP for OC during the nighttime was ~ 1.6 times lower than that observed during the daytime burning period. Further, there was no such difference in the slopes during day and nighttime burning period for the scatter plots between OP_V and WSOC (Fig. 3.16e and f). It can be attributed to some non-polar organic compounds which are fairly soluble in methanol, but not completely soluble in water. The slope for the scatter plot between OP_V with $PM_{2.5}$ mass concentration during the burning period (0.037) is found to be similar to those reported during winter over Atlanta, USA by Fang et al., 2015.

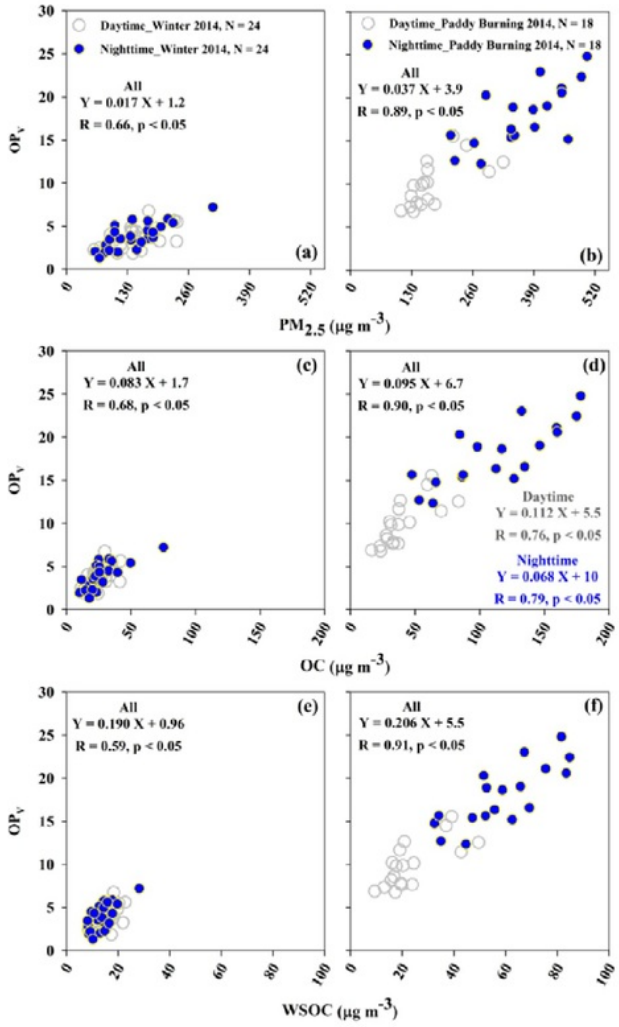

Figure 3. 16. *A comparison of scatter plots between OP_V and mass concentrations of $PM_{2.5}$ (a, b), OC (c, d) and WSOC (e, f) during burning and winter period 2014 over Patiala.*

Moreover, OP_M is found to be significantly correlated with ratio of WSOC to SIA in daytime samples collected during paddy-residue burning ($m = 12$, $R = 0.55$, $p < 0.05$, $N = 18$, Fig. 3.17). The daytime slope during burning period was ~ 8 and 11 times lower compared to that observed during non-foggy days (two data points just after rain events were excluded) and days after foggy nights, respectively, of winter 2014 (Fig. 3.17). WSOC during winter was reported to be predominantly of

secondary origin whereas during autumn, it was a mixture of primary (from BB) and secondary both. It suggests that WSOC formed through secondary processes are more DTT-active than those emitted directly from primary sources. However, the intrinsic OP of BB derived $PM_{2.5}$, was ~ 1.5 – 3.0 times higher during the burning period than compared to that observed during winter. These observations indicate that chronic exposure to such high levels of ambient $PM_{2.5}$ with their corresponding high level extrinsic and/or intrinsic OP may cause a wide array of health effects over the study region.

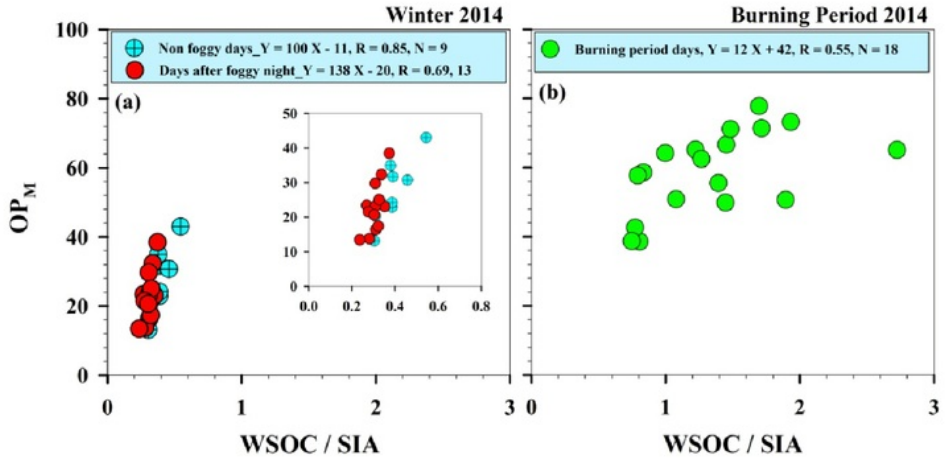

Figure 3. 17. *Scatter plots of OP_M with WSOC/SIA ratio during (a) daytime burning period and (b) daytime of winter period (non-foggy days and days after foggy nights).*

Chapter 4

OXIDATIVE POTENTIAL OF AMBIENT AEROSOL OVER THE REMOTE LOCATIONS

4.1. Introduction

During past several decades, global anthropogenic emissions have increased markedly, particularly in Asia (Kurokawa et al., 2013). To monitor the synoptic scale emissions of particles as well as their precursors from sources and their long-range transport and aging in the air, remote locations such as high-altitude site, open ocean etc. are ideal as they are located far from the anthropogenic sources. Such sites represent regional aerosol composition. Aging processes such as heterogeneous reactions, condensation, coagulation, aggregation, oxidation and reduction during long-range transport of aerosol in the air can alter their physicochemical characteristics. Such studies would show OP of regional aerosol and may help in understanding effect of aerosol aging on their OP.

OP of aerosol near source regions is reported in different parts of the western world (Cho et al., 2005; Hu et al., 2008; Eiguren-Fernandez et al., 2010; Charrier and Anastasio, 2012; McWhinney et al., 2013; Verma et al., 2014). However, the OP of aerosol from remote locations is limited worldwide. To fill this gap, such studies were carried out over a remote high-altitude site and over oceans surrounding India.

4.2. Mount Abu: a high altitude site located in western India

Chemical composition over high altitude sites have been documented over various places in the world, including India (Henning, 2003; Rastogi and Sarin, 2005; Suzuki et al., 2008; Kumar and Sarin, 2010; Ram et al., 2010; Okamoto and Tanimoto, 2016 and references therein). This study reports seasonality in not only chemical composition but also in DTT-based OP of ambient PM_{10} collected during March 2014 to May 2016 at a high altitude site Mount Abu located in western India.

4.2.1. Characterization of ambient PM_{10}

Yearly data was classified into four seasons based on prevailing meteorological conditions over the study site: winter (December–January, n = 10), spring (Late February–April, n = 11), pre-monsoon (May–June, n = 11) and post-monsoon (October-November, n = 10). PM_{10} mass concentration varied from 29 to 273 μg m^{-3} during the study period with the average value of 49 ± 15 μg m^{-3} (1σ), 122 ± 63 μg m^{-3}, 133 ± 56 μg m^{-3} and 72 ± 21 μg m^{-3} during winter, spring, pre-monsoon and post-monsoon, respectively. These values are comparable to those reported over other high-altitude sites such as Nagarkot (81 ± 76 μg m^{-3} in PM_{10} during February-May 1999, Carrico et al., 2003), Manora Peak (83 ± 62 μg m^{-3} in total suspended particulate (TSP) during 2005-2006, Ram et al., 2008), and Dharamshala (39 ± 24 μg m^{-3} in PM_{10} during January-April, 2015, Kaushal et al., 2018). Lower PM_{10} mass concentration during winter was attributed to shallow boundary layer resulted due to low temperature. In winter, the average boundary layer height (using HYbrid Single–Particle Lagrangian Integrated Trajectory (HYSPLIT)-Global Data Assimilation System (GDAS) meteorological fields as an input) over the study site at 14:30 local time was 1494 m, which is lower than the altitude of the sampling location (Guru Shikhar, Mt. Abu, ~1680 m amsl). As a result, the study site was in the free troposphere (i.e. above the boundary layer) most of the time during winter. On the contrary, higher concentrations during pre-monsoon were ascribed to high dust loading under influence of strong westerly/southwesterly (SW) winds (Fig. 4.1).

Using Na^+ as a reference element for sea-salt correction (Keene et al., 1986), the non-sea-salt (nss) components of Ca^{2+}, K^+ and SO_4^{2-} were calculated (average nss-K^+: 90 %, nss-Ca^{2+}: 99 % and nss-SO_4^{2-}: 98 %). The observed nss fractions suggest insignificant sea-salts contribution to these species. Furthermore, chemically analyzed aerosol mass (referred to as $PM_{10\_measured}$) was quantitatively estimated based on nss-Ca^{2+} as a proxy for mineral dust (3.0% Ca in upper continental crust (UCC), Mclennan, 2001), Na^+ as proxy for sea-salts (1/3.5 of seal-salts) and (NH_4^+,

nss-SO_4^{2-} and NO_3^-) as proxy for anthropogenic sources, along with contribution from organic matter and EC (Rastogi and Sarin, 2009). Organic matter concentration was considered as 1.9 times that of OC which is used for aged aerosols (Kiss et al., 2002; Yttri et al., 2007).

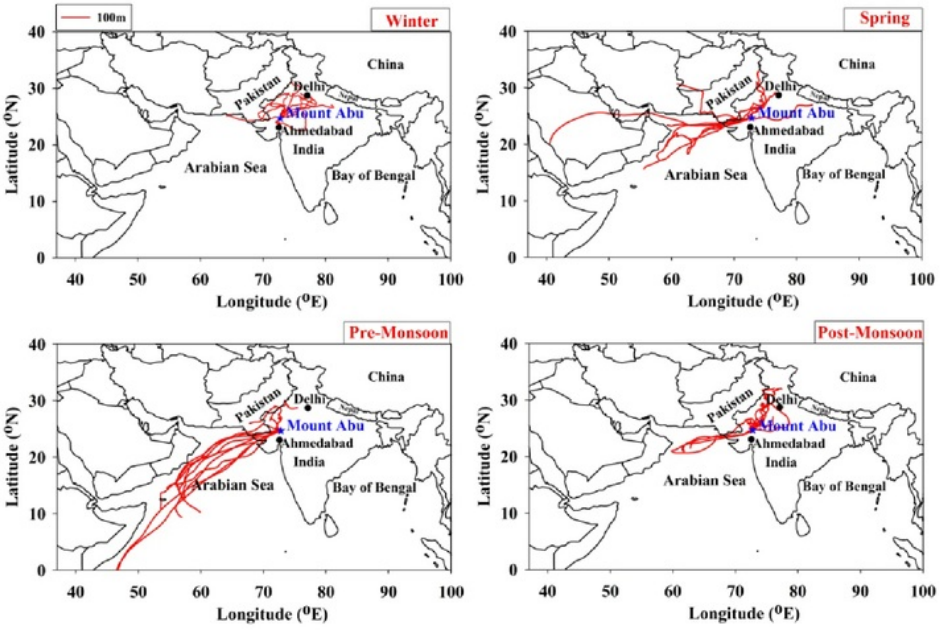

Figure 4. 1. *Five day back trajectories of air-masses arriving 100 m above ground level at Mount Abu during winter (December-January), spring (February-April), pre-monsoon (May-June) and post monsoon (October-November) are plotted using HYbrid Single–Particle Lagrangian Integrated Trajectory (HYSPLIT) model using the Global Data Assimilation System (GDAS, 1 degree, global, 2006-present) as input.*

$\mathbf{PM_{10\_measured}}$ = Mineral dust + Sea-salts + Anthropogenic Inorganics + Organic Matter (OM) + Elemental Carbon (EC)

$= \{[\text{nss-}Ca^{2+}] \times (100/3.0)\} + \{[Na^+] \times 3.5\} + \{[NH_4^+] + [\text{nss-}SO_4^{2-}] + [NO_3^-]\} + \{[OC] \times 1.9\} + \{[EC]\}$

Here, it is relevant to state that water-soluble nss-Ca^{2+} was used for estimating dust fraction in $PM_{10;}$ however, Mclennan (2001) had reported 3.0% total Ca (i.e., soluble + insoluble) in UCC and therefore, the estimated dust shall be considered as the lower limit of mineral dust fraction in PM_{10}. Furthermore, the variability in Ca^{2+} mass concentration during October 2001 to January 2003 (range: 0.59 — 3.32, avg: 1.90 ± 0.76 μg m^{-3}, 1σ, Rastogi and Sarin, 2005) and during January to December 2007 (range: 0.03 — 4.58 μg m^{-3}, Kumar and Sarin, 2010) was found within the range (0.10 — 6.44, avg: 2.03 ± 1.57 μg m^{-3}) observed in the present study over the same study site. Regression parameters (R = 0.83, slope = 0.80, N = 42, fig not shown) for scatter plot between chemically analyzed aerosol mass and gravimetrically measured aerosol mass suggest that on average ~20% fraction of PM_{10} is unknown. Majority of this unknown fraction would be mineral dust because we estimated the lower limit of mineral dust contribution using nss-Ca^{2+}.

Two year average [nss-SO_4^{2-}]/[NO_3^-] ratio in PM_{10} during the present study (3.1) is found to be a factor of two lower than that (5.6) reported by Rastogi and Sarin (2005) in TSP more than a decade ago over the same study site. This difference could arise due to the changes in regional pollution sources over a decadal time scale and/or due to differences in size of sampled particles in these two studies. However, latter case is less likely as one would not expect a big difference between TSP and PM_{10} concentrations over a high altitude site. Furthermore, nss-Ca^{2+} varied from 0.10 to 6.39 μg m^{-3} during the present study, which is higher than that reported earlier (0.59–3.31 μg m^{-3}) (Rastogi and Sarin, 2005). This observation suggests an increase in dust abundance over the study region. An eight times increase in [nss-SO_4^{2-}]/[nss-Ca^{2+}] ratio during the present study (5.6) compared to that (0.67) reported by Rastogi and Sarin (2005) suggests a significant increase of SO_4^{2-} aerosol i.e., anthropogenic contributions exhibited much larger increase over a period of ~15 years. Although less likely, but it could also be due to different SO_4^{2-} and Ca^{2+} abundances in PM_{10} and TSP.

Seasonally averaged contributions of different aerosol components fraction to PM_{10} are summarized in Fig. 4.2. On average, ~ 65% of the total PM_{10} was contributed by mineral dust followed by more or less equal contribution (~ 10 %) from OM and anthropogenic emissions. Further, sea-salts contributed only ~ 2.0 % followed by EC (~1.0 %) over the study site during the study period. High dust loading is common in the atmosphere over the study region during spring and pre-monsoon season (Rastogi and Sarin, 2005, 2006; Kumar and Sarin, 2010), and therefore, higher mass of dust (almost 80–90% of total PM_{10}) was observed. During these months, the boundary layer also experiences a strong temperature inversion due to cooling induced by dust in free troposphere, and resulting horizontal pressure gradient is responsible for strong surface winds (Pawar et al., 2015), which can bring minerals from the Arabian Desert land as well as from the great Thar Desert in absence of precipitation (Figs 4.1 and 4.2). In literature, high Ca^{2+} concentrations at Mauna Loa-USA and Lassen Volcanic National Park-USA during December to July were attributed to Asian dust events (Okamoto and Tanimoto, 2016 and references therein).

Furthermore, it was observed that contributions from OM, EC and anthropogenic emissions were reduced to almost half during spring and pre-monsoon compared to those during winter and post-monsoon. This is attributable to predominant westerly/southwesterly winds during spring and pre-monsoon, which are less polluted (Figs 4.1 and 4.2). Higher contribution from carbonaceous and anthropogenically emitted aerosol to PM_{10} during winter and post-monsoon could also be due to prevailing NE winds bringing pollutants from north Indian regions and enhanced vehicular emissions over the study site (Figs 4.1 and 4.2). Emissions from combustion sources such as a large scale crop-residue burning, bio-fuel and cow dung cakes burning, a variety of large and small scale industries, and numerous thermal power plants make the northern India region as an important source of OC, EC, sulphate, nitrate, ammonium, potassium and metals for downwind regions (Rastogi et al., 2014; Rajput et al., 2014; Singh et al., 2016a and b, Rajput et al., 2018). In

contrast, sea-salts contributed relatively more during spring and pre-monsoon under the influence of SW-winds bringing marine air-mass (Figs 4.1 and 4.2).

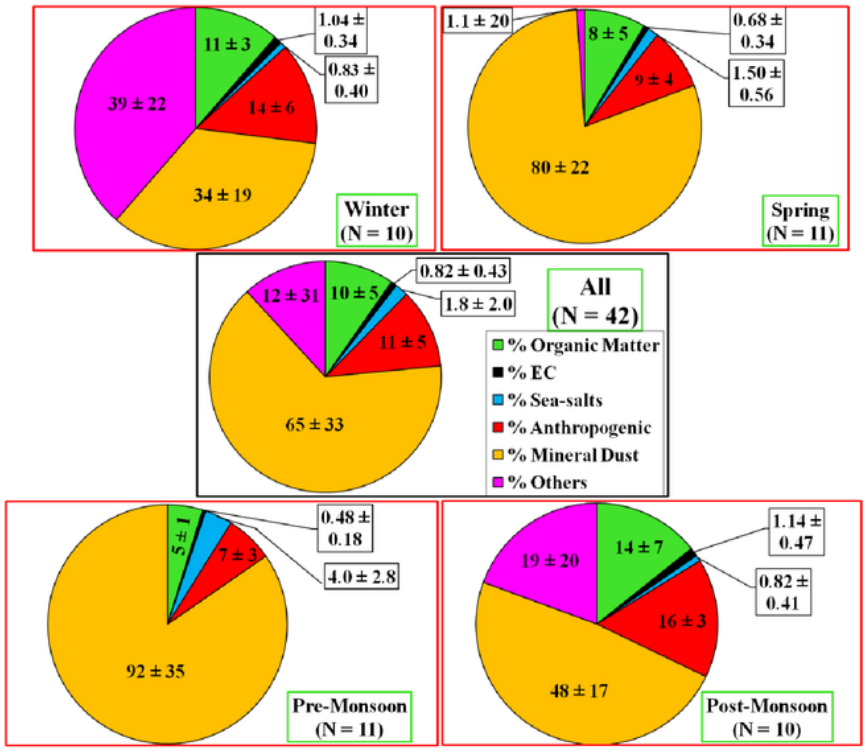

Figure 4. 2. *Seasonally averaged relative contribution (%) of different aerosol components to* PM_{10}.

4.2.2. OP of ambient PM_{10}

Table 4.1 depicts the variability of PM_{10} mass concentrations, chemical species, OP_V and OP_M during the study period. Variability in OP_V (nmol DTT min^{-1} m^{-3}) values observed in this study (0.09 – 3.04 is somewhat higher than those documented over Los Angeles (0.10–0.16, Hu et al., 2008) and Beijing (0.11–0.49, Liu et al., 2014), and similar to that reported over Orinda (0.37 – 2.50, Ntziachristos et al., 2007), Greece (0.84 – 3.10, Argyropoulos et al., 2016), Netherlands (1.4,

Janssen et al., 2014) and Patiala (1.30– 7.20, Patel and Rastogi, 2018a). However, OP_M values (2 – 43 pmol DTT min^{-1} μg^{-1}) observed during this study are found within the range reported worldwide (Ntziachristos et al., 2007; Hu et al., 2008; Liu et al., 2014, Argyropoulos et al., 2016). It means OP_V varies but OP_M does not vary drastically from region to region. This observation has broader implications in assessing effects of aerosol on human health. Seasonally averaged (± standard deviation, 1σ) OP_V over the study site were 0.76 ± 0.52, 1.44 ± 0.48, 1.04 ± 0.57, 1.69 ± 0.80 nmol DTT min^{-1} m^{-3}, whereas OP_M were 14 ± 8, 14 ± 7, 10 ± 7, 23 ± 9 pmol DTT min^{-1} μg^{-1} during winter, spring, pre-monsoon and post-monsoon, respectively. The highest OP_M and OP_V values were found during post-monsoon (October-November). Higher contribution of anthropogenically emitted aerosol to PM_{10} during post-monsoon is attributed to prevailing northeasterly (NE) winds bringing pollutants from north India, as discussed in previous section. The effect of emissions from biomass burning is also reflected in the form of highest contribution of organic matter (OM, 14 ± 7 %) during post-monsoon season in comparison to the rest of the seasons (Fig 4.2). The NE-winds were there in winter also which can bring pollutants from north India. However, lowest PM_{10} mass concentration and OP_V values were observed during winter months likely because the sampling site (Guru Shikhar, 1680 m amsl) remained above the boundary layer (in free troposphere) during winter, as discussed in previous section. On the contrary, OP_V values were reduced to almost half during spring and pre-monsoon. This is attributable to predominant westerly/southwesterly winds, which bring mineral dust and sea-salts (Figs 4.1 and 4.2). Both mineral dust and sea-salts are likely not DTT-active. The highest values of OP_V and OP_M (i.e. 3.04 nmol DTT min^{-1} m^{-3} and 43 pmol DTT min^{-1} μg^{-1}, respectively) observed during post-monsoon season were likely associated with "Diwali" festival, which is celebrated everywhere in India with large amount of firecrackers burning on the festival day occurring in October or November.

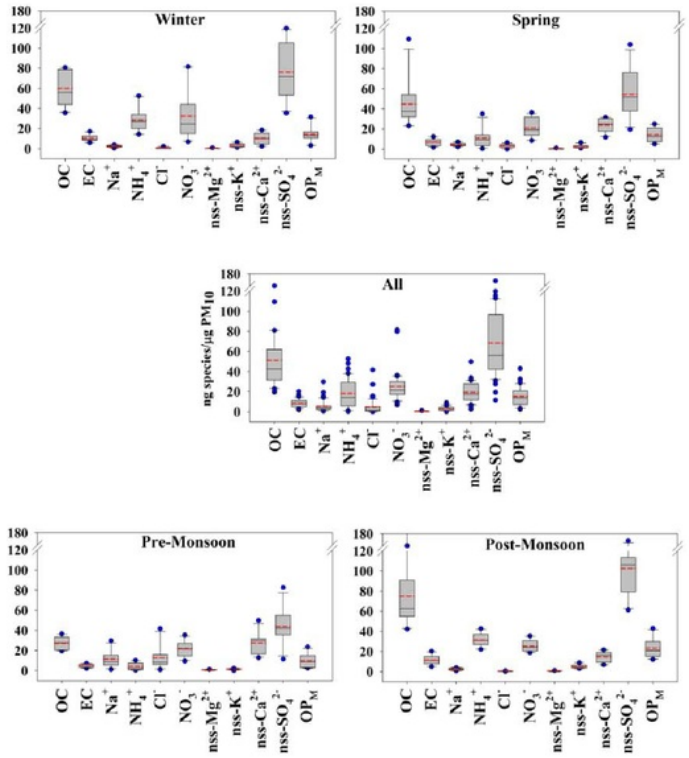

Figure 4. 3. *Box whisker plot depicting mass fractions of chemical species (ng species/µg PM_{10}) and OP_M. The boundary of the box closest to zero indicates the 25th percentile, black and red lines within the box represent median and mean, respectively, and the boundary of the box farthest from zero indicates the 75th percentile. Error bars above and below the box indicate the 90th and 10th percentiles respectively. Blue circles are indicative of outliers.*

In contrast, during spring and pre-monsoon seasons (March-June), higher PM_{10} mass concentrations were found to be associated with high dust loading along with relatively more sea-salts aerosol over the study region. This was primarily due to predominant strong SW/W winds (Figs 4.1 and 4.2). Further, in the absence of significant local sources and due to high latitudinal pressure gradient, the abundance of chemical species over this high altitude study site is expected to be affected by long-range transport during these months (Pawar et al., 2015). The observed lowest OP_M values during pre-monsoon were associated with high dust fraction (almost 90%) and relatively high sea-salts (about a factor of 4 times higher than that in winter

and post-monsoon), suggesting these natural aerosol are relatively not DTT-active. However, the increased activity of DTT based OP_V (0.19–0.49 nmol DTT min^{-1} m^{-3}) was reported during the dust storm over Beijing, China by Liu et al., 2014, which was less than those observed in present study during pre-monsoon. Further, OP_V and OP_M values were found somewhat higher during spring compared to pre-monsoon months likely due to mix (both from NE and SW) air-masses (Fig. 4.1). The OP_V values in spring (1.44 ± 0.48 nmol DTT min^{-1} m^{-3}) and pre-monsoon (1.04 ± 0.57 nmol DTT min^{-1} m^{-3}) are found to be a factor of ~2 and ~1.4 times higher than that during winter (0.76 ± 0.52 nmol DTT min^{-1} m^{-3}).

Seasonal changes were further different when expressed in OP_M. The OP_M during winter (14 ± 8 pmol DTT min^{-1} μg^{-1}) was found similar with those during spring (14 ± 7 pmol DTT min^{-1} μg^{-1}) and pre-monsoon (10 ± 7 pmol DTT min^{-1} μg^{-1}); whereas, significantly lower than that observed during post-monsoon (23 ± 9 pmol DTT min^{-1} μg^{-1}). Mass fraction of OC, NH_4^+, NO_3^-, Ca^{2+} and SO_4^{2-} components in PM_{10} were not consistent throughout the study period (Fig. 4.3). The variability found in OP_M was likely due to these aerosol species. The supply of these species to the study site was not continuous throughout the year as it depends upon their source(s), strength(s) and wind speed/direction. Large variability in OC during winter and post-monsoon seasons under the influence of NE air-masses suggest large variability in their sources, as discussed earlier.

Table 4. 1. *Statistical data (range, average standard deviation (±1σ) and sample number (N)) of measured species concentrations (μg m^{-3}) in aerosol along with OP_V and OP_M over Mt. Abu, and a few other sites reported in literature.*

Sampling Site	Period	Mass conc.	Constituents										OP_V	OP_M	N
			OC	EC	Na^+	NH_4^+	Mg^{+2}	K^+	Ca^{+2}	Cl^-	NO_3^-	SO_4^{2-}			
Present study Mt. Abu	Winter (Dec-Jan)	(29-74)[#] (49±15)	1.46-5.56 2.92±1.22	0.24-0.9 0.5±0.2	0.02-0.27 0.13±0.08	0.52-3.88 1.53±1.16	[#]BDL-0.1 0.03±0.04	0.05-0.36 0.18±0.12	0.10-1.02 0.53±0.37	[#]BDL -0.17 0.05±0.05	0.22-6.02 1.9±2.09	1.29-8.31 4.05±2.48	0.09-1.66 0.76±0.52	3-32 14±8	10
	Spring (Feb-April)	66-273 122±63	2.41-10.2 4.9±2.29	0.47-0.93 0.67±0.15	0.14-0.92 0.53±0.29	0.09-2.3 0.99±0.59	[#]BDL-0.31 0.1±0.09	0.16-0.43 0.27±0.08	0.78-5.05 2.95±1.49	[#]BDL -1.32 0.46±0.43	1.25-3.49 2.22±0.75	4.32-7.61 5.72±1.16	0.69-2.17 1.44±0.48	5-25 14±7	11
	Pre-Monsoon (May-June)	75-232 133±56	1.97-7.73 3.54±1.65	0.35-0.89 0.58±0.20	0.26-3.07 1.34±0.87	0.05-0.99 0.47±0.36	[#]BDL -0.54 0.22±0.18	0.12-0.32 0.21±0.07	2.07-6.44 3.38±1.21	0.23-4.34 1.52±1.32	1.81-3.43 2.59±0.55	2.73-7.64 5.46±1.55	0.42-2.03 1.04±0.57	2-24 10±7	11
	Post-Monsoon (Oct-Nov)	49-121 72±21	3.04-8.52 5.19±2.08	0.32-1.12 0.78±0.28	0.05-0.34 0.16±0.09	1.15-3.02 2.21±0.54	[#]BDL -0.12 0.06±0.04	0.17-0.58 0.36±0.15	0.44-1.64 1.01±0.33	[#]BDL -0.08 0.04±0.02	1.29-2.43 1.76±0.37	3.70-9.24 7.21±1.75	0.74-3.04 1.69±0.80	12-43 23±9	10
	All (Mar'14 – May'16)	29-273 96±56	1.46-10.2 4.14±2.03	0.24-1.12 0.63±0.23	0.02-3.07 0.56±0.67	0.05-3.88 1.27±0.95	[#]BDL -0.54 0.11±0.13	0.05-0.58 0.26±0.12	0.10-6.44 2.03±1.57	[#]BDL -4.34 0.54±0.92	0.22-6.02 2.13±1.14	1.29-9.24 5.61±2.04	0.09-3.04 1.23±0.68	2-43 15±9	42
[a]Milan, Northern Italy_ Traffic side	Winter (Jan-Feb, 2013)	129±60	26±17	6.2±2.9		3.9±1.4		5.6±2.4	2.6±1.2	3.7±3.4	16.5±6.6	4.0±1.5	0.04±0.03	0.33±0.18	5
	Summer (Jul, 2013)	50±7	7.5±0.8	1.5±0.4		2.7±0.4		0.27±0.05	1.6±0.3	0.1±0	5.7±2.2	3.5±0.3	0.1±0.05	1.92±1.07	7
	Late Summer (Oct, 2013)	57±19	9.0±3.2	2.6±1.1		4.2±2.9		0.71±0.74	1.6±0.7	0.7±0.8	10.9±6.6	4.2±2.6	0.15±0.06	3.34±2.94	10
[b]Los Angeles, USA	March-May 2007	2.2-12.5 8.5±3.6	5.5-12.7 8.4±2.4	0.6-1.8 1.1±0.4	9.7-16.9 12.4±2.5	0.7-2.8 1.4±0.8		0.5-1.1 0.6±0.2			11.2-23.4 17.6±4.8	3.8-8.9 5.9±1.7		8-18 13±4	6
[c]Los Angeles Basin, USA	Jan, 2005	8.3	21	0.4							3.5	1.4		17	1
San Francisco, Orinda, Bore 1	Sept, 2004	0.5	38	1.2							3.3	2.7		19	1
San Francisco, Orinda, Bore 2	Sept, 2004	0.7	14	0.4							0.6	2.2		32	1
[d]Mar-May, 2012 Peri-urban Site	Non dust Storm Days	(50-410) 140			1.06±0.48	0.89±0.3	0.25±0.08	0.25±0.08	5.14±0.88	0.75±0.26	1.65±1.32	1.84±1.31	(0.12-0.28)		18
	Dust Storm				1.83±0.52	1.4±0.13	0.43±0.10	0.46±0.12	8.99±1.75	1.61±0.51	2.63±1.34	3.71±1.87	(0.29-0.49)		9
Central Beijing Site	Non dust Storm Days	(20-270) 100			1.57±0.52	1.85±0.57	0.60±0.19	0.41±0.15	4.73±1.04	1.31±0.41	3.99±1.69	2.97±0.62	(0.10-0.24)		18
	Dust Storm				1.79±0.52	1.98±0.65	0.72±0.25	0.48±0.12	6.65±1.41	1.87±0.56	4.58±1.22	3.65±1.09	(0.19-0.31)		9

ǂvariability, (average ± SD, 1σ)
#Below detection limit
[a] Perrone et al., 2016; OP_V - nM DTT min^{-1} m^{-3}; OP_M - nM DTT min^{-1} μg^{-3}
[b]Hu et al., 2008; Coarse; constituent values are in %,
[c]Ntziachristos et al., 2007; Coarse; constituent values are in %,
[d]Liu et al., 2014; $PM_{2.5}$

4.2.3. Linear regression analysis between OP and PM_{10} constituents

Pearson's correlation between OP values (OP_V and OP_M) and PM species (respective volume and mass normalized based) measured in the present study were assessed, and depicted in Table 4.2. During winter, majority of species, except OC, Mg^{2+} and Ca^{2+}, showed positive ($R > 0.60$) and significant correlation with OP_V whereas large scatter was observed with OP_M. This suggests uniformity of PM composition during these months (Table 4.2, Fig. 4.3). Intrinsic OP (OP_M) of PM species during spring months was associated with NH_4^+ and SO_4^{2-} whereas the same was associated with EC, K^+ and NO_3^- during pre-monsoon months. Present study shows a significant positive correlation between OP_M and secondary inorganic aerosol (SIA, such as NH_4^+, NO_3^- and SO_4^{2-} mass fractions) during spring, which is inconsistent with the previous study carried out over Patiala (Patel and Rastogi, 2018a), as well as the other studies (Hu et al., 2008; Verma et al., 2012, 2014) (Table 4.2). The SIA would not be responsible for the observed OP as they were reported to be DTT-inactive through laboratory experiment (Patel and Rastogi, 2018a). Most of aerosol species collected over the present study site are expected to travel far from the emission sources before reaching to the sampling region. It is possible that DTT-active species also travelled along with SIA and that is why this correlation is observed. A positive and significant correlation of OP_M with EC and K^+during pre-monsoon (Table 4.2) is consistent with our previous study (Patel and Rastogi, 2018a), which documented that combustion sources are the source of DTT-active species. The OP_V during spring and pre-monsoon were not strongly correlated with NH_4^+ and K^+ ($R < 0.40$, when 70-80% of PM_{10} mass was dust), unlike that during winter and pre-monsoon ($R = \sim 0.70$ at $p<0.05$, when dust contribution was 25-40%) (Fig. 4.2,

Table 4.2). This further suggests that sources/transport which contribute NH_4^+ and K^+ could be responsible for the observed OP during winter and pre-monsoon months.

Since sea-salts are not found to be DTT-active, nss fraction of species were calculated and used for relevant species. On annual scale, combustion derived (such as EC and nss-K^+) and other anthropogenically derived inorganic species (such as NH_4^+ and nss-SO_4^{2-}) or, unmeasured species transported along with these species are expected to be responsible for the observed OP (both OP_M and OP_V) (Table 4.2). Cho et al., 2005 have documented that EC correlate positively with DTT-activity, and attributed it to the co-emissions of EC and DTT-active species from same source. Similar observation was also reported by Patel and Rastogi (2018a).

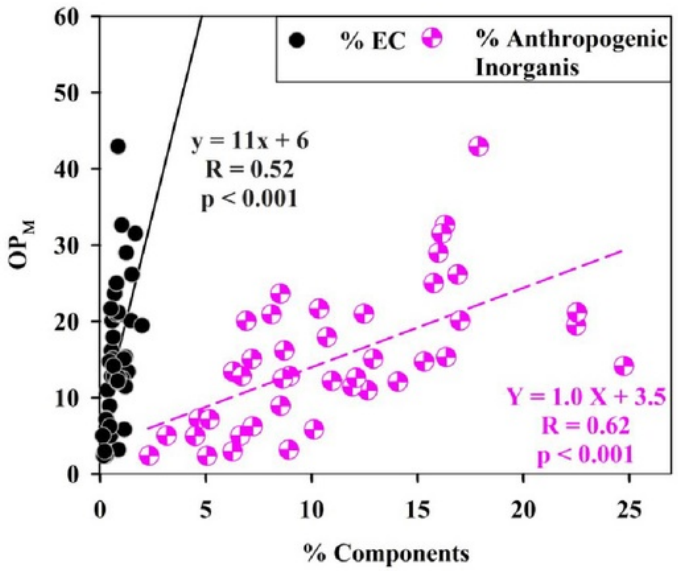

Figure 4. 4. *Scatter plot of OP_M with % EC mass fraction and % anthropogenically derived inorganic mass fraction.*

Furthermore, the temporal variability in PM_{10} and the percentage contribution of its component's sources (i.e. mineral dust, EC, anthropogenic inorganics, organic matter, sea-salt) with both OP_V and OP_M show that OM, EC and anthropogenically derived inorganics followed the same trend which is shown by OP (both OP_V and

OP_M) (fig not shown). On the contrary, dust and sea-salts didn't follow the temporal trend of OP, as expected. In present study, the contribution of OM, EC and anthropogenically derived inorganics to PM_{10} had increased during post-monsoon and winter under the influence of NE winds (as discussed in previous section). It is inferred that the source (s) emitting EC also emit other species, which are more DTT-active than those species which are emitted along with anthropogenically derived inorganic species throughout the study period (Fig. 4.4).

Table 4. 2. *Correlation coefficient (R) of volume and mass normalized species concentrations with OP_V and OP_M respectively. Values marked in red and bold font are significant at $p < 0.05$.*

Red and bold, p<0.05		Present study					Milan, Northern Italy[$]	Los Angeles, USA[Φ]	Central Atlanta[@]	
		All	Winter	Spring	Pre-Monsoon	Post-Monsoon			Water extract	Methanol Extract
Number of samples (n)		42	10	11	11	10	22	18	8	8
OP_V	OC	**0.37**	0.37	0.07	-0.14	0.38	-0.30			
	EC	**0.51**	**0.85**	-0.05	0.57	0.15	-0.27			
	Na^+	-0.16	**0.67**	0.11	-0.41	0.07				
	NH_4^+	**0.46**	**0.70**	0.33	0.35	**0.69**	0.06			
	Mg^{+2}	-0.25	0.02	-0.31	-0.56	-0.27				
	K^+	**0.63**	**0.64**	-0.17	0.43	**0.69**	**0.39**			
	Ca^{+2}	0.07	0.49	-0.08	0.10	0.22	-0.19			
	Cl^-	-0.23	**0.78**	-0.02	-0.52	0.09	-0.35			
	NO_3^-	0.18	**0.65**	-0.13	0.17	0.22	-0.11			
	SO_4^{2-}	**0.56**	**0.77**	0.36	-0.08	0.51	0.16			
OP_M	OC	**0.43**	-0.28	0.58	0.53	0.08			**0.78**	**0.84**
	EC	**0.52**	0.51	0.52	**0.86**	0.03			0.3	**0.74**
	Na^+	-0.26	0.47	-0.01	0.03	-0.03		**−0.80**		
	NH_4^+	**0.57**	0.32	**0.76**	0.34	0.41		0.38	−0.57	**−0.83**
	Mg^{+2}	**-0.32**	-0.24	-0.43	-0.10	-0.48				
	K^+	**0.69**	0.54	0.57	**0.84**	0.48		**−0.53**		
	Ca^{+2}	-0.13	0.50	-0.21	0.43	-0.05				
	Cl^-	**-0.34**	**0.64**	-0.49	-0.20	0.03				
	NO_3^-	0.24	0.38	0.33	**0.62**	-0.22		**−0.74**	−0.37	**−0.68**
	SO_4^{2-}	**0.65**	0.55	**0.75**	0.49	0.27		0.27	−0.65	**−0.79**

[$] *Perrone et al., 2016, TSP, methanol extract*
[Φ] *Hu et al., 2008, All size (Quasi-UF, Accumulation, Coarse), aqueous particle suspension in MQ*
[@] *Verma et al., 2012, $PM_{2.5}$, Jan-Feb, 201*

4.3. Marine Environments

4.3.1. Introduction

Atmospheric deposition of aerosol is among the major sources of nutrients to the open ocean (Jickells TD et al., 2005; Mahowald et al., 2005). Micro-nutrients (trace metals) are not only important in regulating the primary productivity, but also shown to be associated with negative effects (Sunda, 2013). One of the negative effects can be the production of higher levels of ROS in ocean waters (Lesser, 2006). ROS are ubiquitous in the ocean surface water, and the H_2O_2 has the longest life time (Lesser, 2006).

Field studies showed particle associated production of superoxide anion in the ocean, which indicate its biological origin (Rose et al., 2008; Schneider et al., 2016). Further, biological production of superoxide anion through dismutation also plays an important role in seawater H_2O_2 production. In addition to in-situ production of ROS by phytoplankton during photosynthesis and respiration as a part of their metabolism in the marine system, atmospheric deposition of some aerosol may also enhance ROS concentration in surface water. ROS can be produced in the atmosphere and bound to ambient particles, which are known as particle-bound or exogenous ROS. Atmospheric deposition of such particle-bound ROS may result in significant increase in ROS concentrations in surface waters (Cooper et al., 1987; Gerringa et al., 2004; Yuan and Shiller, 1999). Further, Tolar et al., 2016 reported several pathways for the ROS production in marine environments, which include by-products of photosynthesis, photochemical reactions of colored dissolved organic matter (CDOM) and metals, atmospheric exchange and rain, and production by heterotrophic bacteria through respiration. By any means when the level of ROS exceeds the defense mechanisms, oxidative stress is generated which can pose a threat to cell by causing damage to bio-molecules such as DNA, lipids and nucleic acids (Lesser, 2006).

To understand the transformation in aerosol physicochemical properties during the transportation from continents to the open ocean, locations like the Arabian Sea and the Bay of Bengal (BoB) in certain seasons are ideal. Continental outflow from south Asia and the Arabian Desert to the Arabian Sea is conspicuous characteristic during pre-monsoon months (Kumar et al., 2008a; Lawrence and Lelieveld, 2010; Srinivas and Sarin, 2013). The BoB, situated in the eastern part of northern Indian Ocean and confined by land from three sides, is one of the ideal regions to study the impact of continental aerosol transported to the marine environment. This region is largely affected by the winds originating from north/north-eastern region of Indian subcontinent as well as from south-east Asian countries during the late northeast monsoon. Srinivas et al., 2012 documented the difference in chemical characteristics of mineral dust reaching to two different oceanic regions (the Arabian Sea and the BoB) due to different chemical processing during the long-range transport. Such processes can also alter aerosol OP.

No studies worldwide, to the best of our knowledge, have reported OP of ambient aerosol over the marine environments. The present study reports chemical composition and DTT-based OP of ambient PM_{10} over the Arabian Sea during April, 2017 and the Port Blair (BoB) during February to April, 2013.

4.3.2. The Arabian Sea

4.3.2.1. PM_{10} composition

PM_{10} mass concentration over the MABL of the Arabian Sea varied from 61 to 184 μg m^{-3} (avg: 105, sd: 26, 1σ), which is attributable to winds bringing aerosol from different type of sources (anthropogenic, marine, mineral dust). Using Na^+ as a reference element for sea-salt correction (Keene et al., 1986), the non-sea-salt (nss) fraction of K^+, Mg^{2+}, Ca^{2+} and SO_4^{2-} were calculated. A clear contrast in nss fractions was observed during the study period with initial 10 samples showing very less contribution from sea-salts (average nss-K^+: 93%, nss-Ca^{2+}: 97% and nss-SO_4^{2-}: 98%); whereas sea-salts contributions were noticeable during the latter period of the

cruise (nss-K^+: 63% nss-Ca^{2+}: 91% and nss-SO_4^{2-}: 87%) (Fig. 4.6). A significant fraction of Mg^{2+} was observed to be emitted from sea-salt in most of the samples (nss-Mg^{2+}: ranging from 1 to 66%).

To identify the source (s) of air masses for the collected samples, five-day air mass back trajectories ending at 1000 m above mean sea level were investigated using the GDAS (1°, global, 2006–present) meteorological data set as input in the HYSPLIT model, and samples were accordingly classified in two categories. Initial 10 samples (defined as Class-A) were found to be associated with the air masses travelled from Indian continent, whereas the latter study period (Class-B) received the air masses from open ocean and from the Arabian continent (Fig. 4.5).

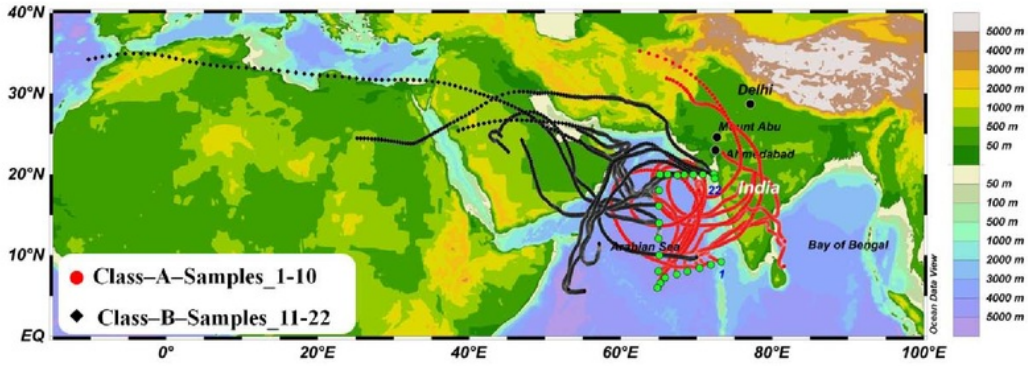

Figure 4. 5. *Five-day air mass back trajectories ending 1000 m above sampling locations using GDAS meteorological data (1 degree, global, 2006-present) as input in HYSPLIT model. Green circles show the start and stop point of aerosol sampling location over the Arabian Sea.*

Further, chemically analyzed aerosol mass was used for quantitative estimation of contributions from different sources using the approach given in Rastogi and Sarin (2009) and Patel and Rastogi (2018b). Estimated mass was calculated using nss-Ca^{2+} as a proxy for mineral dust (3.0% Ca in upper continental crust (UCC) (Mclennan, 2001)), Na^+ as proxy for sea-salts (1/3.5 of seal-salts) and (NH_4^+, NO_3^-, nss-SO_4^{2-}) as proxy for anthropogenic inorganic sources, along with

contribution from organic matter (OM = OC × 1.9) and EC. Gravimetrically obtained mass was reasonably similar to estimated aerosol mass (slope = 0.72, R^2 = 0.79, N = 17). Here, five samples (from Class-B) were excluded from this regression as outliers. Air mass back trajectories for excluded samples were found to be originated from the Arabian continent which indicates the possibility of overestimation of dust fraction in PM_{10}. Further, (NH_4^+ + nss-K^+) were found to be non-linear with acidic species (nss-SO_4^{2-} + NO_3^-), unlike that reported over continental sites (Rastogi et al., 2016, 2014). However, initial eight samples (from continental site) showed linearity among these species. These observations suggest that different air masses might have traveled to the study region during the sampling period. In general, ammonia plays a major role in converting the sulfuric acid to its neutral form (ammonium sulfate). Further, reaction between ammonia and nitric acid forms ammonium nitrate which requires "free ammonia". Based on their concentrations (in equivalent unit), it was estimated that (NH_4^+ + nss-K^+) neutralize about thirty percent of the total acidic species (NO_3^- + nss-SO_4^{2-}) in the initial eight samples, when the air masses were associated with the Indian continent. This observation suggests the presence of ~ 70% excess acid (given by (NO_3^- + nss-SO_4^{2-}) – (NH_4^+ + nss-K^+)) in the samples under Class-A. However, concentration of nss-K^+ was insignificant in comparison to that of NH_4^+. Further, mineral dust (nss-Ca^{2+} + nss-Mg^{2+}) was found to be neutralizing ~ 74% of the total excess acid. This observation suggests that there was still some free acid (~ 26%), estimated as (NO_3^- + nss-SO_4^{2-}) – ((NH_4^+ + nss-K^+ + nss-Ca^{2+} + nss-Mg^{2+}) in Class–A samples. This free acid was found to be strongly and positively correlated (slope = 0.85, R^2 = 0.90, $p < 0.001$) with sea-salt aerosol (i.e. Na^+). As a result, these Class–A samples showed ~ 95% depleted-Cl^- (Fig. 4.6f). The amount of depleted-Cl^- is found to be significantly correlated with the free acid (R^2 = 0.90, $p < 0.001$). Previous studies over the marine region surrounding India also reported Cl^--depletion due to the polluted air masses (Kumar et al., 2008; Sarin et al., 2010). Interestingly, % depleted-Cl^- was also positively and significantly correlated (slope = 1.14, R^2 = 0.70, fig not shown) with OP_M, suggesting the importance of free acid in

the catalytic generation of ROS. It could be due to enhanced solubility of DTT-active metals in presence of free acid. In contrast, the mass fraction of mineral dust was ~ 2.3 times higher in Class-B samples in comparison to Class-A samples (Fig. 4.6a). In addition, acidic species in PM_{10} of Class-B were found to be more or less fully neutralized by mineral dust (slope = 1.17, R^2 = 0.66). Further, sea-salt abundance (based on Na^+) in Class-B samples were ~ 6 times higher than that in Class-A samples (Fig. 4.6e); however, free acid concentration didn't increase proportionally. Therefore, relatively less depleted-Cl^- was observed in these samples (Fig. 4.6f).

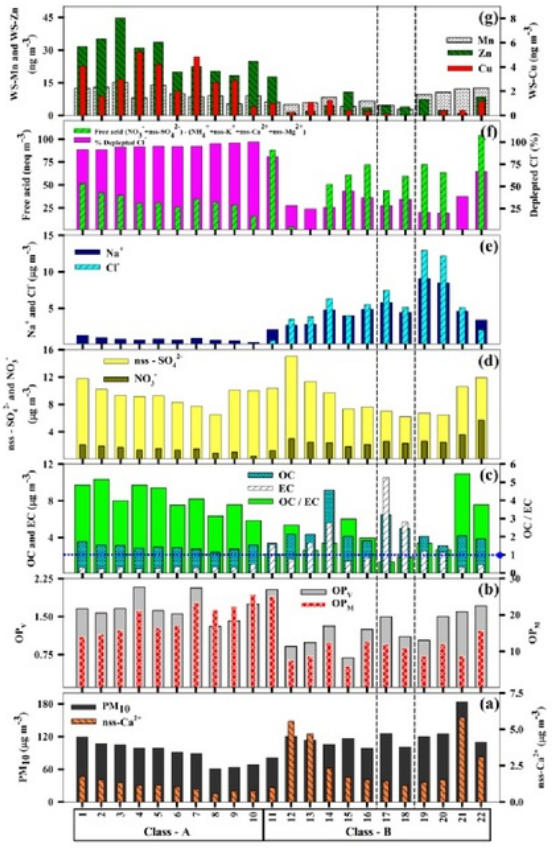

Figure 4. 6. *Temporal variability of (a) PM_{10} and nss-$\boldsymbol{Ca^{2+}}$ concentrations, (b) OP_V and OP_M, (c) OC and EC concentration along with OC/EC ratio, (d) nss-$\boldsymbol{SO_4^{2-}}$ and $\boldsymbol{NO_3^-}$ concentration, (e) $\boldsymbol{Na^+}$ and $\boldsymbol{Cl^-}$ concentration, (f) estimated free acid and depleted–$\boldsymbol{Cl^-}$, and (g) WS–Mn, WS–Zn and WS–Cu metals concentration. Two*

samples, highlighted between black dotted lines, are likely affected by chimney emissions. In (c), OC/EC ratio value of 1.0 is shown by horizontal dotted line.

4.3.2.2. OP and PM_{10} composition

The OP_V varied from 0.69 to 2.08 nmol DTT min^{-1} m^{-3} (1.47 ± 0.37; average ± 1σ) during the study period (Table 1). These OP_V values are higher than those observed over Hangzhou city, China (range; 0.11 – 1.66 nmol DTT min^{-1} m^{-3}, Wang et al., 2019), Beijing (0.018 ± 0.28 nmol DTT min^{-1} m^{-3}, Liu et al., 2014) and Shanghai (average; 0.13 nmol DTT min^{-1} m^{-3}, Lyu et al., 2018); whereas, lower than those observed over the Indo-Gangetic Plain, India (1.3 – 7.2; 3.8 ± 1.4 nmol DTT min^{-1} m^{-3}, Patel and Rastogi, 2018a), and similar to those observed over Mt. Abu, India during spring season (0.69 – 2.17; 1.44 ± 0.48 nmol DTT min^{-1} m^{-3}, Patel and Rastogi, 2018b). On the other hand, the OP_M values varied from 6 to 26 pmol DTT min^{-1} μg^{-1} (15 ± 6) during the study period, which are comparable with those observed over Mt. Abu during spring season (5 – 25; 14 ± 7 pmol DTT min^{-1} μg^{-1}, Patel and Rastogi, 2018b), Los Angeles Beach Port (average 13 pmol DTT min^{-1} μg^{-1}, Hu et al., 2008) and Lecce urban-background (10.7 ± 6.6 pmol DTT min^{-1} μg^{-1}, Pietrogrande et al., 2018), whereas lower than those observed over Downey Riverside (23 ± 9 pmol DTT min^{-1} μg^{-1}, Ntziachristos et al., 2007). Also, OP_V (1.30 ± 0.38) and OP_M (12 ± 5) associated with Class-B samples showed ~ 1.5 times lower values as compared to OP_V (1.67 ± 0.25) and OP_M (19 ± 4) associated with Class-A samples.

EC mass fraction is found to be positively correlated with OP_M in Class-A samples (slope = 8.6, R = 0.73, $p < 0.05$, Fig. 4.7a) in which aerosol are expected to be transported from the Indian continent. On the contrary, no significant relationship between these components was observed in Class-B samples, where aerosol composition is expected to be dominated by desert dust and/or marine emissions. This observation suggests that the source (s) emitting EC in Indian continent also emit other species which may be responsible for the observed OP. The EC is a marker of incomplete combustion of fossil fuel and biomass burning. EC is reported to be

positively correlated with DTT-based OP elsewhere also (Cho et al., 2005; Patel and Rastogi, 2018a, 2018b). The slope (8.6) between EC mass fraction and OP_M observed in this study is found to be similar to that documented over a high altitude site Mt Abu (11, Patel and Rastogi, 2018b), but a factor of 2 higher than that documented over a semi-urban city Patiala (4.6, Patel and Rastogi, 2018a) This observation suggest that the aging of aerosol make it more DTT-active, as both the Arabian Sea and the Mt Abu predominantly receive aged aerosol.

Furthermore, when the categorized data was investigated for WSOC mass fraction, it was also found to be significantly and positively correlated with OP_M in Class-A samples (slope = 4.8, R = 0.88, Fig. 4.7b). However, the relationship of OP_M with WSOC mass fraction was not as prominent as observed with EC mass fraction (see the slopes of Figs. 4.7a and 4.7b). Further, WSON mass fraction for all the samples were observed to be positively correlated with OP_M (slope = 24, R = 0.79, N = 21, Fig. 4.7c). Highest OP_M (25 pmol DTT min^{-1} μg^{-1}) is found to be associated with the highest mass fraction of WSON. This observation suggests that likely water-soluble nitrogenous organics are highly DTT-active. Such an observation is not reported in literature, to the best our knowledge. On an average, contribution of WSON to total nitrogen was ~ 15% which is consistence with the previous studies (Chen et al., 2006; Rastogi et al., 2011; Srinivas and Sarin, 2013). From ocean biogeochemistry perspective also, it is important to note that WSON is a significant fraction of reactive nitrogen over the study region. Long-range transport of DTT-active species from continents to the marine environments, and their subsequent deposition may enhance the surface ROS concentration that may further influence the marine biogeochemistry of nitrogen species (Tolar et al., 2016). This observation has an important implication in the ocean biogeochemical cycle.

Table 4. 3. *Statistical parameters (min – max; avg ± sd) of PM_{10} and its chemical components (μg m^{-3}) along with volume normalized OP (OP_V) and mass normalized OP (OP_M).*

(Min – Max); (Avg ± SD, 1σ)	Present study			Johansen and Hoffmann, (2004)				Kumar et al., (2008)
Components	All (N = 22)	Class-A (N = 10)	Class-B (N = 12)	March, 1997 Group 1 (IO97-01- IO97- 10)		March, 1997 Group 2 (IO97-11- IO97- 27)		March – May, 2006 (N =19)
				Fine (N = 26)	Coarse (N = 25)	Fine (N = 26)	Coarse (N = 25)	
PM_{10}	61 – 184; 105 ± 26	61 – 119; 90 ± 20	81 – 184; 117 ± 25	–	–	–	–	8.2 – 46.9; 24.7 ± 10.4
$^{\#}OP_M$	6 – 26; 15 ± 6	14 – 26; 19 ± 4	6 – 25; 12 ± 5	–	–	–	–	–
$^{\dagger}OP_V$	0.69 – 2.08; 1.47 ± 0.37	1.31 – 2.08; 1.67 ± 0.25	0.69 – 2.03; 1.3 ± 0.38	–	–	–	–	–
OC	2.38 – 9.14; 3.87 ± 1.49	2.38 – 3.54; 2.95 ± 0.32	3.07 – 9.14; 4.63 ± 1.67	–	–	–	–	BDL – 0.68; 0.21 ± 0.15
EC	0.58 – 10.52; 2.15 ± 2.4	0.58 – 1.11; 0.74 ± 0.15	0.76 – 10.52; 3.33 ± 2.77	–	–	–	–	BDL – 0.2; 0.08 ± 0.03
WSOC	1.46 – 4.05; 2.29 ± 0.7	1.46 – 2.33; 1.83 ± 0.27	1.9 – 4.05; 2.68 ± 0.72	–	–	–	–	–
WSON	0.09 – 0.61; 0.27 ± 0.16	0.2 – 0.61; 0.35 ± 0.13	0.09 – 0.59; 0.2 ± 0.15	–	–	–	–	–
Na^+	0.37 – 9.08; 2.95 ± 2.56	0.37 – 1.28; 0.79 ± 0.25	2.1 – 9.08; 4.75 ± 2.15	0.22 – 0.64; 0.35 ± 0.14	0.19 – 0.64; 0.46 ± 0.14	0.13 – 0.65; 0.35 ± 0.15	0.21 – 1.01; 0.52 ± 0.21	0.22 – 10.27; 1.92 ± 2.43
NH_4^+	0.4 – 2.54; 1.32 ± 0.67	1.4 – 2.54; 1.95 ± 0.36	0.4 – 1.36; 0.8 ± 0.29	*566 – 1410; 904 ± 248	*11.8 – 84.3; 50.8 ± 22.3	*232 – 1210; 508 ± 238	*12.8 – 76.2; 31.7 ± 13.1	BDL
Mg^{2+}	0.13 – 1.09; 0.47 ± 0.29	0.13 – 0.32; 0.2 ± 0.06	0.33 – 1.09; 0.68 ± 0.21	*25.5 – 58.6; 44.0 ± 11.2	*30.5 – 97.5; 63.7 ± 22.4	*31.1 – 88.2; 54.9 ± 17.4	*24.2 – 131; 70.7 ± 31.2	0.04 – 1.13; 0.2 ± 0.26
nss-Mg^{2+}	$^{\$}$BDL – 0.28; 0.11 ± 0.07	0.06 – 0.16; 0.11 ± 0.03	BDL – 0.28; 0.11 ± 0.1	*BDL – 23.1; 2.91 ± 13.4	*BDL – 27.7; 9.11 ± 11.75	*BDL – 43.4; 13.5 ± 12.9	*BDL – 47; 8.76 ± 19.80	–
K^+	0.35 – 0.69; 0.46 ± 0.08	0.35 – 0.58; 0.43 ± 0.07	0.37 – 0.69; 0.48 ± 0.09	*105 – 277; 192 ± 58	*12.8 – 65.7; 34.0 ± 13.9	*52.6 – 385; 139 ± 90	*11.1 – 65.7; 25.9 ± 12.4	0.04 – 0.42; 0.12 ± 0.08
nss-K^+	0.18 – 0.61; 0.35 ± 0.11	0.33 – 0.57; 0.4 ± 0.07	0.18 – 0.61; 0.31 ± 0.12	*96.5 – 253; 179.4 ± 56.2	*5.9 – 42.1; 17.0 ± 10.5	*43.3 – 361; 125.7 ± 86.8	*BDL – 4.21; 6.63 ± 8.69	–
Ca^{2+}	0.61 – 5.99; 2.03 ± 1.53	0.61 – 1.81; 1.12 ± 0.38	1.09 – 5.99; 2.78 ± 1.74	*8.23 – 132; 72.0 ± 42.8	*126 – 482; 257 ± 134	*56.2 – 300; 121 ± 69	*59.1 – 705; 327 ± 184	0.12 – 2.24; 0.85 ± 0.56
nss-Ca^{2+}	0.58 – 5.81; 1.92 ± 1.51	0.58 – 1.76; 1.09 ± 0.37	1.01 – 5.81; 2.6 ± 1.77	*BDL – 119; 58.8 ± 41.5	*111 – 459; 240 ± 131	*43.1 – 288; 108.1 ± 69.1	*44.2 – 680; 307 ± 184	–
Cl^-	BDL – 12.93; 3.15 ± 3.92	BDL – 0.2; 0.07 ± 0.06	0.61 – 12.93; 5.72 ± 3.68	0.1 – 0.07; 0.02 ± 0.02	0.15 – 0.9; 0.47 ± 0.22	0.03 – 0.4; 0.09 ± 0.08	0.13 – 1.55; 0.75 ± 0.41	BDL – 15.26; 2.16 ± 3.88
NO_3^-	0.46 – 5.69; 2.1 ± 1.09	0.46 – 2.15; 1.38 ± 0.5	1.27 – 5.69; 2.7 ± 1.1	0.04 – 0.26; 0.11 ± 0.07	0.71 – 1.41; 0.99 ± 0.27	0.08 – 0.36; 0.18 ± 0.10	0.31 – 0.99; 0.66 ± 0.21	BDL – 1.34; 0.4 ± 0.4

SO_4^{2-}	6.7 – 15.8; 10 ± 2.1	6.7 – 12.1; 9.4 ± 1.5	7.3 – 15.8; 10.4 ± 2.4	2.47 – 5.25; 3.70 ± 0.83	0.11 – 0.46; 0.35 ± 0.11	1.46 – 3.16; 2.35 ± 1.24	0.18 – 0.58; 0.34 ± 0.12	–
nss-SO_4^{2-}	6.2 – 15.1; 9.2 ± 2.2	6.5 – 11.8; 9.2 ± 1.5	6.2 – 15.1; 9.2 ± 2.7	2.41 – 5.09; 3.61 ± 0.81	0.06 – 0.33; 0.23 ± 0.08	1.36 – 3.11; 2.27 ± 1.22	0.04 – 0.33; 0.18 ± 0.10	1.3 – 5.7; 2.9 ± 1.2
*WS–Al	6 – 174; 36 ± 34	15 – 39; 28 ± 8	6 – 174; 42 ± 45	–	–	–	–	0.21 – 1.89; 0.85 ± 0.47¥
*WS–Ti	1.86 – 26; 8 ± 7	1.86 – 6; 4 ± 2	3.12 – 26; 11 ± 8	–	–	–	–	–
*WS–V	0.91 – 3.48; 1.83 ± 0.8	0.91 – 3.06; 1.68 ± 0.76	0.98 – 3.48; 1.96 ± 0.85	–	–	–	–	–
*WS–Fe	0.4 – 111; 18 ± 22	5.2 – 22; 12 ± 5	0.4 – 111; 23 ± 29	–	–	–	–	0.09 – 1.01; 0.44 ± 0.27¥
*WS–Mn	2.8 – 15.2; 8.7 ± 3.5	5.2 – 15.2; 10.4 ± 3.1	2.8 – 12.5; 7.3 ± 3.2	–	–	–	–	–
*WS–Ni	0.18 – 1.92; 0.76 ± 0.44	0.36 – 1.2; 0.76 ± 0.33	0.18 – 1.92; 0.75 ± 0.53	–	–	–	–	–
*WS–Cu	0.01 – 5.25; 1.8 ± 1.65	0.73 – 5.25; 3.13 ± 1.46	0.01 – 1.23; 0.59 ± 0.44	–	–	–	–	–
*WS–Zn	1.1 – 45; 16 ± 13	18 – 45; 28 ± 8	1.1 – 18; 6 ± 5	–	–	–	–	–
*WS–As	BDL – 0.39; 0.14 ± 0.1	0.06 – 0.39; 0.18 ± 0.1	BDL – 0.12; 0.07 ± 0.04	–	–	–	–	–
*WS–Se	0.21 – 0.8; 0.38 ± 0.16	0.21 – 0.42; 0.32 ± 0.07	0.21 – 0.8; 0.44 ± 0.2	–	–	–	–	–
*WS–Sr	2.3 – 87; 14 ± 20	2.3 – 8.7; 5.9 ± 2.3	5.7 – 87; 23 ± 28	–	–	–	–	–
*WS–Cd	BDL – 0.26; 0.11 ± 0.07	0.08 – 0.26; 0.15 ± 0.05	BDL – 0.09; 0.03 ± 0.04	–	–	–	–	–
*WS–Sb	BDL – 0.19; 0.09 ± 0.06	0.08 – 0.19; 0.13 ± 0.04	BDL – 0.11; 0.05 ± 0.03	–	–	–	–	–
*WS–Pb	0.06 – 3.5; 1.29 ± 1.01	0.92 – 3.5; 2.19 ± 0.78	0.06 – 1.15; 0.55 ± 0.35	–	–	–	–	–
*WS–Bi	1 – 99; 49 ± 31	35 – 99; 71 ± 24	1 – 76; 31 ± 24	–	–	–	–	–

*#nmol DTT min^{-1} µg^{-1}, !nmol DTT min^{-1} m^{-3}, *ng m^{-3}, $below detection limit, ¥total (acid soluble) metal concentration in µg m^{-3}*

The OP_M is also found to be positively correlated with the mass fraction of SIA (sum of NH_4^+, NO_3^- and nss-SO_4^{2-}) species in all the samples with the similar slope (1.0) that was documented for a high altitude site Mt Abu (1.0, Patel and Rastogi, 2018b) (Fig. 4.7d). However, SIA species are reported to be DTT-inactive (Patel and Rastogi, 2018a). This observation suggests that species emitted and/or formed and/or transported along with secondary inorganic species can also be partially responsible for the observed OP_M. Secondary formation processes of ambient aerosol during the long-range transport can play an important role in altering aerosol OP. The highest OP_V and OP_M values found in Class-A samples are attributable to long-range transport of anthropogenically emitted pollutants brought by air-masses from the Indian continent. It is inferred that the species emitted from the sources of EC are ~ 8 times DTT-active compared to the species from sources of secondary inorganic species, which is consistent with our pervious study over the high altitude site, Mt. Abu (Patel and Rastogi, 2018b).

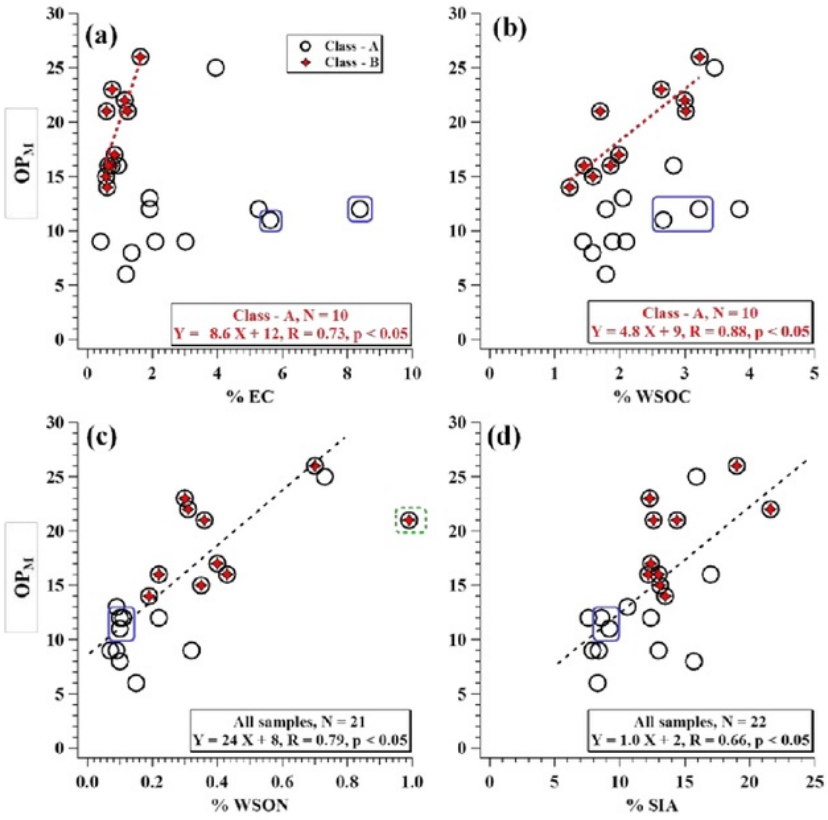

Figure 4. 7. *Linear regression plots of mass normalized OP (OP_M) with mass fraction (in %) of (a) EC, (b) WSOC, (c) WSON and (d) SIA. Encircled samples (in blue) are likely affected from ship emissions. In (c), the sample encircled with green dotted line is excluded from the regression analysis.*

It is observed that the mass fraction of nss-K^+, a marker of biomass burning, showed a significant linear positive correlation with the OP_M, indicating that the biomass burning derived aerosol species also play an important role in the aerosol OP over the study region. Interestingly, the relationship between OP_M and nss-K^+mass fraction over the Arabian Sea (slope = 25, R = 0.83, $p < 0.05$) is found similar to that documented over a high altitude site Mt Abu (R = 0.69) (Patel and Rastogi, 2018b) (fig not shown).

Temporal variability in the mass concentrations of various PM_{10} chemical constituents such as NH_4^+, nss-K^+, WSOC, WSON, WS–Al and WS–Fe are shown in

Figure 4.8. Figure 4.9 shows the temporal variability of different characteristics ratios of chemical constituents. As described earlier, dissolved organic matter (DOM) along with trace metals and dissolved oxygen are among the main sources of ROS in aquatic environments. Interestingly, we observed that the OP_M is correlated positively with mass fraction of WS–Mn (R = 0.58), WS–Cu (R = 0.66), and WS–Zn (R = 0.73) at good significance level ($p < 0.05$) over the Arabian Sea for all the samples (Fig. 4.10). These DTT-active trace metals present in the PM_{10} are redox active species. These metals can contribute through catalytic activity in the formation of superoxide anion that could enhance OP_M in Class-A samples (Fig. 4.6g). On the contrary, Class-B samples are found to be dominated by mineral dust (based on nss-Ca^{2+} as a reference) where despite of higher PM_{10} mass concentration, WS-Mn, WS-Cu and WS-Zn fractions were low and, possibly therefore OP_V and OP_M were also low (Fig. 4.6g). Species derived through Indian continental air masses have higher ROS generation capability over MABL which can be toxic to marine organisms. Catalytic formation of superoxide anion due to deposition of high OP species can act as either an oxidant or a reductant in biological systems. It further undergoes dismutation which can lead to the formation of hydrogen peroxide (H_2O_2). This dismutation either occurs spontaneously or catalyzed by the antioxidant enzyme present in the organisms (Asada, 1984). The H_2O_2 may cause significant damage because it is not restricted to its point of synthesis but diffuses across biological membranes. Exposure to H_2O_2 can damage many cellular constituents directly such as DNA and enzymes involved in ocean biogeochemical cycle. A high level of H_2O_2 in seawater is also shown to inhibit nitrification which is governed by Thaumarchaeotes (Ammonia Oxidizing Archaea (AOA)) (Tolar et al., 2016). If H_2O_2 is further reduced, it can produce the most damaging hydroxyl radical that may induce oxidative damage to AOA and/or other organisms. One of sources of electrons for this reduction in biological systems can be transition metals such as WS–Fe (i.e. via Fenton chemistry and/or Haber–Weiss reaction) (Lesser, 2006). Even though WS-Fe is not correlated with DTT-based OP, the availability of free iron in the form of Fe^{2+} is considered paramount for ROS toxicity due to their role in catalyzing the formation of the most

damaging hydroxyl radical (Cadenas, 1989; Gutteridge and Halliwell, 1989; Lesser, 2006). Trace metals such as WS–Mn are found to be interacting synergistically with dissolved organic compounds such as quinones in the DTT oxidation (superoxide/H_2O_2 formation) (Yu et al., 2018). In present study, a strong correlation between mass normalized WS–Cu and OP_M is observed (slope = 2.1, R = 0.66, $p < 0.05$, Fig. 4.10b). The WS–Cu has been reported to be important contributor from ambient PM in the formation of H_2O_2 and OH· (Charrier et al., 2015; Charrier and Anastasio, 2012; DiStefano et al., 2009; Shen and Anastasio, 2011; Vidrio et al., 2008).

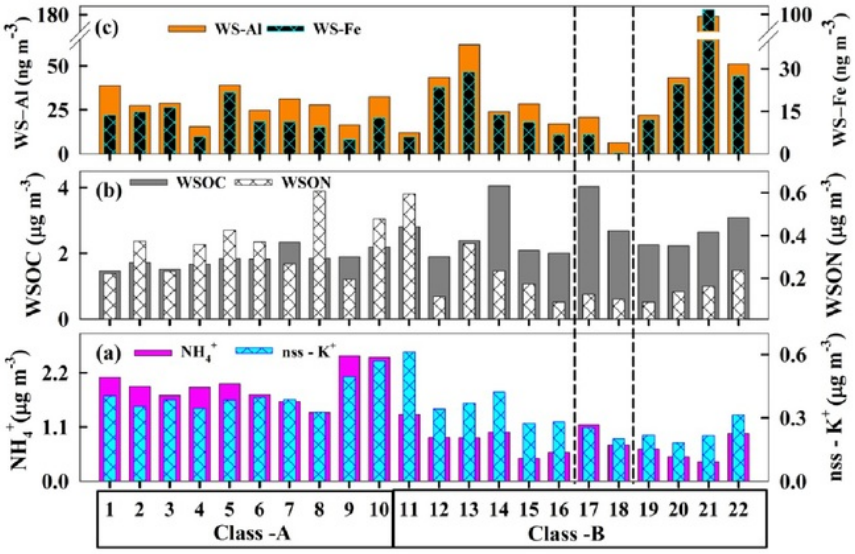

Figure 4. 8. *Time series shows PM_{10} chemical species mass concentration such as (a) NH_4^+ and nss - K^+, (b) WSOC and WSON, (c) WS–Al and WS–Fe. Two samples appeared to be affected by chimney emissions and highlighted between dotted lines.*

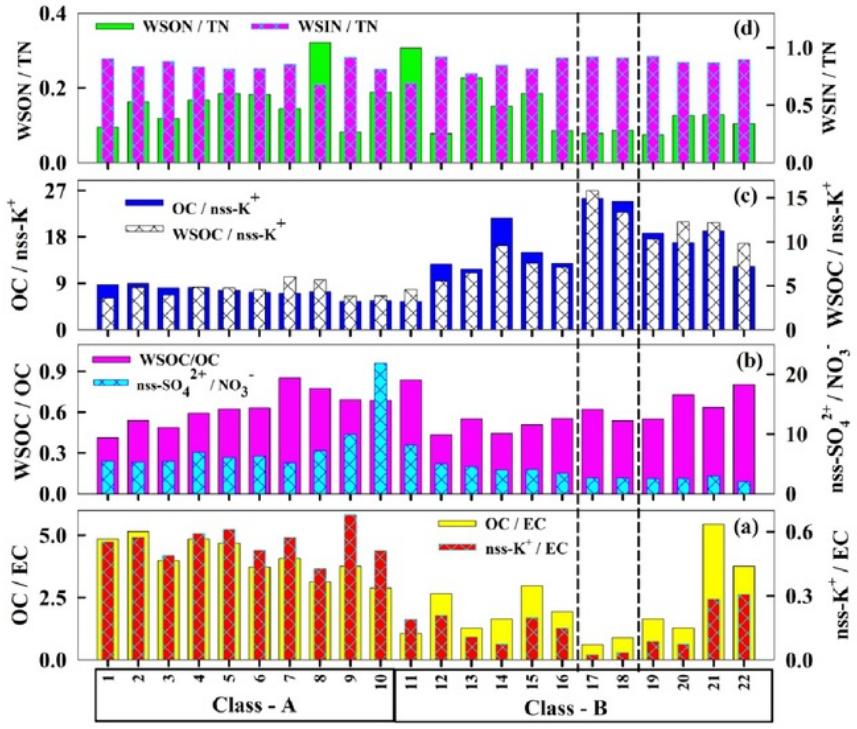

Figure 4. 9. *Temporal variability of different characteristic ratios such as (a) OC/EC and nss-K^+/EC (b) WSOC/OC and nss-SO_4^{2-}/NO_3^- (c) OC/nss- K^+ and WSOC/nss-K^+ and (d) WSON/TN and WSIN/TN.*

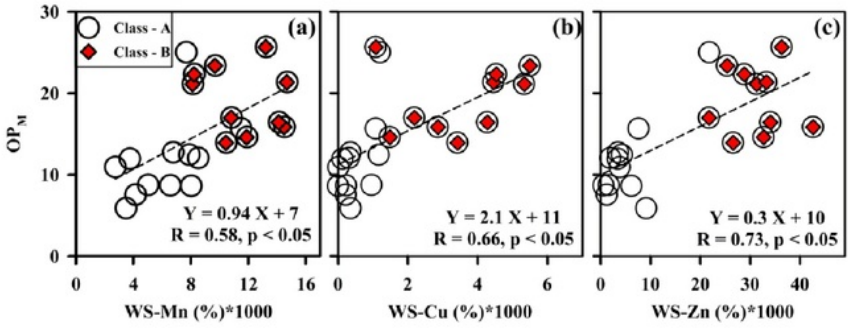

Figure 4. 10. *Scatter plot for OP_M with percentage fraction of water-soluble trace metals such as (a) WS–Mn, (b) WS–Cu, (c) and WS–Zn.*

4.3.2.3. Deposition fluxes of biogeochemically important and OP responsible PM_{10} species

A large anthropogenic influence of continental outflow to the Northern Indian Ocean is documented in several studies (Kumar et al. 2008, Srinivas et al. 2011, Srinivas and Sarin, 2013). In addition to be important as the supplier of macro- and micro-nutrients in regulating the primary productivity, atmospheric deposition of biogeochemically important species are also shown to be associated with the negative effects such as higher level of ROS (Cooper et al.,1987; Lesser, 2006; Kieber et al., 2003; Sunda, 2013). Recent modeling study by Paytan et al., (2009) suggested the effect of WS–Cu deposition to low nutrients low chlorophyll (LNLC) areas in the Bay of Bengal with relevance to changes in marine community structure. Fluvial supply of nutrients can be efficiently trapped in near-coastal areas and cannot reach to open oceans (Jickells et al., 2005). Hence, the dominant external input of nutrients to the surface of the open ocean is Aeolian transport, mainly from the surrounding continents. Therefore, it is also important to assess their ROS generation capability along with atmospheric abundances.

Dry deposition fluxes are calculated based on the concentrations of biogeochemically important aerosol species (Fig. 4.11). Dry deposition velocity for both Classes (A and B) are considered as 0.1 cm s^{-1} for OM, EC, nss-SO_4^{2-}, NH_4^+, nss-K^+, Cu and Zn, 0.3 cm s^{-1} for NO_3^-, and 1.0 cm s^{-1} for Mn as suggested by Duce et al., 1991. It was observed that the ambient mass concentration of water-soluble Al, Fe, Ti and Sr were ~ 2 to 3 times higher for the Class-B samples compared to those observed for Class-A samples. This observation further suggests the effect of the dominance of air masses arriving from the Arabian Desert area on the abundances of these species (Figs. 4.5, 4.6 and 4.8).

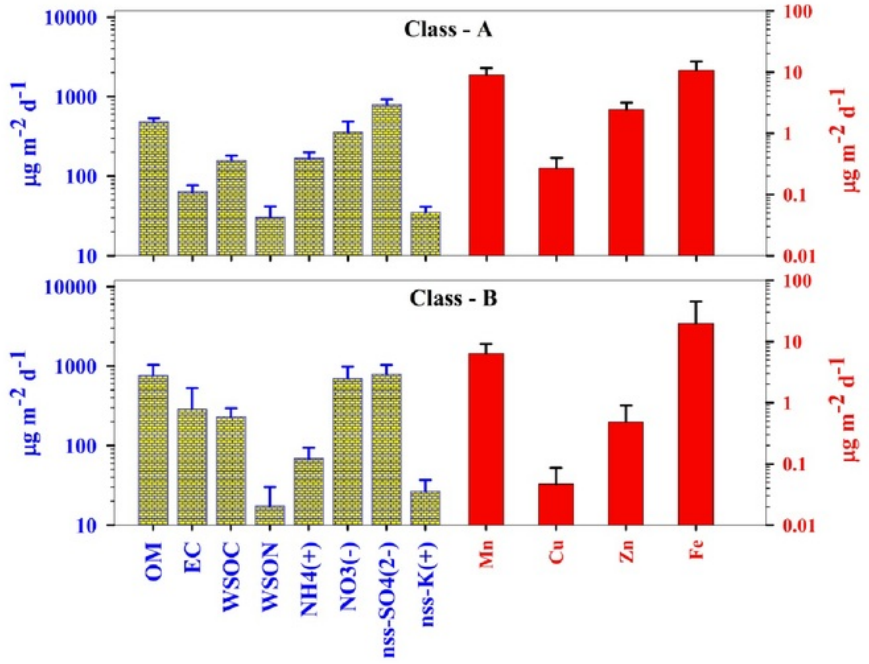

Figure 4. 11. *Dry deposition fluxes of biogeochemically important aerosol species over the Arabian Sea.*

Atmospheric deposition of reactive nitrogen over the different oceanic regions of India had been reviewed by Rengarajan et al. (2010). The deposition fluxes of NH_4^+ (34 – 219; 114 ± 58 µg m^{-2} d^{-1}) observed over the Arabian Sea during the present study are comparable with those reported by Krishnamurti et al., 1998 for the year of 1996 and Reddy et al., 2008 for 2006, whereas, ~ 8 – 17 times higher compared to those reported by Gibb et al., 1999 for 1994. Furthermore, NH_4^+ and NO_3^- deposition fluxes estimated during the present study over the Arabian Sea are similar with those estimated by Srinivas et al., 2013 for the year of 2006. NO_3^- deposition fluxes over the Arabian Sea in the present study (118 – 1475; 544 ± 283 µg m^{-2} d^{-1}) is ~1.9 times higher than that observed by Sarin et al., 1999 for the year of 1994, whereas, ~ 5 times higher than those reported for 2006 by Kumar et al., 2008. The observed differences are attributable to their different source inputs, as well as source strength and meteorological conditions. The WSON (8 – 53; 23 ± 13 µg m^{-2} d^{-}

^{1}) deposition fluxes estimated during the present study are ~ 3 times higher than that observed for the year of 2006 by Srinivas et al., 2013. The WS–Fe deposition flux observed during the present study is ~ 13 times lower than that estimated by Srinivas et al., 2013 for the year of 2006. The Fe may generate the most damaging hydroxyl radical via Fenton chemistry and/or Haber–Weiss reaction that may further affect ocean biogeochemical cycle (Lesser, 2006). It is important to note that the large deposition fluxes for OM, Mn and Zn associated with Class-A may cause threat by generating oxidative stress in surface water that ultimately affects ocean biogeochemical cycle.

4.3.3. Port Blair (Bay of Bengal)

4.3.3.1. PM_{10} chemical composition

PM_{10} mass concentraton varied from 24 to 65 (42 ± 11; avg ± 1σ) μg m^{-3} during the study period (February to April) over the Port Blair. Average PM_{10} mass concentration over the Port Blair (42 ± 11) was factor of ~ 2.5 lower than those observed over MABL of the Arabian Sea (105 ± 26) and a high altitude site, Mount Abu (96 ± 56). Five day air mass back trajectories were computed using GDAS meteorological data (1 degree, global, 2006-present) as input in HYSPLIT model. It showed typical contrasts in composition for the trajectories of aerosol reaching to MABL during February to April over the Port Blair (some of them were from southeast Asian continents and rest were from the open ocean). During February and beginning of March month (initial 15 samples) showed trajectories from the IGP of India and southeast Asia, representing continental outflow. Rest of the period (sample number 16 – 50) was influenced by the trajectories from north, northwest and southwest of the Port Blair. Further, sea-salt fraction for K^+, Ca^{2+}, Mg^{2+}, and SO_4^{2-} were corrected using Na^+ as a reference element (Keene et al., 1986). The non-sea-salt (nss) fraction of K^+ (1.01 ± 0.02; avg ± std error), Ca^{2+} (1.02 ± 0.01), and SO_4^{2-} (1.01 ± 0.01) suggest insignificant sea-salts contribution to these species. In contrast,

Mg^{2+} showed significant contribution from sea-salts for the initial samples also when trajectories were associated with IGP outflow.

The contribution of various components such as OM, EC, SIA (sum of NH_4^+, NO_3^- and nss-SO_4^{2-} and denoted as anthropogenic emissions) and mineral dust to PM_{10} were estimated as per the description given in Rastogi and Sarin, (2009) (Fig. 4.12). Briefly, the contribution of sea-salts was estimated using measured Na^+ concentrations and estimated Cl^--depletion (sea-salts = $[Na^+ \times 3.5] - [Cl^-_{depleted}]$). The contribution of SIA was estimated by adding measured concentrations of NH_4^+, NO_3^- and nss-SO_4^{2-}. The OM was considered 1.9 times of measured OC concentration, presuming OC was aged (Kiss et al., 2002). Mineral dust contribution was estimated using measured Al concentration (Al × [100/8]). Remaining mass concentrations (i.e. PM_{10} gravimetric mass concentration – sum of all estimated) was termed as 'others'. On average, percentage contribution of OM, EC, sea-salts, SIA and mineral dust components to PM_{10} were found to be 28 ± 6%, 5 ± 1%, 3 ± 3%, 24 ± 8% and 25 ± 8%, respectively.

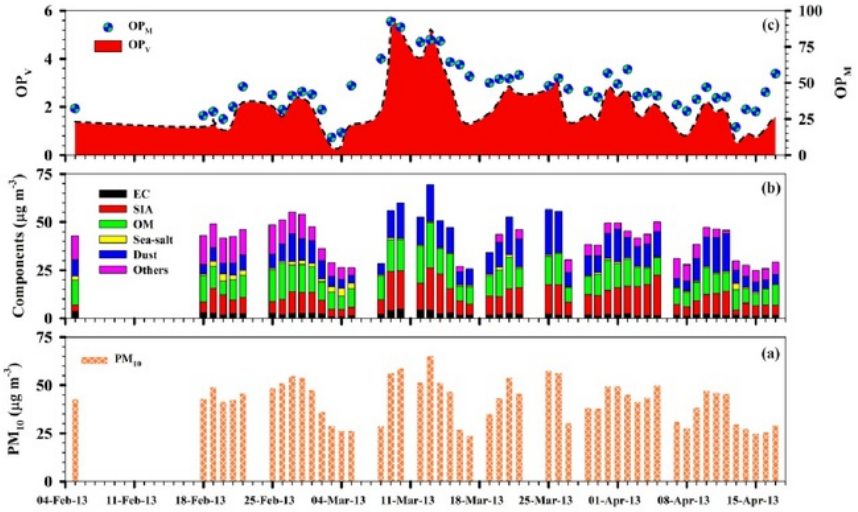

Figure 4. 12. *Time series of (a) PM_{10} mass concentration and (b) chemical components along with their (c) OP_V and OP_M.*

Linear relationships between mass concentrations of OC and EC, nss-K^+ and EC, OC and nss-K^+ and WSOC and OC are depicted in Figure 4.13. Here, EC showed a positive and linear correlation with OC (R = 0.75, slope = 1.6, intercept = 3.0) and nss-K^+ (R = 0.85, slope = 0.12, intercept = 0.22), suggesting contribution of carbonaceous aerosol were both from fossil fuel burning as well as biomass burning emissions (Figs. 4.13a and b). Further, a positive linear relationship between OC and nss-K^+ (R = 0.75, slope = 9.5, intercept = 1.8), suggests their co-emission from the biomass burning (Fig. 4.13c). However, the slope for the regression between OC and EC (1.6), OC and nss-K^+ (9.5) are ~ 2 and ~ 1.5 times lower than the average OC/EC and nss-K^+/EC ratios. The intercepts for the same (i.e. 3.0 and 1.8, respectively) were also significant with respect to averaged OC mass concentration (6.3), that further suggest that a considerable fraction of OC was from non-combustion sources, which may be of secondary origin. The averaged OC/EC ratio (1.8 – 5.9, 3.3 ± 0.9) over Port Blair was significantly lower than that reported over Patiala in the IGP for winter (6.0) and similar for spring (3.2) (Rastogi et al., 2016). The averaged nss-K^+/EC ratio (0.12 – 0.46, 0.25 ± 0.08) over Port Blair was significantly lower than that reported over Patiala in the IGP for winter (0.41) and similar for spring (0.26) (Rastogi et al., 2016). A significant positive linear relationship between WSOC and OC (R = 0.85, slope = 0.45, intercept = 0.16) with a negligible intercept suggests that almost half of the OC was from secondary origin (Fig. 4.13d). It is noteworthy that that WSOC can be often used as a measure of secondary OC (Ervens et al., 2011). The averaged WSOC/OC ratio over Port Blair (0.34 – 0.74, 0.47 ± 0.09) was somewhat higher than that observed over urban city in the IGP such as Hisar (0.32, Rengarajan et al. 2007), Delhi (0.37 for daytime and 0.25 for nighttime, Miyazaki et al. 2009), Allahabad (0.35, Ram and Sarin, 2010), whereas significantly lower than that observed for winter (0.70, Jan-Feb) and spring (0.66, Mar-Apr) over Patiala (Rastogi et al., 2016).

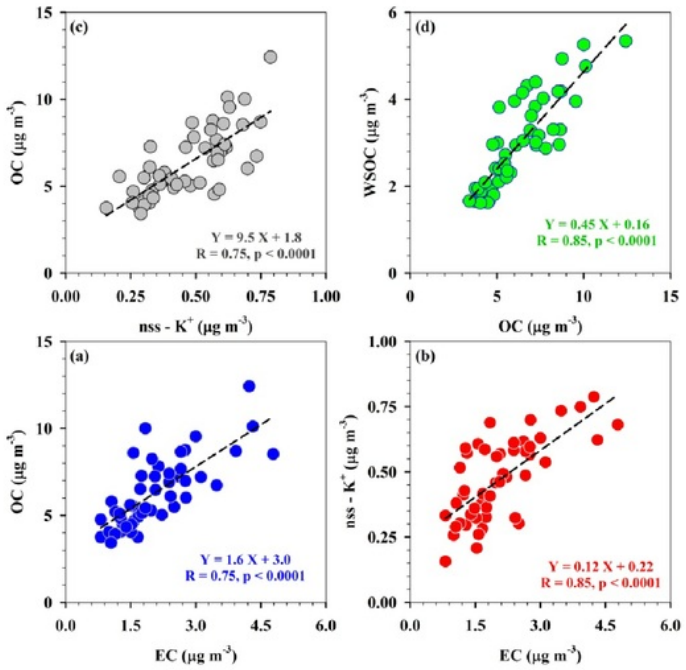

Figure 4. 13. *Scatter plot beetwen (a) OC and EC (b) nss-**K**$^{+}$ and EC (c) OC and nss-**K**$^{+}$ and (d) WSOC and OC.*

4.3.3.2. PM_{10} chemical composition and OP

The OP_V varied from 0.35 to 5.22 nmol DTT min^{-1} m^{-3} (2.03 ± 1.14; average ± 1σ) during the study period. These OP_V values are higher than those observed over the Mt. Abu during spring season (0.69 – 2.17, 1.44 ± 0.48 nmol DTT min^{-1} m^{-3}), the MABL of the Arabian Sea (0.69 – 2.08; 1.47 ± 0.37 nmol DTT min^{-1} m^{-3}), China (0.11 – 1.66 nmol DTT min^{-1} m^{-3}, Wang et al., 2019) and Beijing (0.018 – 0.28 nmol DTT min^{-1} m^{-3}, Liu et al., 2014), whereas lower than those observed over the Indo-Gangetic Plain, India (1.3 – 7.2, 3.8 ± 1.4 nmol DTT min^{-1} m^{-3}, Patel and Rastogi, 2018a). OP_M values varied from 12 to 92 pmol DTT min^{-1} μg^{-1} (46 ± 17) during the study period, which are higher than those observed over Mt. Abu during spring season (5 – 25; 14 ± 7, Patel and Rastogi, 2018b), the MABL of the Arabian Sea (6 –

26, 15 ± 6), the IGP, India (13 – 50, 27 ± 8, Patel and Rastogi, 2018a), and Hangzhou city, China (2 – 23, 6.4, Wang et al., 2019).

The fractions of OM, EC and SIA over the Port Blair are found to be ~ 4.0, ~ 2 – 5, and ~ 2.0 times higher, respectively, than those observed over the Arabian Sea during April and over the Mount Abu during January to April. On the contrary, mineral dust was the predominant contributor to PM_{10} over the Arabian Sea and the Mount Abu (~ 1.5 – 3.0 times higher than the Port Blair). Likely as a result of increased fraction of anthropogenic inputs (such as OM, EC and SIA) over the Port Blair, OP_M was ~ 3.0 times higher as compared to those observed over the Arabian Sea and the Mount Abu. A noteworthy fact is that PM_{10} mass concentration over the Arabian Sea and the Mount Abu was ~ 2.5 times higher compared to that observed over the Port Blair. It further indicates the dependence of aerosol OP on chemical composition rather than mass concentration.

In consistence with our previous studies over Patiala (Patel and Rastogi, 2018a) and Mount Abu (Patel and Rastogi, 2018b) and the Arabian sea, mass normalized EC for the trajectories from north, northwest and southwest of the Port Blair also showed a significant positive correlation with OP_M, suggesting co-emission of EC with OP responsible species (Fig. 4.14). Intrinsic OP for EC (i.e. slope) over the Port Blair (0.76, $p < 0.05$) is found similar to that over the Arabian Sea (0.86, $p < 0.05$), whereas, ~ 1.5 times higher than those observed over Patiala (0.46, $p < 0.05$) and ~ 1.5 times lower than Mount Abu (1.11, $p < 0.05$).

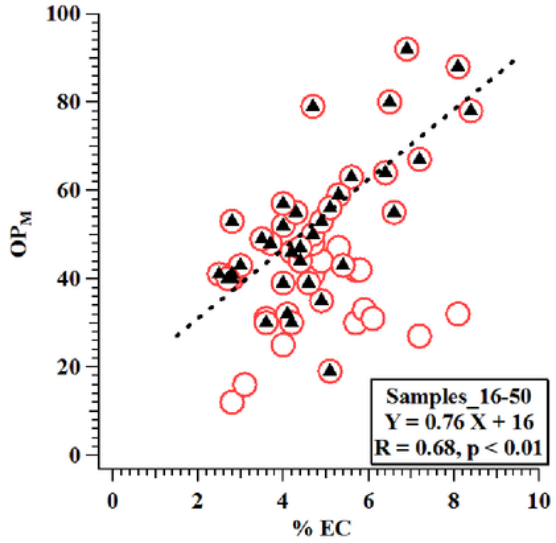

Figure 4. 14. *Scatter plot between % EC and OP_M. Linear regression parameters are given for the black triangles (samples 16 – 50).*

Moreover, a strong linear relationship between acids (nss-SO_4^{2-} + NO_3^-) and bases (NH_4^+ + nss-K^+) is depicted by figure 4.15a. The observed slope (1.15) was slightly higher than the expected (i.e. 1.0) with a significant intercept (39), suggesting presence of ~ 12% excess acid (un-neutralized acid, subtraction of equivalent quantity of bases from acids). The significant positive and linear correlation for the excess acid and nss-Ca^{2+} + nss-Mg^{2+} (bases representing mineral dust) was observed (R = 0.83, slope = 1.26, intercept = 15) during the period of trajectories from north, northwest and southwest of the Port Blair. However, the slope further suggests significant presence of free acid (subtraction of equivalent mineral dust contained bases from the excess acid) over the study region. The acid processing of mineral dust for this period was further resulted into simultaneous increase in the OP_M (plotted as a color scale in Fig. 4.15b). It is most likely due to the increased solubility of the DTT-active trace metals as a result of acid processing of mineral dust in these samples. The acid processing of mineral dust was resulted into 1 – 2 order of

magnitude higher fractional solubility of aerosol Fe over the Bay of Bengal (1.4 – 24%) compared to the Arabian Sea (0.02 – 0.4%) (Bikkina et al., 2011). PM_{10} during this period were found to have ~ 1.5 times higher SIA as well as mineral dust, and ~ 3.0 times lower sea-salts contribution compared to the period during the trajectories from IGP. On the contrary, excess acid during the period when trajectories from IGP (comprising relatively less mineral dust and higher sea-salts) was found to be reacting with the sea-salts and therefore depleted the Cl^- concentration (Fig. 4.13c).

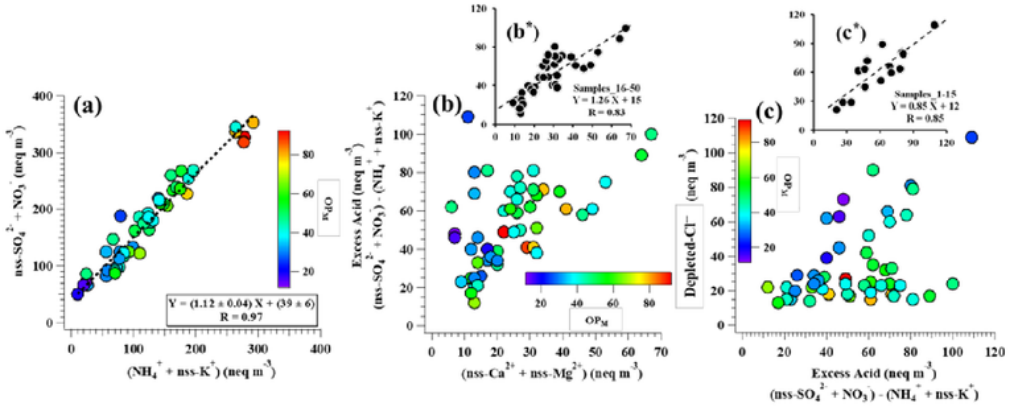

Figure 4. 15. *Scatter plots between (a) acids (nss-SO_4^{2-} + NO_3^-) and bases (NH_4^+ + nss-K^+) (b) Excess acid {(nss-SO_4^{2-} + NO_3^-) - (NH_4^+ + nss-K^+)} and (nss-Ca^{2+} + nss-Mg^{2+}) (c) Excess acid {(nss-SO_4^{2-} + NO_3^-) - (NH_4^+ + nss-K^+)} and depleted–Cl^-. OP_M in each plot is shown by color scale. Inset figures b* and c* shows the respective scatter plot for the samples (16-50 for b) and samples (1-15 for c).*

Total trace metal (acid soluble) concentrations in PM_{10} over the study site were considerable and followed the order Al > Ca > Fe > Mg > Zn > Ti > Mn > Pb > Cu > Sr > Cr > Ni > Cd. To investigate the dominant source of trace metals (continental crust vis-à-vis anthropogenic activity) over the study region, EFs of Ca, Mg, Fe, Mn, Ni, Cu, Zn and Pb were estimated using Equation (1) where Al is used as a reference element for upper continental crust (UCC) (Arimoto et al., 1989; Rastogi and Sarin, 2009).

$$EF_x = (X/Al)_{aerosol} / (X/Al)_{UCC} \quad \ldots\ldots\ldots (1)$$

Higher EFs values for a given trace element suggest its larger contribution from anthropogenic sources (Patel and Rastogi, 2018a). The EFs values >10 for Ni, Cu, Zn and Pb suggest their predominant contribution from anthropogenic sources, whereas Ca, Mg and Fe showed their predominant contribution from mineral dust (EFs < 2). Further, EF of Mn (1.5 to 6.6) suggest that a considerable portion of Mn was from anthropogenic sources in addition to noticeable portion from UCC over the study region. Furthermore, PM_{10} during the period for trajectories from IGP were found to have ~ 1.5 times lower dust contribution compared to rest of the period. As a result, anthropogenic inputs of Ni, Cu, Zn and Pb during the trajectories from IGP were ~ 2.0 times higher compared to the rest period. As discussed above the rest period was influenced by the acid processing of mineral dust which may increase the solubility of the DTT-active trace metals such as Mn, Cd and Zn and hence found to be linearly and positively correlated with the OP_M at high significance level (Fig. 4.16).

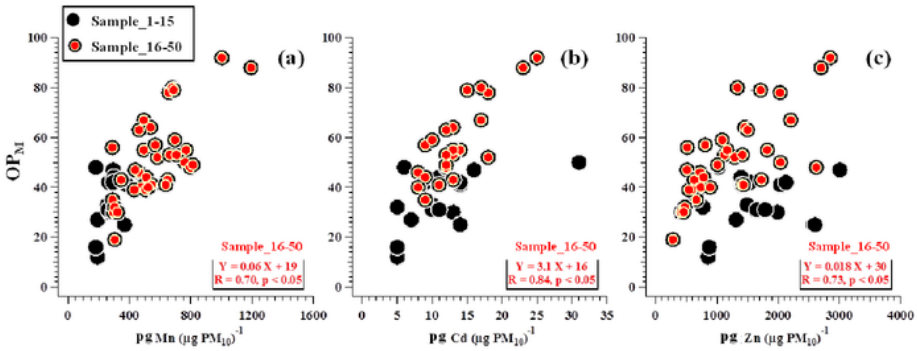

Figure 4. 16. *Scatter plots of OP_M with (a) Mn (b) Cd and (c) Zn fraction in PM_{10}. Sample numbers 1 to 15 are shown by black circles, and numbers 16 to 50 are shown by red circles. Linear regression parameters (slope, intercept, R along with p value) are performed for sample numbers 16 to 50.*

Chapter 5

OXIDATIVE POTENTIAL OF AMBIENT AEROSOL OVER DIFFERENT MICRO-ENVIRONMENTS OVER A BIG URBAN CITY IN THE WESTERN INDIA, AHMEDABAD

5.1. Introduction

Air pollution exposure especially in urban areas is one of the world's leading environmental health risks, causing approximately 7 million deaths worldwide in 2012 (WHO, *25 March 2014*). Therefore, it is necessary to study chemical composition of atmospheric PM along with its ROS generation capability over urban areas across the country. DTT assay is widely used to assess the potential of PM to generate ROS (also known as oxidative potential, OP) (Li et al., 2003; Cho et al., 2005). As a part of the present research work, ROS generation capability of ambient aerosol over different microenvironments of a big urban city (Ahmedabad) of western India was assessed. Ahmedabad's population (~ 5.6 million as per 2011 population census) makes it the fifth-most populous and seventh-largest metropolitan area of India and the largest city in Gujarat. Total number of motor vehicles across Ahmedabad has been increased from ~ 1.5 during the year 2007 to ~ 3.5 million during year 2016 (*https://www.statista.com/statistics/665754/total-number-of-vehicles-in-ahmedabad-india/*). Ahmedabad is the commercial capital of the State and is also known as the textile capital of India. Ahmedabad district accounts for 21.5% of factories in the State. Further, the emissions from two coal-based thermal power plants, situated in the northeast (Sabarmati: 350 MW per day and Gandhinagar: 700 MW per day), can add significantly to the secondary aerosol over the city.

This chapter presents DTT based-OP of PM_{10} collected during May-June, 2017 over five different sites (i.e. Bapunagar (N = 6), Narol, (N = 8), Paldi (N = 7), Income Tax (N = 6) and Science City (N = 7)) representing different emission sources over Ahmedabad. Here, Bapunagar, Paldi and Science City are residential zones in different parts of Ahmedabad (Fig. 5.1), where liquefied petroleum gas (LPG) and piped natural gas (PNG) are being used as fuel in kitchen (*https://www.gujaratgas.com/our-business/png-commercial/*). Income Tax is a big commercial zone with heavy traffic. As per the statistics of existing traffic volume and travel characteristics over the sampling sites, ~ 50,000 of total Passenger Car Unit (PCU, a metric used in transportation engineering to assess traffic-flow rate)

measured for 16 hours have been recorded from Regional Transport Office (RTO) to Paldi via Income Tax cross road (*Ahmedabad Traffic Management And Information Control Centre: Operations Document*). Narol is an industrial site with unpaved Gujarat Industrial Development Corporation (GIDC) inter-connecting road (i.e., Industrial Zone) and nearby (~7 kms) Pirana dumping site. A large number of industries related to textiles, chemicals, machinery, metal products, pharmaceutical, engineering, plastics, electrical appliances, dye, electronics, passenger cars etc. are located in the district (*Brief Industrial Profile of Ahmedabad District, www.msmediahmedabad.gov.in*).

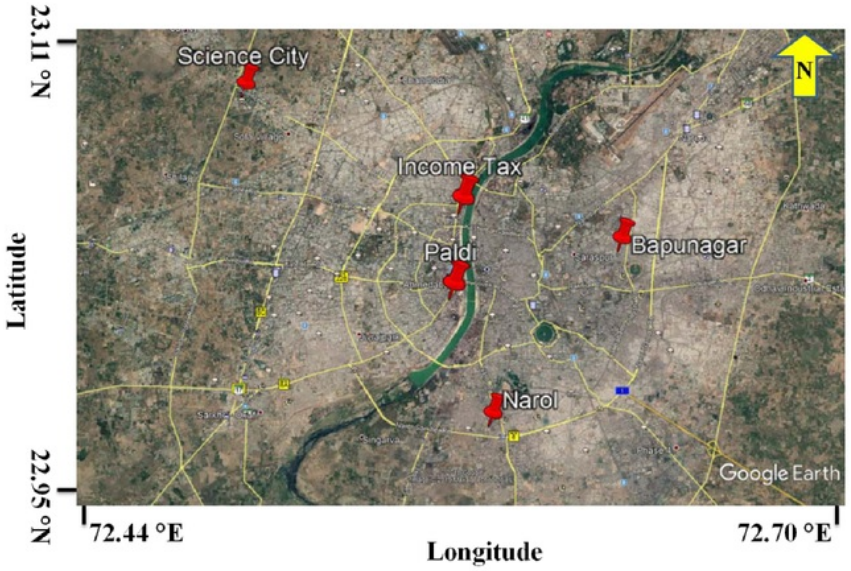

Figure 5. 1. *Map demonstrates Ahmedabad city in which location of sampling sites (Bapunagar, Narol, Paldi, Income Tax and Science City) are shown with red pin.*

5.2. Chemical composition and oxidative potential of ambient aerosol over five sites representing different emission sources over Ahmedabad

5.2.1. PM_{10} chemical composition

Non-sea-salt (nss) fractions of K^+, Ca^{2+}, Mg^{2+} and SO_4^{2-} were estimated using Na^+ as a reference for sea-salts (Keene et al., 1986). The nss fractions of K^+ (95%), Ca^{2+} (98%) and SO_4^{2-} (94%) suggest insignificant sea-salts contribution to these species. However, significant sea-salt fraction to Mg^{2+} was observed (nss fraction, 0 – 70%, 19 ± 18, average ± SD, 1σ) over all the sites. Moreover, chemically analyzed aerosol mass was quantitatively estimated based on Al as a proxy for mineral dust (8% Al in upper continental crust (UCC), Mclennan, 2001), Na^+ as proxy for sea-salts (1/3.5 of seal-salts) and (NH_4^+, nss-SO_4^{2-} and NO_3^-) as proxy for anthropogenic secondary inorganic sources, along with contribution from organic matter (OM) and EC. OM concentration was considered as 1.6 times that of OC which is used for aerosols over urban area (Yttri et al., 2007; Rastogi and Sarin, 2009). The regression parameters of the linear plot (R^2 = 0.96, slope = 0.83) in Fig. 5.2 suggest the quality of chemical analysis techniques. This information can be helpful while assessing regional and global scale climate models (Ramanathan et al., 2001). Figure 5.4 shows percentage contribution of each estimated component (OM, EC, anthropogenic secondary inorganics, sea-salts and dust) to PM_{10} mass. The air quality over Ahmedabad seems complex because of its close proximity to the great Thar desert in Rajasthan and the Arabian sea. The rapid winds from west and/or south-west to the study site especially during the study period (i.e. pre–monsoon, April – June months) often results into the high contribution of sea-salts and mineral dust to PM_{10} (Fig. 5.4e and f).

On an average, PM_{10} mass concentration were 116 ± 36, 228 ± 43, 133 ± 29, 101 ± 21 and 70 ± 20 μg m^{-3} over Bapunagar, Narol, Paldi, Income Tax and Science City, respectively (Fig. 5.4a). PM_{10} values observed during the present study were always exceeding the World Health Organization (WHO) Air Quality Guideline values (i.e. 50 μg m^{-3} for 24-hour mean). PM_{10} values observed over Bapunagar,

Paldi, Income Tax and Science City were comparable whereas, ~ 2 – 3 times higher over Narol than those observed over Ahmedabad during the year of 2005 (Rastogi and Sarin, 2009) and Mexico City (De Vizcaya-Ruiz et al., 2006). Seasonal variability of different aerosol components contribution to total suspended particulate (TSP) was summarized over Ahmedabad by Rastogi and Sarin, 2009, wherein the uniform contribution of mineral dust (average ~ 70%) to TSP was observed throughout the year. The present study also reports ~ 45% average contribution from the mineral dust to PM_{10} over all the study sites (Fig. 5.4f).

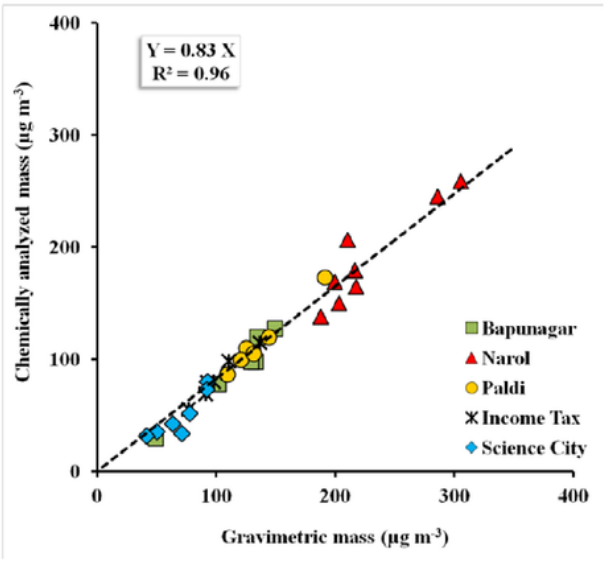

Figure 5. 2. *Scatter plots showing the relation between gravimetrically analyzed mass and estimated mass using chemical analysis. Slope indicates the quality of chemically analyzed aerosol mass.*

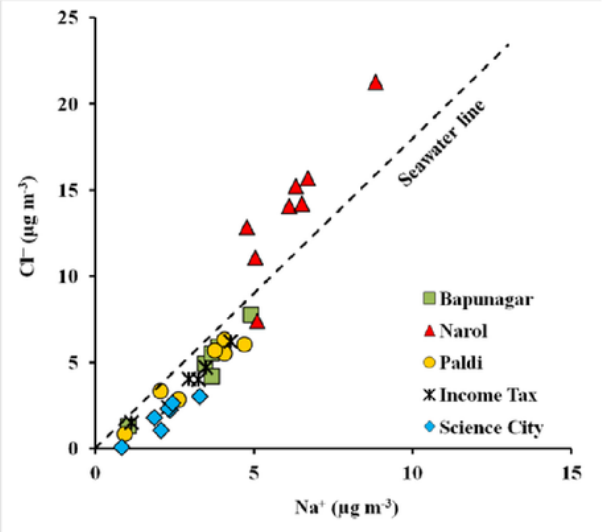

Figure 5. 3. *Scatter plots between* $\boldsymbol{Na^+}$ *and* $\boldsymbol{Cl^-}$ *with respect to seawater line (*$\boldsymbol{Cl^-}$ *= 1.8* $\boldsymbol{Na^+}$*) suggest that both the ions are largely derived from sea-salts over all the sites except that over the industrial site (Narol).*

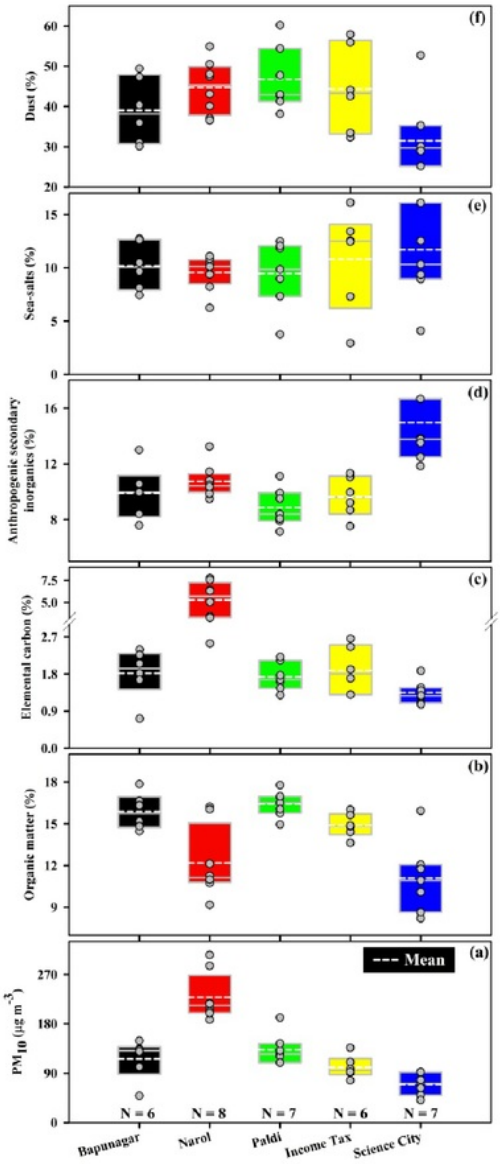

Figure 5. 4. *Box plots showing variability of (a) PM_{10} mass concentration along with percentage contribution of estimated components such as (b) organic matter (c) elemental carbon (d) anthropogenic secondary inorganics (e) sea-salts and (f) dust, to PM_{10} mass over different sites in Ahmedabad. Mean is shown by white dashed line in each box. The box portion of the box plot is given by two lines at the 25^{th} and 75^{th} percentile, whereas a solid line is drawn inside the box at the 50^{th} percentile*

represents median value. Short dashed white line within the box represents mean. Grey closed circles in each plot show the actual data points.

Higher levels of PM_{10} over western India compared to WHO Air Quality Guideline values are clearly visible likely due to elevated dust content in atmospheric PM. Dust is perennial over Ahmedabad because of it's being a part of semi-arid region. Nevertheless, Science City can be considered as a background site (minimum of anthropogenic contribution to PM_{10} mass) among all the study sites. Increase in PM_{10} mass concentration over other sites with respect to Science City can be conceived as local anthropogenic inputs to PM_{10}. Narol, an industrial site, receives ~ 2 – 3 times higher PM_{10} mass compared to rest of the study sites (Fig. 5.4a). Use of coal, a least expensive fuel, is very high in different industrial units of Narol. Furthermore, OC/EC ratios (average ~ 5 to 6) were similar over all the sites except Narol (1.8), suggesting that carbonaceous aerosol over these sites were contributed relatively more from bio-fuel or biomass combustion, and/or secondary organic aerosol formation. Relatively low OC/EC ratio (0.9 – 4.0, 1.8 ± 1.2) over Narol suggests that fossil-fuel combustion (primarily coal) was the major source of carbonaceous aerosol over this site (Fig. 5.5e). Typically, Narol (representing industrial emission) receives ~ 6 times more EC mass with respect to Science City (background site), which might be reason of much higher (~ 4 times) OPv values over Narol (Fig. 5.5a), as discussed in latter section.

Further, Na^+ and Cl^- concentrations closely followed the sea-salts proportion with marginal excess of Na^+ over all the sites except that over Narol (Fig. 5.3). Ambient Cl^- can come from coal combustion processes (Zhang et al., 2018). Hence, it could be inferred that the excess of Cl^- to that over Na^+ over Narol was likely resulted from coal combustion. Moreover, an average ratio of WSOC/OC was 0.48 ± 0.05, 0.86 ± 0.23, 0.63 ± 0.07, 0.58 ± 0.02 and 0.91 ± 0.23 over Bapunagar, Narol, Paldi, Income Tax and Science City, respectively (Fig. 5.5k), reflecting the secondary organic carbon fraction over these sites. Further, WSON fraction of TN over Narol was comparable to all other sites except Science City which suggest WSON from

industrial emission is not significant (Fig. 5.5g). Higher PM_{10} mass concentration over Narol is also attributed to suspension of road dust due to unpaved GIDC inter-connecting road (i.e., Industrial Zone) and nearby (~7 kms) waste dumping site (Pirana) of the city.

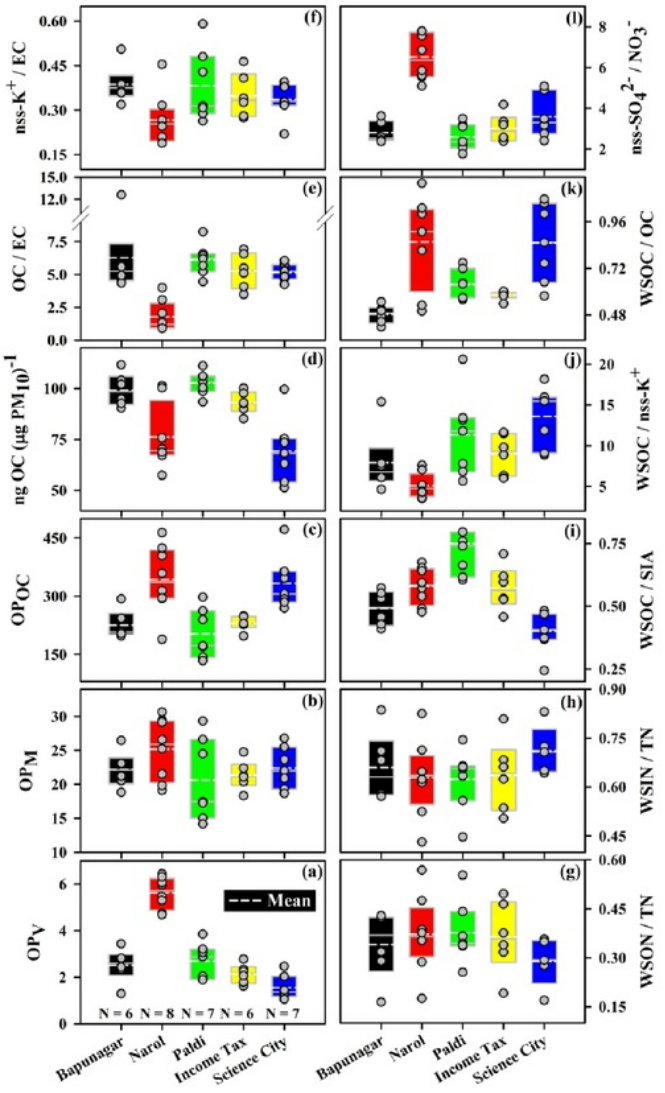

Figure 5. 5. *Box plots show variability of (a) OP_V (b) OP_M (c) OP_{OC} along with different characteristic ratios such as (d) ng OC $(\mu g\ PM_{10})^{-1}$ (e) OC/EC (f) nss-K^+/EC (g) WSON/TN (h) WSIN/TN (i) WSOC/SIA (j) WSOC/nss-K^+ (k) WSOC/OC*

(l) nss-SO_4^{2-}/NO_3^-. For the details of box plot, lines and symbols, refer to caption of Figure 5.4.

Among ten soluble transition metals measured, Ni, Co, Pb, Fe, Cu, Mn and V have substantial capability to catalytically produce ROS (Charrier and Anastasio, 2012). Despite slow rate to catalytically produce ROS, high ambient mass concentration of Fe cannot be ignored (Fig 5.6a). In present study, an enrichment factor (anthropogenic vs crustal sources) of Fe, Pb, Zn, Mn, Cu and Ni were estimated using Al as a reference element for UCC (Arimoto et al., 1989; Rastogi and Sarin, 2009). Estimated EF for Fe and Mn were found closer to unity for all sites, which indicates their predominant contribution from UCC. On the contrary, higher EFs values (> 10) for Pb, Zn and Cu indicate their larger contribution from anthropogenic sources. EF values of Ni over Narol, Income Tax and Science City suggests its anthropogenic source. Ni over Bapunagar and Paldi were likely derived from anthropogenic as well as considerable fraction from road dust.

5.2.2. Oxidative potential of PM_{10}

Fig. 5.5a, b and c display OP_V, OP_M and OP_{OC}, respectively over all the sites. OP_V correlated strongly and positively at high significance level with PM_{10} mass concentration over Bapunagar (slope = 0.019, R = 0.96, $p < 0.05$), Income Tax (slope = 0.018, R = 0.89, $p < 0.05$) and Science City (slope = 0.023, R = 0.89, $p < 0.05$) in contrast to that observed over Narol and Paldi (Table 5.2). The level of OP_V values observed over Narol was ~ 4 times higher compared to Science City, suggesting higher exposure of people to potentially redox-active PM. However, there was no such drastic change in OP_M (intrinsic OP) over Narol compared to the other sites. Among all sites, substantial variability in OP_V and OP_M over Narol and Paldi sites suggests the contrasting mixture of sources resulting in different PM composition over these specific urban atmospheres (Fig. 5.5a and b). On the contrary, variability in OP_V and OP_M over Bapunagar and Income Tax was very low.

Table 5. 1. *Statistical data (min – max; average ± standard deviation (±1σ)) of measured constituent concentrations (μg m^{-3}) and enrichments factors in metals along with OP_V, OP_M and OP_{OC} over five different sites in Ahmedabad.*

Constituents	Bapunagar (N = 6)	Narol (N = 8)	Paldi (N = 7)	Income Tax (N = 6)	Science City (N = 7)
PM_{10}	49 – 149; 116 ± 36	188 – 306; 228 ± 43	109 – 191; 133 ± 29	77 – 136; 101 ± 21	41 – 92; 70 ± 20
OP_V	1.29 – 3.44; 2.51 ± 0.71	4.68 – 6.44; 5.62 ± 0.68	1.89 – 3.85; 2.69 ± 0.76	1.62 – 2.78; 2.14 ± 0.41	1.05 – 2.47; 1.55 ± 0.51
OP_M	19 – 26; 22 ± 3	19 – 31; 25 ± 5	14 – 29; 21 ± 6	18 – 25; 21 ± 2	19 – 27; 22 ± 3
OP_{OC}	197 – 293; 225 ± 37	188 – 463; 343 ± 88	133 – 298; 202 ± 64	197 – 249; 229 ± 19	269 – 472; 333 ± 70
OC	4 – 14; 12 ± 4	11 – 29; 18 ± 6	11 – 20; 14 ± 3	7 – 12; 9 ± 2	2 – 9; 5 ± 2
EC	0.4 – 3.2; 2.2 ± 1	6 – 16; 12 ± 4	1.8 – 3.1; 2.3 ± 0.6	1.4 – 2.2; 1.8 ± 0.3	0.5 – 1.7; 0.9 ± 0.4
WSOC	2 – 8; 6 ± 2	11 – 17; 14 ± 2	6.4 – 11; 9 ± 2	4 – 7; 5 ± 1	3 – 6; 4 ± 1
WSON	0.10 – 0.93; 0.56 ± 0.29	0.54 – 0.99; 0.69 ± 0.17	0.39 – 0.99; 0.67 ± 0.22	0.21 – 0.66; 0.50 ± 0.17	0.23 – 0.59; 0.43 ± 0.17
Na^+	1 – 4.9; 3.4 ± 1.3	4.8 – 8.8; 6.2 ± 1.3	2.1 – 4.7; 3.4 ± 1	1.1 – 4.3; 2.9 ± 1.1	0.8 – 3.3; 2.2 ± 0.7
NH_4^+	0.2 – 0.6; 0.5 ± 0.1	0.3 – 2.5; 0.9 ± 0.7	0.2 – 1.1; 0.6 ± 0.3	0.2 – 0.9; 0.5 ± 0.3	0.3 – 3.3; 1.2 ± 1
nss-K^+	0.1 – 1.2; 0.9 ± 0.4	1.7 – 4.4; 2.9 ± 0.8	0.5 – 1.7; 0.9 ± 0.5	0.5 – 0.9; 0.6 ± 0.2	0.2 – 0.7; 0.3 ± 0.2
nss-Mg^{2+}	#BDL – 0.2; 0.1 ± 0.1	BDL – 0.4; 0.3 ± 0.1	BDL – 0.5; 0.2 ± 0.2	BDL – 0.3; 0.1 ± 0.1	BDL
Nss-Ca^{2+}	1.7 – 6.2; 4.7 ± 1.9	7 – 14; 9 ± 2	3.5 – 6.1; 4.6 ± 1.1	2.4 – 3.8; 3.3 ± 0.6	0.7 – 2.5; 1.5 ± 0.7
nss-SO_4^{2-}	2 – 10; 8 ± 3	14 – 27; 19 ± 4	5 – 10; 7 ± 2	5 – 8; 6 ± 1	4 – 11; 7 ± 3
Cl^-	1.3 – 7.8; 4.9 ± 2.1	7.4 – 21.3; 14 ± 4	2.9 – 6.3; 4.8 ± 1.4	1.5 – 6.2; 3.8 ± 1.7	0.1 – 3.1; 1.9 ± 1
NO_3^-	0.9 – 4.2; 2.7 ± 1.1	1.9 – 4.6; 3.1 ± 0.9	2.1 – 3.4; 2.9 ± 0.5	1.4 – 3.2; 2.1 ± 0.6	1.2 – 2.6; 1.9 ± 0.6
Ni*	3 – 8; 6 ± 2	12 – 192; 59 ± 62	1 – 9; 7 ± 3	6 – 32; 15 ± 11	7 – 216; 50 ± 75
Zn*	61 – 328; 241 ± 94	278 – 533; 383 ± 82	113 – 547; 264 ± 138	178 – 346; 247 ± 62	48 – 286; 154 ± 89
Co*	9 – 13; 11 ± 1	13 – 28; 17 ± 5	2 – 15; 6 ± 5	0.6 – 4.2; 2.2 ± 1.3	1.4 – 2; 1.7 ± 0.4

Pb*	21 – 372; 218 ± 127	71 – 765; 384 ± 250	42 – 145; 68 ± 38	34 – 84; 57 ± 21	9 – 52; 24 ± 18
Fe*	1017 – 4645; 3245 ± 1389	5909 – 11776; 7998 ± 2257	3039 – 7613; 4203 ± 1613	1745 – 5192; 2968 ± 1240	705 – 2723; 1412 ± 724
Cu*	32 – 121; 69 ± 33	45 – 169; 83 ± 37	27 – 51; 42 ± 9	16 – 74; 35 ± 21	6 – 30; 16 ± 7
Mn*	19 – 89; 64 ± 27	102 – 194; 138 ± 35	57 – 163; 81 ± 37	43 – 104; 61 ± 23	14 – 59; 31 ± 16
V*	3 – 18; 12 ± 5	19 – 40; 27 ± 8	10 – 24; 14 ± 5	0 – 14; 5 ± 6	0.7 – 2.4; 1.3 ± 0.6
Ga*	0.8 – 2.8; 1.7 ± 0.7	3.7 – 7.1; 5.2 ± 1.1	0.6 – 3.1; 1.5 ± 0.9	0.4 – 1.7; 1.1 ± 0.6	0.1 – 1.2; 0.7 ± 0.6
Al*	1176 – 5896; 3781 ± 1717	5927 – 11604; 8236 ± 2319	3610 – 9208; 5089 ± 1975	1986 – 6312; 3707 ± 1629	953 – 3895; 1822 ± 1067
EF-Fe	1.8 – 2.1; 2 ± 0.1	2.1 – 2.3; 2.2 ± 0.1	1.7 – 2; 1.9 ± 0.1	1.6 – 2; 1.8 ± 0.1	1.5 – 2.3; 1.8 ± 0.3
EF-Pb	90 – 562; 300 ± 197	59 – 504; 231 ± 141	39 – 114; 68 ± 26	37 – 173; 87 ± 46	45 – 100; 64 ± 21
EF-Zn	57 – 99; 72 ± 16	35 – 79; 54 ± 16	23 – 79; 58 ± 19	61 – 138; 81 ± 29	55 – 135; 94 ± 26
EF-Mn	2 – 2.5; 2.3 ± 0.2	2.1 – 2.5; 2.2 ± 0.1	1.9 – 2.4; 2.1 ± 0.2	1.8 – 2.9; 2.3 ± 0.4	1.8 – 3.5; 2.3 ± 0.6
EF-Cu	35 – 266; 86 ± 91	23 – 49; 34 ± 11	19 – 43; 29 ± 8	11 – 72; 36 ± 22	16 – 54; 34 ± 16
EF-Ni	2 – 12; 7 ± 3	7 – 127; 31 ± 40	1 – 9; 6 ± 3	0 – 26; 13 ± 10	10 – 827; 166 ± 294

*ng m^{-3}

#Below detection limit

Table 5. 2. *Correlation coefficient (R) of volume and mass normalized PM_{10} constituents with OP_V and OP_M, respectively. Values in red color are significant at $p < 0.05$.*

PM_{10} Constituents	Bapunagar		Narol		Paldi		Income Tax		Science City	
	OP_V	OP_M	OP_V	OP_M	OP_V	OP_M	OP_V	OP_M	OP_V	OP_M
PM_{10}	0.96	-	0.23	-	0.23	-	0.89	-	0.89	-
OC	0.94	-0.18	0.21	-0.07	0.17	-0.25	0.91	0.59	0.98	0.55
EC	0.92	-0.57	0.47	0.45	0.70	0.74	-0.19	0.49	0.97	0.80
WSOC	0.90	-0.39	0.20	0.44	0.25	0.07	0.92	0.60	0.82	0.26
WSON	0.82	-0.09	-0.07	0.26	0.81	0.79	0.58	0.33	0.73	-0.09
Na^+	0.73	-0.55	0.29	0.37	0.24	0.48	-0.69	0.27	0.56	0.73
NH_4^+	0.01	0.75	0.00	-0.37	-0.25	-0.50	0.83	-0.27	-0.06	-0.54
$nss - K^+$	0.94	-0.50	0.06	0.38	0.80	0.71	0.45	0.68	0.98	0.54
$nss - Mg^{+2}$	0.81	-0.38	0.16	-0.27	0.03	-0.55	0.81	-0.50	0.55	-0.05
$nss - Ca^{+2}$	0.80	-0.64	0.47	0.21	-0.22	-0.65	0.51	-0.15	0.89	0.39
$nss - SO_4^{2-}$	0.92	-0.10	0.43	0.24	0.77	0.80	0.88	0.84	0.47	-0.43
Cl^-	0.70	-0.79	0.37	0.52	0.12	0.34	-0.67	0.20	0.36	0.77
NO_3^-	0.99	-0.17	0.43	0.16	0.12	0.12	0.29	0.31	0.83	0.19
Excess Acid	0.95	-0.29	0.41	0.28	0.81	0.79	0.48	0.69	0.96	0.71
Cr	0.96	-0.63	0.47	0.03	0.11	-0.35	0.81	-0.41	0.81	0.28
Ni	0.56	0.24	-0.40	-0.15	-0.27	-0.30	-0.19	-0.44	-0.09	-0.46
Zn	0.96	-0.72	0.79	0.77	0.29	0.10	0.63	-0.27	0.94	0.25
Co	0.24	-0.85	0.10	-0.14	0.21	-0.11	0.82	-0.41	-	-1.00
Cd	0.65	0.12	0.51	0.31	-0.17	-0.16	0.58	0.69	0.82	0.25
As	0.58	-0.26	-0.24	-0.24	0.70	0.57	0.41	0.71	0.69	0.18
Pb	0.40	-0.60	0.76	0.30	0.33	0.02	0.55	0.49	0.95	0.43
Fe	0.91	-0.61	0.34	-0.03	0.10	-0.57	0.84	-0.45	0.87	0.43
Cu	-0.34	0.57	0.36	-0.19	0.45	0.43	-0.41	-0.52	0.80	0.58
Mo		-	-0.31	-0.18	0.85	0.90	-0.15	-0.47	-0.53	-0.07
Mn	0.92	-0.68	0.33	-0.06	0.14	-0.41	0.82	-0.47	0.88	0.37
V	0.96	-0.51	0.37	-0.05	0.25	-0.08	-	-	0.95	-
Ti	0.92	-0.47	0.35	-0.17	-0.01	-0.81	-	-	-	-
Sr	0.92	-0.71	0.34	0.10	-0.02	-0.74	0.68	-0.28	0.80	0.47
Ga	0.94	0.25	0.78	0.73	0.57	0.42	0.86	0.80	1.00	0.89
Ba	0.84	-0.31	0.00	-0.39	0.28	0.04	0.48	-0.62	0.05	-0.33
Al	0.93	-0.48	0.38	-0.01	0.12	-0.42	0.83	-0.43	0.80	0.33

Table 5. 3. *Correlation coefficient (R) of different characteristic ratios with OP_V and OP_M. Values in red color are significant at $p < 0.05$.*

Constituent Ratios	Bapunagar		Narol		Paldi		Income Tax		Science City	
	OP_V	OP_M	OP_V	OP_M	OP_V	OP_M	OP_V	OP_M	OP_V	OP_M
OC/EC	-0.86	0.74	-0.12	-0.32	-0.60	-0.77	0.73	-0.43	0.54	-0.39
nss − K^+/EC	0.22	-0.01	-0.28	0.07	0.85	0.57	0.79	0.32	0.69	-0.15
WSOC/OC	0.40	-0.40	-0.21	0.24	0.22	0.21	0.20	0.05	-0.74	-0.56
WSOC/nss − K^+	-0.85	0.66	-0.18	-0.41	-0.72	-0.63	0.09	-0.65	-0.86	-0.34
WSOC/SIA	-0.28	-0.23	-0.60	0.32	-0.41	-0.56	0.19	-0.48	-0.16	0.20
nss − SO_4^{2-}/NO_3^-	0.03	-0.03	-0.23	0.01	0.81	0.58	0.50	0.12	-0.06	-0.36
WSON/TN	0.75	-0.45	-0.52	0.23	0.85	0.74	-0.17	0.17	0.47	0.33
WSIN/TN	-0.75	0.45	0.52	-0.23	-0.85	-0.74	0.17	-0.17	-0.47	-0.33
WSON/WSOC	0.55	-0.05	0.00	0.12	0.91	0.81	0.00	0.87	0.00	-0.12
EF_Fe	-0.45	-0.18	-0.31	-0.01	-0.15	-0.16	-0.32	0.27	-0.16	-0.08
EF_Pb	0.09	-0.39	0.73	0.33	0.41	0.31	-0.16	0.63	0.66	0.30
EF_Zn	0.06	-0.20	0.26	0.62	0.27	0.36	-0.68	0.13	0.32	-0.24
EF_Mn	-0.04	-0.34	-0.51	-0.05	0.12	-0.11	-0.53	0.22	-0.03	-0.15
EF_Cu	-0.88	0.66	0.17	-0.10	0.30	0.53	-0.76	-0.35	-0.23	0.13
EF_Ni	-0.51	0.41	-0.47	-0.11	-0.39	-0.18	0.04	-0.28	-0.18	-0.48

Table 5. 4. *Correlation coefficient (R) of AMS and BrC based OC composition with OP_V and OP_M. Values in red color are significant at $p < 0.05$.*

AMS and BrC based parameters	Bapunagar		Narol		Paldi		Income Tax		Science City	
	OP_V	OP_M	OP_V	OP_M	OP_V	OP_M	OP_V	OP_M	OP_V	OP_M
f43	-0.50	0.65	-0.26	0.38	0.45	0.49	0.07	0.51	0.03	0.86
f44	0.86	-0.52	-0.45	-0.51	-0.53	-0.60	0.06	-0.53	-0.55	-0.54
f57	-0.90	0.32	0.00	-0.32	0.00	-0.43	0.77	0.25	0.00	-0.06
f60	0.51	-0.38	0.04	-0.19	0.53	0.51	0.02	0.91	0.24	0.34
OM/OC	0.89	-0.44	-0.32	-0.02	-0.51	-0.37	-0.45	-0.59	0.07	0.27
H/C	-0.92	0.53	-0.17	0.08	0.16	0.33	-0.87	-0.42	-0.78	-0.46
O/C	0.89	-0.44	-0.33	-0.03	-0.53	-0.41	-0.43	-0.58	0.10	0.29
N/C	0.87	-0.33	-0.39	-0.18	0.35	0.00	0.01	-0.50	-0.11	0.50
S/C	0.86	-0.52	-0.19	-0.25	0.16	0.41	-0.63	0.12	-0.10	0.31
b_{abs_365}	0.86	-	-0.11	-	0.85	-	0.25	-	0.95	-
b_{abs_370}	0.85	-	-0.11	-	0.86	-	0.26	-	0.95	-
b_{abs_390}	0.85	-	-0.14	-	0.85	-	0.24	-	0.94	-
b_{abs_420}	0.83	-	-0.12	-	0.87	-	0.26	-	0.95	-
b_{abs_450}	0.80	-	-0.09	-	0.87	-	0.27	-	0.95	-
b_{abs_565}	0.68	-	0.03	-	0.89	-	0.43	-	0.90	-
$b_{abs\_370} / b_{abs\_365}$	-	-0.33	-	0.39	-	0.42	-	-0.13	-	-0.77
$b_{abs\_390} / b_{abs\_365}$	-	-0.59	-	-0.04	-	0.62	-	0.41	-	0.42
$b_{abs\_420} / b_{abs\_365}$	-	0.76	-	0.36	-	0.83	-	0.66	-	-0.01
$b_{abs\_450} / b_{abs\_365}$	-	0.77	-	0.37	-	0.84	-	0.80	-	-0.31
$b_{abs\_565} / b_{abs\_365}$	-	0.84	-	0.37	-	0.90	-	0.55	-	-0.60

5.2.3. Oxidative potential and trace metals

Average concentrations of metals (Ni, Co, Pb, Fe, Cu, Mn, V) along with OP_V, and their mass normalized concentrations along with OP_M for all the sites are shown in Fig. 5.6. OP_M over Narol showed significant and positive linear relationship with mass fraction of Zn (R = 0.77). It could be because of coal-combustion and waste incineration processes in this industrial area which can contribute significant Zn fraction as well as DTT-active species to ambient PM (Spiro et al., 1986; Zhou et al., 2010, Fomba et al., 2015).

Coal contains high fractions of the heavy metals, including Sc, Cr, Ni, Cu, Zn, Cd, Pb, Sb Ga, As and Se, of which two elements (Sc and Ga) are of rising environmental and health concern (Uryu et al. 2003; Wynne et al. 2008; Zhai et al., 2009). It is noteworthy fact that various units of industries at Narol use the coal as a fuel. This is supported by a strong correlation between Zn and Pb ($R = 0.93$, $p < 0.05$) that further suggests their co-emission from high-temperature combustion processes (such as coal combustion and/or waste incineration) as well as from non-metallurgic industrial processes. However, Pb didn't show a relation with OP over Narol. It is important to note the limitation of the present study that the acid-soluble metal contents (i.e., total metal content in PM_{10}) are compared with OP of (water + methanol) soluble PM_{10}.

Interestingly, OP_M showed significant positive linear relationship with Ga mass fraction over Narol (slope = 0.85, R = 0.73, N = 8), Paldi (slope = 2.0, R = 0.99, N = 5, two data points were excluded from the regression) and Income Tax (slope = 0.47, R = 0.93, N = 5, one data point is excluded from the regression) (Table 5.2). The slope indicates the intrinsic OP of Ga that was almost a factor of 2 and 4 higher over Paldi compared to that over Narol and Income Tax, respectively. Cu mass fraction did not show any relation with OP_M. However, a large fraction of Cu over Bapunagar compared to other sites should not be ignored as it is shown to have high DTT activity (Charrier and Anastasio, 2012).

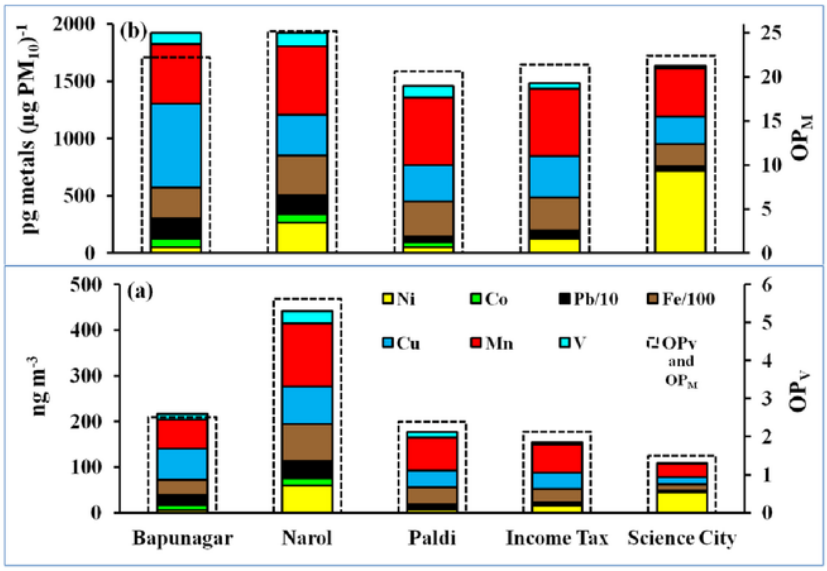

Figure 5. 6. *Stacked bar shows (a) average contribution of volume normalized metal concentration along with average OP_V and, (b) average mass normalized metals along with average OP_M at each site.*

5.2.4. Oxidative potential and organic aerosol

OC mass concentrations over Bapunagar and Science City followed quite similar trend with EC mass concentration, suggesting their contribution from common source (s). It is interesting to note that the minimum OC/EC ratio (4.4) over Bapunagar is quite similar to the slope obtained from linear regression analysis between OC and EC (slope = 3.5, R = 0.97, intercept = 3.7, $p < 0.05$, fig not shown), but due to significant value of intercept (3.7), the average value of OC/EC is 6.3. As discussed in literature (Turpin and Huntzicker, 1995; Castro et al.,1999; Sandrini et al 2014), minimum OC/EC ratio can be considered due to primary emissions from the combustion sources, and increase in OC/EC ratio can be explained in terms of secondary OC formation. This observation over Bapunagar suggests that abundance of OC is dominated by primary sources with considerable fraction coming from secondary formation processes as well. Bapunagar is considered as residential zone, which is upwind of major urban areas during the study period. Sometimes open trash burning was observed near the site. Over Science City, on the contrary, a negligible

intercept was observed in linear regression analysis between OC and EC (slope = 6.0, intercept = -0.87, R = 0.97, $p < 0.05$, fig not shown), suggesting the dominance of carbonaceous aerosol from primary and secondary emissions. However, the scenario was totally different for Narol, Paldi and Income Tax, where OC and EC were not correlated significantly (poor R). A significant positive linear relationship of OP_V with OC mass concentrations (slope = 0.18, R = 0.94, $p < 0.05$, Table 5.2) as well as EC mass concentration (slope = 0.64, R = 0.92, $p < 0.05$, Table 5.2) over Bapunagar suggests predominant contribution of ROS responsible carbonaceous aerosol from combustion sources and secondary formation processes. Science City also showed a significant positive linear relationship of OP_V with OC mass concentrations (slope = 0.21, R = 0.98, $p < 0.05$, Table 5.2) and with EC mass concentration (slope = 1.3, R = 0.97, $p < 0.05$, Table 5.2), suggesting that considerable contribution of ROS species emitted from primary emissions.

Table 5. 5 *Correlation coefficient (R) of AMS and BrC based parameters and OP_{OC}. Values in red color are significant at $p < 0.05$.*

Constituent Ratios	OC mass normalized OP (OP_{OC})				
	Bapunagar	Narol	Paldi	Income Tax	Science City
OC/EC	-0.87	-0.81	-0.73	0.00	-0.85
WSOC/OC	-0.36	0.82	0.33	0.28	0.81
WSON/WSOC	-0.35	-0.11	0.87	0.89	-0.70
f44	-0.43	-0.01	-0.29	-0.63	-0.26
f43	0.36	0.41	0.40	0.62	0.43
f57	0.41	-0.61	-0.44	0.71	0.52
f60	-0.72	-0.21	0.36	0.50	0.24
OM/OC	-0.42	0.28	-0.03	-0.86	-0.40
H/C	0.47	0.23	0.21	-0.56	0.32
O/C	-0.42	0.28	-0.04	-0.85	-0.42
N/C	-0.48	0.27	0.12	-0.80	0.28
S/C	-0.63	0.16	0.30	-0.35	0.31
MAE_365 nm	-0.71	0.39	0.84	0.20	0.37
MAE_370 nm	-0.71	0.39	0.84	0.21	0.41
MAE_390 nm	-0.71	0.39	0.81	0.23	0.21
MAE_420 nm	-0.67	0.42	0.85	0.26	0.26
MAE_450 nm	-0.63	0.43	0.86	0.29	0.32
MAE_565 nm	-0.31	0.55	0.82	0.42	0.42
b_{abs}_370 / b_{abs} _365	-0.61	0.56	0.10	0.30	0.43
b_{abs} _390 / b_{abs} s_365	-0.81	0.26	0.45	0.51	-0.13
b_{abs} _420 / b_{abs} _365	0.76	0.49	0.44	0.74	-0.12
b_{abs} _450 / b_{abs} _365	0.80	0.43	0.34	0.88	-0.19
b_{abs} _565 / b_{abs} _365	0.85	0.42	0.16	0.81	0.31
f-familyCH	0.45	-0.32	-0.20	0.85	0.46
f-familyCHO1	0.09	0.38	0.33	-0.59	-0.31
f-familyCHO>1	-0.43	-0.19	-0.26	-0.51	0.01
f-familyCHN	-0.50	0.28	0.24	-0.89	0.12
f-familyCHO>1N	0.26	-0.08	-0.12	0.33	0.45
f-familyCS	-0.71	0.09	0.36	-0.11	0.27
f-C2H3O	-0.23	0.58	0.46	-0.10	-0.47
f-C3H5	0.44	-0.38	-0.36	0.86	0.46
f-C4H9	0.37	-0.67	-0.38	0.54	0.66
f-C6H10O	-0.48	-0.51	-0.11	0.80	-0.13
f-C6H4O	-0.35	-0.01	0.34	0.79	0.34
f-C3H5O	0.39	-0.18	0.09	0.76	-0.46
f-CH3S	-0.43	-0.13	0.12	-0.22	-0.02
f-CH2SO2	0.17	-0.26	0.23	0.53	-0.08
f-CH3SO2	-0.16	0.11	0.43	0.62	0.20
f-CH4SO3	-0.22	0.08	0.12	0.76	0.06
f-C3H5SO2	0.49	-0.31	-0.16	0.26	0.56
f-C4H5SO2	-0.24	-0.03	0.38	0.71	0.09

*fraction of organic families or species in total organics

In present study, water soluble organic aerosol (WSOA) were measured using aerosol mass spectrometer (AMS) to study their characteristics and evolution. Some parameters were compared with (methanol + water) soluble OP. To get the information about aging of organics, people often plot f44 (ratio of m/z 44 signal, representing CO_2^+, to total water-soluble organics signal) as a function of f43 (ratio of m/z 43 signal, representing $C_2H_3O^+$, to total water-soluble organics signal). The m/z 44 ion in OOA is thought to be mostly due to organic acids or their derivatives, such as esters (Duplissy et al., 2011). The m/z 43 ion is predominantly due to non-acid oxygenates. A general understanding for organic aerosol (OA) is that hydrocarbon like OA (HOA) components have f44 < 0.05; semi volatile oxidized OA (SV–OOA) have 0.05 < f44 < 0.10 and low volatile oxidized OA (LV–OOA) components have f44 > 0.10 (Ng et al., 2010, 2011). The dotted lines in Fig. 5.7 define the triangular space wherein ambient oxidized OA (OOA) components fall. The less aged SV–OOA usually concentrates in the lower half, and those becomes LV–OOA with aging occupies the upper half of the triangle. In present study, we have SV–OOA (0.05 < f44 < ~ 0.12) type OA over all the sites, and they are concentrated in the lower half of the triangle (Fig. 5.7). Overall, samples with higher f44 were associated with less intrinsic OP_{OC} and vice-versa (Fig. 5.7). This observation reflects the variable composition of fresher secondary OA (SOA) formed from site-specific precursors and sources. However, AMS-derived parameters reflect the properties of WSOA only whereas, OP can due to both water- and methanol-soluble OA.

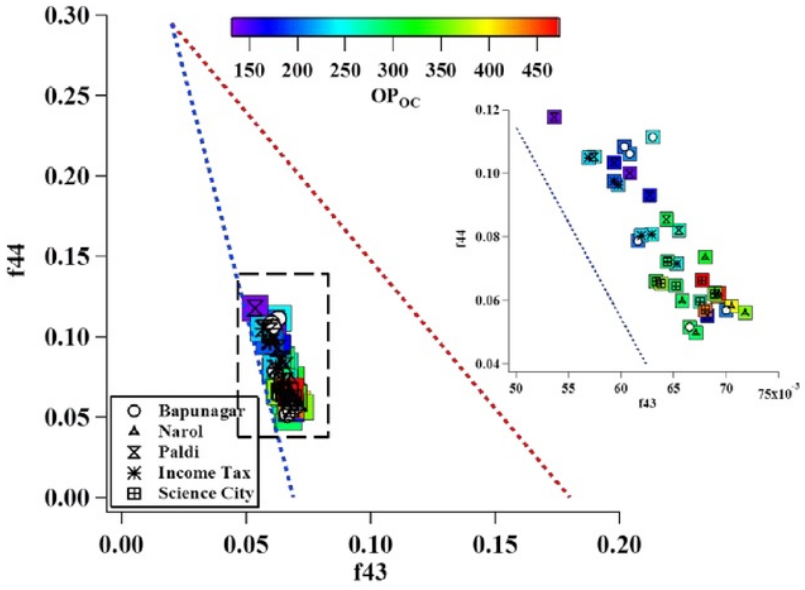

Figure 5. 7. *f44 vs. f43 for all the OOA components from different sites over Ahmedabad. The dotted lines are added to define the triangular space where ambient OOA components fall. The slope and intercept of these dotted lines are discussed in Ng et al., 2010.*

Fig. 5.8 indicates the relationship between f44 and f60 (ratio of m/z 60 signal, representing $C_2H_4O_2^+$, to total water-soluble organics signal, a marker for biomass burning). The background level of f60 is marked with a vertical dashed line and triangular space in this plot belongs to OA from biomass burning (Cubison et al. 2011). The present study shows that biomass burning was not a major source of OA rather it could be from anthropogenic sources/biogenic emission. This observation is consistent with earlier study over Ahmedabad by Singh et al., (2019) where they have shown that biomass burning was not a major source of OA during the post-monsoon season.

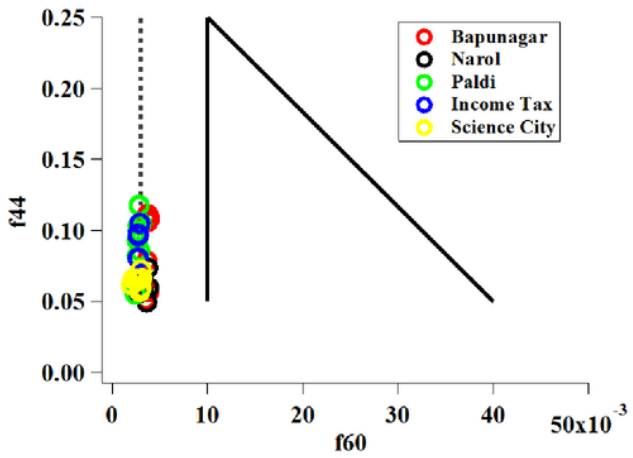

Figure 5. 8. *Relationship between f44 and f60 over different sites in Ahmedabad is shown. The background level of f60 (0.003) is marked with a vertical dashed line and data points right to this dashed line denote the primary organic aerosol. Triangular space in this plot belongs to primary organic aerosol from biomass burning.*

Furthermore, as indicated above, OP_{OC} was used to identify the relationship of soluble organic aerosol with ROS. This intrinsic OP_{OC} is driven by ROS active organic species present in PM_{10}. Overall, OP_{OC} when plotted against f43, showed a significant positive linear relationship (Fig. 5.9). It suggests that oxidized OA contributed from fossil fuel are more responsible for ROS production. This is further confirmed when we introduced H/C and fraction of CHO>1 as a color scale along with f43 (Fig. 5.9a and b). OP_{OC} was found to be increasing along with f43 and H/C whereas decreasing along with the fraction of CHO>1 (aging). These observations suggest that less aged OOA (high f43, less f44) are more DTT-active and as they aged (less f43, high f44) their OP_{OC} decreases over Ahmedabad. It is important to note the limitation of this case study that water-soluble OA (measured with AMS) is compared with (water + methanol) soluble OP_{OC} over Ahmedabad.

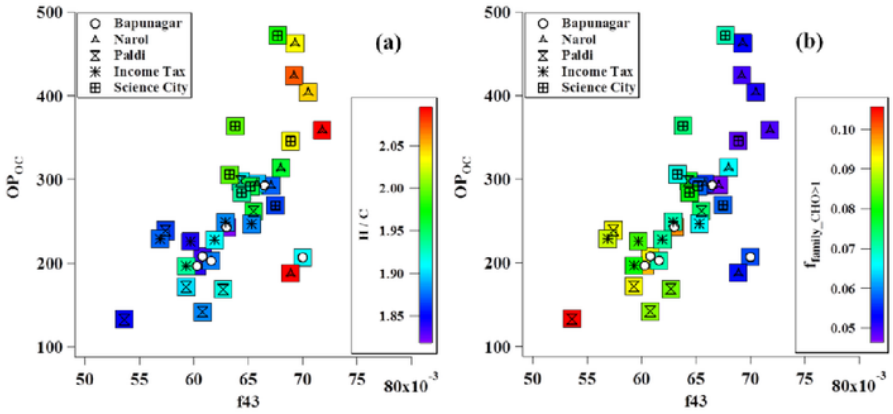

Figure 5. 9. *Scatter plots of OP_{OC} with f43 are shown along with color scale (a) H / C ratio and (b) fraction of family CHO>1 in total soluble organics.*

The role of OP_{OC} was further investigated for the organic aerosol composition. It was found to be correlated positively and linearly with the WSON/WSOC ratio over Paldi and Income Tax (Fig. 5.10 and b, Table 5.5). The red dashed lines in each scatter plot of Figure 5.10 suggest there is a 95 % probability that the true best-fit line for the population lies within the confident interval. We followed the approach given by Satish and Rastogi, 2019 and used brown carbon (BrC) spectra as a tool to understand broader composition and characteristics of organic aerosol in this study. In general, humic like substances (HULIS) are primary oxygenated organics and are similar to terrestrial and aquatic humic and fulvic acids. These types of primary organics absorb strongly at near UV regions (i.e. 365 nm) of spectrum and known as BrC. Fossil fuel combustion and biomass burning emissions are the significant sources of these species (or its precursors) in the atmosphere (Ramanathan et al., 2007; Stone et al., 2009; Chakrabarty et al., 2010; Lin et al., 2012). Variety of atmospheric aging processes in presence of NOx often involves in the formation of nitrogenous organic aerosol compounds which consist of a secondarily formed oxygenated organic aerosol. While investigating organic aerosol composition, b_{abs} at 420 nm (b_{abs_420}, represents 3-Nitrophenol, Lin et al., 2015) and 450 nm (b_{abs_450}, represents 2,5-Dinitrophenol, Lin et al., 2015) were normalized with 365 nm (b_{abs_365}, represents HULIS), and subsequently correlated with WSON/WSOC ratio. The WSON/WSOC ratio over Paldi and Income Tax was found to be correlated

significantly with b_{abs_420} / b_{abs_365} and b_{abs_450} / b_{abs_365}. This observation implies that considerable fraction of BrC chromophores could be nitro-phenolic compounds which were probably the cause of observed intrinsic OP_{OC} over Paldi and Income Tax. These findings also suggest that nitro-phenolic compounds emitted particularly from the traffic related sources (i.e. over Paldi and Income Tax) could respond more to OP in contrast to those emitted likely from some other sources over Bapunagar, Narol and Science City.

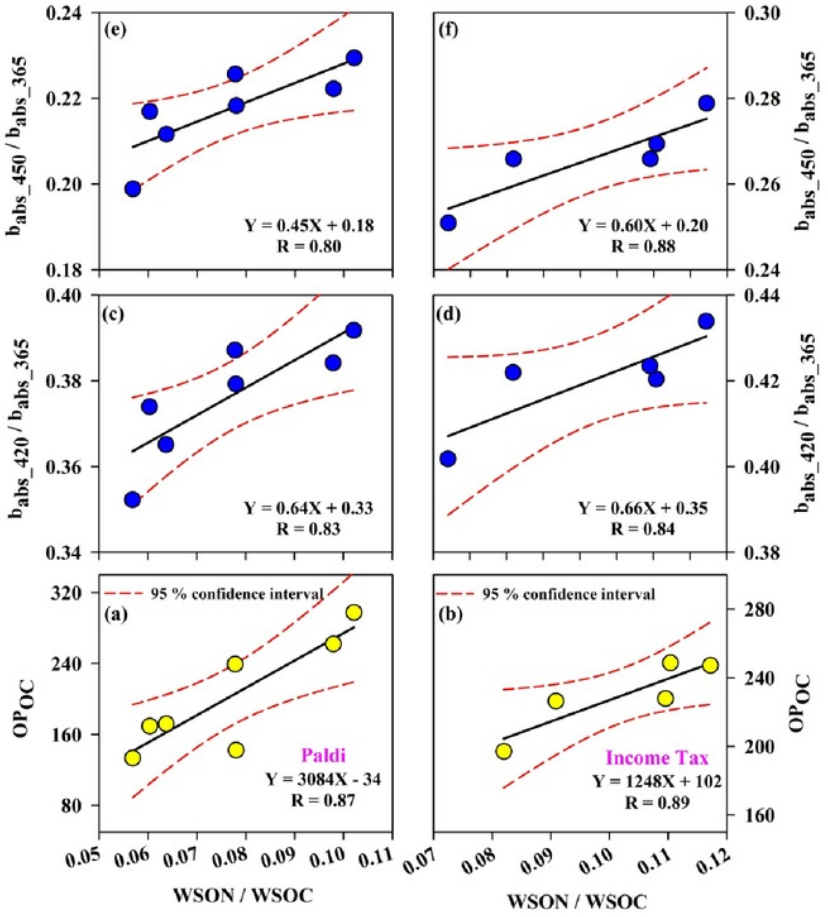

Figure 5. 10. *Scatter plots of WSON/WSOC ratio with OP_{OC}, b_{abs_420} / b_{abs_365} ratio, b_{abs_450} / b_{abs_365} ratio over Paldi (a, c, e, respectively) and Income Tax (b, d, f, respectively). Red dashed lines in each plot shows 95 % probability that the true best-fit line for the population lies within this confident interval.*

Chapter 6

SYNTHESIS AND FUTURE SCOPE

6.1. Synthesis

This chapter summarizes the key findings made in this study and addresses certain issues indicating the scope of further research. Our results suggest that aerosol OP over different regions of India and surrounding oceans are influenced by emissions from different sources, their atmospheric processing, and meteorological conditions. It covers how the change in chemical composition responds to their OP. It also hints how the atmospheric aging influences the chemical composition and thus OP. One of our key finding showed relationship of OPV and OPM with PM2.5 mass concentration, which suggests particle composition is more relevant than mass concentration in deciding the OP of PM. However, both are important as PM2.5 mass concentration decides the amount of dose reaching to the human respiratory tract, whereas PM2.5 composition decides its OP. Region wise summary and conclusions are described below.

Indo-Gangetic Plain

As mentioned in chapter 2, the IGP spread over northern India receives large amount of air pollutants due to various anthropogenic activities such as emissions from vehicles, industries and bio-fuel burning during winter months (December – February), which result into deterioration of ambient air quality. Over Patiala (northern IGP), it was observed that the dominance of carbonaceous aerosol in $PM_{2.5}$ enhances OP_M of ambient particles, and dominance of secondary inorganic aerosol, being DTT-inactive, appear to reduce it. It is suggested to use WSOC/SIA ratio as a measure of DTT activity of secondary particle over the study region. Biomass burning derived carbonaceous aerosol are found to be likely more DTT-active as compared to those derived from fossil fuel burning. Enhancement in the slope of OP_M and WSOC/SIA ratio linear relationship for samples collected during daytime following the foggy nights in comparison to that for samples collected during non-foggy period might be due to the production of redox-active species by fog processing. These results suggest a need of taking up online measurement of OP

during foggy and non-foggy period to better understand and assess the role of meteorological condition in particle DTT activity.

Though there was no statistically significant difference in $PM_{2.5}$ mass concentration, the average values of OP_V and OP_M observed over the middle of IGP (i.e. Kanpur) were significantly higher ($p < 0.001$) than those observed over northern IGP (i.e. Patiala, the upwind region). Significantly higher OC fraction and higher WSOC/SIA over Kanpur compared to Patiala could be the reason for observed higher averaged OP_V and OP_M.

Furthermore, $PM_{2.5}$ over Patiala (upper IGP) and Kanpur (middle IGP) during winter had been reported to be composed of 20 to 50% of OM. On the contrary, $PM_{2.5}$ composition over Shillong (lower IGP) ambience was found to be dominated by higher OM fraction (50 – 70%) during winter. DTT assay has been reported to be mainly active for organics (Cho et al., 205), which is likely the reason of very high (a factor of 2) OP_M over Shillong. These observations also reflect a relatively high exposure risk and intrinsic oxidative toxicity of aerosol over Shillong.

Moreover over Patiala, emission of aerosol and their gaseous precursors from post-harvest paddy-residue burning during October–November every year results into poor air quality downwind in the IGP. This study highlights the significant impact of biomass burning on aerosol chemical composition and OP. The OP_V values (7 – 25 nmol DTT min^{-1} m^{-3}) found during the burning period were 10 – 14 times higher than those reported worldwide. This is an important observation as the inhaled dose of $PM_{2.5}$ with high OP can severely affect the health of people living in the study region. Higher individual OP_V values were found to be associated with higher (> 1.0) BC_{370}/BC_{880} ratios, suggesting that the emissions from BB sources are more responsible for OP. It inferred that aging of nitro-aromatics (Brown carbon chromophores) emitted from paddy burning can be more responsible for OP.

Remote Locations

The highest PM_{10} concentrations over a high altitude site (Mt Abu) during pre-monsoon were ascribed to high dust loading whereas, the lowest PM_{10}

concentrations during winter were attributable to shallow boundary layer that made the site in free troposphere. The temporal variability in PM_{10} and the percentage contribution of its component's sources (i.e. mineral dust, EC, anthropogenic inorganics (also defined as SIA), OM, sea-salt) with both OP_V and OP_M showed that OM, EC and anthropogenically derived inorganics are following the same trend which is shown by OP (both OP_V and OP_M). On the contrary, dust and sea-salts are not following the temporal trend of OP, suggesting natural inorganic aerosol are not DTT-active. It was inferred that the source (s) emitting EC also emit other species, which are more DTT-active than those species which are emitted along with anthropogenically derived inorganic species (i.e. SIA).

PM_{10} mass concentration over the MABL of the Arabian Sea varied significantly from 61 to 184 $\mu g\ m^{-3}$, which is attributable to winds bringing aerosol from different type of sources (anthropogenic, marine, mineral dust). It was observed that the Arabian Sea received aerosol from two different classes of long-range transported air masses; i.e. continental and Desert / marine. The continental air masses were found to be associated with free acid, which further reacted with sea-salt and resulted in ~ 95% depleted-Cl^-. The Cl^--depletion was positively and significantly correlated with OP_M, suggesting the importance of free acid in the catalytic generation of ROS. Average OP_V and average OP_M over the Arabian Sea associated with continental air masses showed ~ 1.5 times higher values as compared to those associated with Desert / marine air masses. Further, mass fraction of WSON, WS–Mn, WS–Cu, and WS–Zn correlated positively with OP_M at high significance level.

The relationship between EC mass fraction and OP_M observed over the Arabian Sea is found to be similar to that documented over a high altitude site Mt Abu, but with a factor of 2 higher slope than that documented over a semi-urban city Patiala. This observation suggest that the aging of aerosol make it more DTT-active, as both the Arabian Sea and the Mt Abu predominantly receive aged aerosol.

The fractions of anthropogenically derived PM components such as OM, EC and SIA over the Port Blair are found to be ~ 4.0, ~ 2 – 5, and ~ 2.0 times higher, respectively, than those observed over the Arabian Sea (during April) and over the

Mount Abu (during January to April). On the contrary, mineral dust component was the predominant contributor to PM_{10} over the Arabian Sea and the Mount Abu (~ 1.5 – 3.0 times higher than the Port Blair). As a result of increased fraction of anthropogenic inputs over the Port Blair, intrinsic oxidative potential (i.e. OP_M) was increased almost 3.0 times as compared to those observed over the Arabian Sea and the Mount Abu.

Micro-Environments

OP over the five sites, representing different micro-environment, of a big urban city in western India (i.e. Ahmedabad) was carried out. Narol is an industrial site, Income Tax is a big commercial zone with heavy traffic, whereas, Bapunagar, Paldi and Science City are residential zones in different parts of Ahmedabad. Higher levels of PM_{10} over western India compared to WHO Air Quality Guideline values are clearly visible likely due to elevated dust content in atmospheric PM. Dust is perennial over Ahmedabad because of it's being a part of semi-arid region. The level of OP_V values observed over Narol was ~ 4 times higher compared to Science City, suggesting higher exposure of people to potentially redox-active PM. However, there was no such drastic change in OP_M (intrinsic OP) over Narol compared to the other sites. Overall, PM_{10} over all the sites in Ahmedabad was found to be dominated by ~ 50% mineral dust, which could be the reason for similar OP_M over the city. Furthermore, It was inferred that less aged oxidized OA (high f43, less f44) are more DTT-active and as they aged (less f43, high f44) their OP_{OC} decreases over Ahmedabad. It is important to note the limitation of this case study that water-soluble OA is compared with (water + methanol) soluble OP_{OC} over Ahmedabad. It was observed that considerable fraction of nitro-phenolic compounds (Brown carbon chromophores) were probably the cause of observed intrinsic OP_{OC} over Paldi and Income Tax. These findings also suggest that nitro-phenolic compounds emitted particularly from the traffic related sources (i.e. over Paldi and Income Tax) could respond more to OP in contrast to those emitted likely from some other sources over Bapunagar, Narol and Science City.

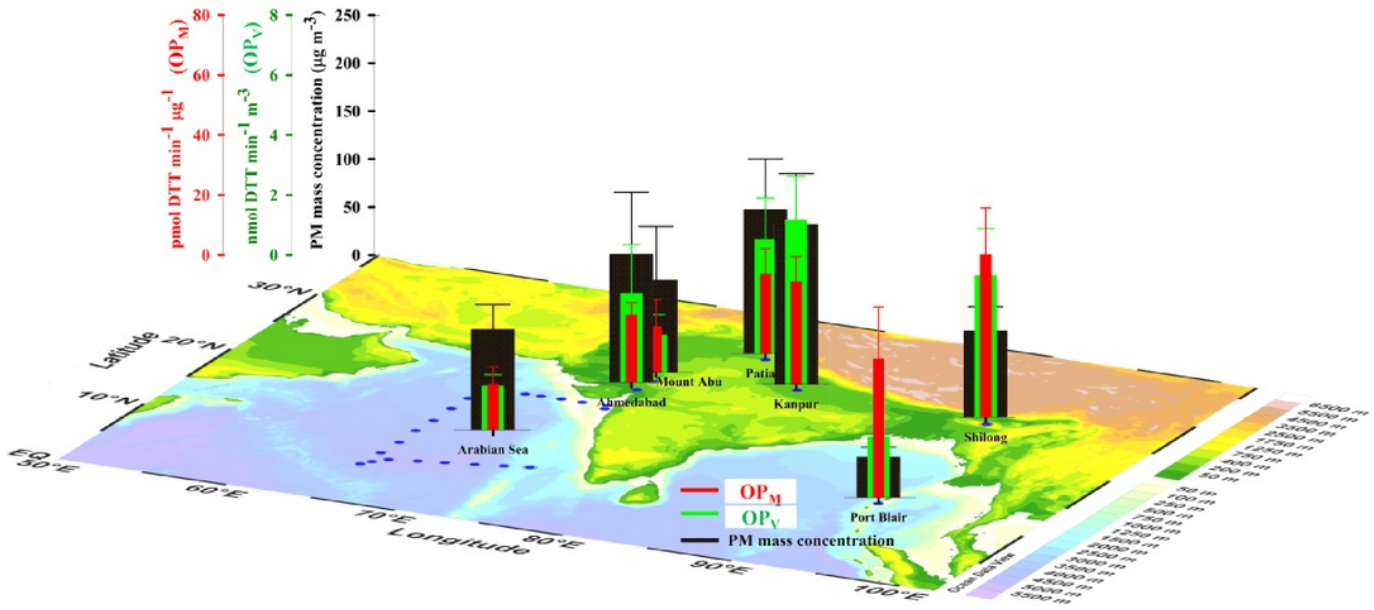

Figure 6. 1. *Summary of the oxidative potential of ambient aerosol over different environments in India.*

6.2. Future Scope

This study broadly covers the OP of ambient aerosol over sites dominated by different emission sources such as intense biomass burning, mixed sources of biomass and fossil fuel burning, emission from industries, residential zone etc., and different meteorological conditions such as foggy – non-foggy conditions, seasonal variation over high altitude site, impact during long-range transport etc., over India and surrounding oceans. The potential role of aerosol derived from both anthropogenic as well as natural sources in determining the impact on OP has been covered in detail in this study. This study also attempted to identify the major sources responsible for the OP. However, the study carried out during this Ph.D. considers only the soluble fraction of aerosol, whereas insoluble aerosol species can also contribute to OP and should be considered when assessing health effects.

Although there has been substantial research on the toxicity of ambient aerosol in relation to particle size, there are no studies on the OP of size-segregated aerosol over India and very limited in the world. The size distributions of OP along with the major chemical players of both water–soluble and –insoluble will give the total picture of aerosol and their ROS generation capability over India. This information has an important implication while assessing effects of aerosol on the human health.

To better understand the emission sources and physicochemical transformations processes affecting aerosol OP, semi–continuous measurements of OP along with chemical composition in different environments are vital. It will be further useful during foggy and non-foggy conditions to understand what influences the OP of ambient aerosol after fog dissipation.

ROS can be studied using several assays such as Dithiothreitol, Ascorbic Acid, Dichloro-Dihydro-Fluorescein Diacetate, p-Hydroxyphenyl Acetic Acid Dimerization etc. However, none of these assays respond to all the chemical components present in atmospheric aerosol. Aerosol OP should be measured with all available and need to focus on the identification of specific species responsible for the in-situ production of ROS followed by looking into its correlation with the mortality and morbidity factors. This information can be important while assessing

effects of aerosol on the human health and should be of tremendous value to the government for imparting their resources in reducing pollution in India.